Přírodovědecká fakulta Univerzity Palackého v Olomouci

Katedra optiky



Bakalářská práce

Recyklace Fockových stavů na stlačené stavy

Petr Zapletal

Faculty of Science Palacký University Olomouc

Department of Optics



Bachelor Thesis

Recycling of Fock states to squeezed states

Petr Zapletal

Přírodovědecká fakulta Univerzity Palackého v Olomouci

Katedra optiky



Bakalářská práce

Recyklace Fockových stavů na stlačené stavy

Vypracoval: Petr Zapletal

Studijní program: B1701 Fyzika

Studijní obor: Obecná fyzika a matematická fyzika, 3. ročník

Forma studia: prezenční

Vedoucí bakalářské práce: Doc. Mgr. Radim Filip, Ph.D.

Práce odevzdána dne: 12. 5. 2014

Abstrakt

Fockovy stavy diskrétních proměnných a stlačené stavy spojitých proměnných jsou kvantové stavy využívané jako zdrojové stavy pro kvantovou fyziku. Cílem je studovat a navrhnout proveditelnou metodu recyklace mnoha kopií neperfektních Fockových stavů na stlačené stavy světla s využitím pouze lineární optiky a homodynní detekce. Speciální pozornost je věnována recyklaci kvantových ne-Gaussovských stavů s pozitivní Wignerovou funkcí na stlačené stavy. To otevírá směr kvantové recyklace i pro širší třídu zdrojových stavů, které i když nejsou aplikovatelné v určité úloze, mohou být po recyklaci aplikované v jiné úloze.

Klíčová slova

Kvantové stlačení, Fockův stav, Gaussovský stav, recyklace, Gaussovská operace, Gaussovský filtr

Abstract

Both discrete-variable Fock states and continuous-variable squeezed states are basic resources of quantum physics. The aim is to study and propose a feasible method of a recycling of many copies imperfect Fock states to the quantum squeezing using only linear optics and homodyne detection. In particular, the recycling of quantum non-Gaussian states with positive Wigner function to the squeezed states will be addressed. It also opens a direction of quantum recycling for a class of resource states, which are not applicable for some task but, after the recycling, they still can be useful for another task.

Keywords

Quantum squeezing, Fock state, Gaussian state, recycling, Gaussian operation, Gaussian filter

| Poděkování |
|--|
| Chtěl bych poděkovat panu Doc. Mgr. Radimovi Filipovi, Ph.D. za odborné vedení bakalářské práce a za pomoc a poskytnuté rady, které mi pomohly při vypracování této práce. Dále bych chtěl poděkovat své rodině za psychickou podporu. |
| |
| |
| Čestné prohlášení |
| Čestně prohlašuji, že jsem baklářskou práci vypracoval samostatně za použití uvedé literatury a pod dohledem vedoucího práce. Dále souhlasím s tím, aby práce byla použita pro studijní a výzkumné účely. |
| Bakalářská práce byla vypracována souběžně s připravovanou publikací R. Filip a P. Zapletal, Recycling of wasted quantum states into useful squeezing. |
| |
| |
| V Olomouci dne 12. 5. 2014 |
| |

Contents

| 1 | Introduction | 1 |
|---|--|----------------------------------|
| 2 | Theoretical background 2.1 Quantization of electromagnetic field 2.2 Wigner function of quantum states 2.3 Gaussian states 2.4 Fock states 2.5 Linear Gaussian operations 2.6 Threshold detector and photocounters 2.7 Homodyne and heterodyne detection | 10 11 |
| 3 | Recycling strategies with Gaussian tools | 13 |
| 4 | Single-copy Gaussian recycling 4.1 Universal single-copy recycling | 15 16 18 |
| 5 | Two-copy Gaussian recycling 5.1 Universal two-copy recycling | 24 25 31 |
| 6 | Multi-copy Gaussian recycling6.1 Tree-structure multi-copy Gaussian recycling6.2 Linear-structure multi-copy Gaussian recycling6.3 Universal multi-copy recycling6.4 Single-layer partially-universal multi-copy recycling6.5 Multi-layer partially-universal multi-copy recycling6.6 Non-universal multi-copy recycling | 36 36 37 46 47 48 |
| 7 | Non-Gaussian detectors 7.1 Threshold detectors | 5; 5; 5; 5; 5; |
| 8 | Conclusion | 60 |
| 9 | Outlook | 62 |

1 Introduction

Non-classical squeezed states are very important resources for quantum information processing [1]. Their non-classicality is characterized by reduced noise in some observable bellow threshold of vacuum noise. First experimental observation of squeezed states was made in Refs. [2, 3]. Recently, squeezed states are key resource for continuous-variable quantum information processing like: quantum metrology [4], continuous-variable quantum teleportation [5], preparation of cluster states [6], quantum key distribution [7] and hybrid approach to quantum information processing [8].

Squeezing is very sensitive to noise and can be very easily lost in a channel. Squeezing distillation was developed to reverse the disturbing process and reach squeezing again. Important fact is that squeezing cannot be distilled from Gaussian states [9]. Distillation from non-Gaussian states arising by amplitude fluctuations [10] and phase fluctuation [11, 12] were studied. On the other hand, the squeezed states can be purified by Gaussian operations based on linear optics and feedforward [13]. Squeezing distillation has purification effect as well [14]. Moreover, multi-copy distillation was introduced to improve squeezing recovery [15]. Multi-copy distillation has also Gaussification effect [16, 17] and provides harmonic mean of input state variances of observables [18].

An extension of the squeezing distillation is squeezing extraction [19]. Squeezing extraction universally generates squeezing from general quantum states in contrast to squeezing distillation obtaining squeezing from specific disturbed states which are originally squeezed. Universal multi-copy squeezing extraction based on multiple interference and position measurement was introduced and analyzed in Ref. [19]. Interestingly, extractable squeezing by universal multi-copy recycling is determined by relative concavity of input state probability distribution of generalized coordinate in point of global maximum. It is a method which exploits hidden features of only one variable distribution of quantum states, therefore it advantageously does not require complete knowledge of quantum state. The universal squeezing extraction was then applied to various examples of non-Gaussian states.

If the squeezing extraction is applied to an imperfect version of another resource states, for example imperfect single-photon states, we actually could recycle wasted resource to another useful one. Highly non-classical single-photon states are another very important resources for quantum processing. They have zero uncertainty in energy and their strong non-classicality is represented by negativity of Wigner function. Single-photon states were detected at first in Refs. [20, 21] and their full tomography was done in Ref. [22]. Single-photon states are important resource for many quantum processing implementations like preparation of entanglement for qubits [23], quantum key distribution [25, 24] and linear optical quantum computing [26]. Moreover, broad scale of quantum states could be prepared from ideal single-photon states [27]. However, imperfect single-photon states are typically mixture of vacuum state and pure single-photon state which appears by attenuation of original pure single photon. Highly attenuated single-photon state loses its negativity but they are still non-classical [28]. Its non-classicality is now represented by non-Gaussian character which means that the state is incompatible with mixture of Gaussian states [29, 30]. It is not clear whether these imperfect states can be still recycle to useful states, for example squeezed states.

Important no-go theorem is that portion of single photon in wasted single-photon states cannot be increased by linear optics, any destructive measurement, post-selection or feedforward [31]. Attenuated single-photon state in form $\eta|1\rangle\langle 1|+(1-\eta)|0\rangle\langle 0|$ is considered where presence of higher Fock states than one is excluded since higher Fock states can be eliminated. Imperfection of attenuated single-photon state is then described by factor η representing the portion of single photon. This attenuation factor cannot be increased if only linear optical components, any destructive measurements, post-selection and feedforward are allowed and presence of higher Fock state components in distilled state is forbidden [31]. Simultaneously, attenuated single-photon state has positive Wigner function for $\eta \leq 0.5$. As a result, wasted single-photon state with positive Wigner function cannot be distilled to state with negative Wigner function. Therefore, they might be useless for original purpose of single-photon states if it depends on negativity of Wigner function. On the other hand, wasted single-photon state with positive Wigner function can be used as input state for squeezing recycling where its non-Gaussianity is enough to produce squeezing.

In this thesis, squeezing recycling from wasted single-photon state is studied in detail. Novel non-universal approach is introduced to improve the universal squeezing extraction [19]. Mainly, we focus on possibility to extract squeezing from states with positive Wigner function. Fundamental questions arise: can squeezing be extracts from arbitrary attenuated single-photon state and how much squeezing can be asymptotically extracted for large number of input states? Remarkably, we will show that squeezing can be extracted from arbitrary attenuated single-photon state. We will introduce novel partially-universal method to estimate extractable squeezing from large number of input states. This method extracts squeezing from relative concavity and newly from relative steepness of input state probability distribution of generalized coordinate. Moreover, we are involving recycling strategies to produce as high as possible squeezing from pure single-photon state or as an extension from higher Fock states. Interesting usage of recycling protocols can be producing squeezed states in ultraviolet region of electromagnetic spectrum where standard sources of squeezing are not available but still single-photon states can be produced [32, 33].

2 Theoretical background

2.1 Quantization of electromagnetic field

Quantization of electromagnetic field can be found comprehensively in Ref. [8]. For this Thesis, we will only sketch a basic results to introduce a reader to the field. Vector potential \mathbf{A} , which is just ancillarly observable in classical electrodynamics, has a crucial role in discretization of electromagnetic field in quantum electrodynamics. Its quantum version, vector potential operator $\hat{\mathbf{A}}$ of electromagnetic field in box of finite spatial volume L^3 can be expressed in quantized form

$$\hat{\mathbf{A}}(\mathbf{r},t) = \sum_{k} \left(\frac{\hbar}{2\omega_{k}\varepsilon_{0}L^{3}} \right)^{1/2} \mathbf{e}^{(\lambda)} \left[\hat{a}_{k} \ e^{i(\mathbf{k}\cdot\mathbf{r} - \omega_{k}t + \phi)} - \hat{a}_{k}^{\dagger} \ e^{-i(\mathbf{k}\cdot\mathbf{r} - \omega_{k}t + \phi)} \right]$$
(1)

where the sum is over all modes in the box with wave vector \mathbf{k} and angular frequency ω_k . Vector $\mathbf{e}^{(\lambda)}$ is unit polarization vector, the index $\lambda = 1, 2$ is polarization index, ε_0 is electric permittivity of free space and \hbar is Dirac constant. Dimensionless complex constants in classic theory are here replaced by operators \hat{a}_k and \hat{a}_k^{\dagger} which represent annihilation and creation operators satisfying $[\hat{a}_k, \hat{a}_k^{\dagger}] = 1$. Phase factor ϕ represents phase with respect to reference phase. Electric intensity given as $\hat{\mathbf{E}} = -\frac{\partial \hat{\mathbf{A}}}{\partial t}$ reads

$$\hat{\mathbf{E}}(\mathbf{r},t) = i \sum_{k} \left(\frac{\hbar \omega_{k}}{2\varepsilon_{0} L^{3}} \right)^{1/2} \mathbf{e}^{(\lambda)} \left[\hat{a}_{k} \ e^{i(\mathbf{k} \cdot \mathbf{r} - \omega_{k} t + \phi)} + \hat{a}_{k}^{\dagger} \ e^{-i(\mathbf{k} \cdot \mathbf{r} - \omega_{k} t + \phi)} \right]$$
(2)

and Hamiltonian of electromagnetic field can be expressed as

$$\hat{H} = \sum_{k} \hbar \omega_k \left(\hat{a}_k^{\dagger} \hat{a}_k + \frac{1}{2} \right), \tag{3}$$

where $\hat{N}_k = \hat{a}_k^{\dagger} \hat{a}_k$ is photon number operator of kth mode. The optical detectors are only sensitive to electric field [34]. Electric intensity of kth mode with single polarization

$$\hat{E}_k(\mathbf{r},t) = E_0 \left[\hat{a}_k \ e^{i(\mathbf{k}\cdot\mathbf{r} - \omega_k t + \phi)} + \hat{a}_k^{\dagger} \ e^{-i(\mathbf{k}\cdot\mathbf{r} - \omega_k t + \phi)} \right]$$
(4)

can be expressed as

$$\hat{E}_k(\mathbf{r},t) = E_0 \left[\hat{x}_k \cos \left(\mathbf{k} \cdot \mathbf{r} - \omega_k t + \phi \right) + \hat{p}_k \sin \left(\mathbf{k} \cdot \mathbf{r} - \omega_k t + \phi \right) \right], \tag{5}$$

where constant E_0 contains all the dimensional prefactors. In-phase quadrature $\hat{x}_k = \hat{a}_k^{\dagger} + \hat{a}_k$ and out-of-phase quadrature $\hat{p}_k = i(\hat{a}_k^{\dagger} - \hat{a}_k)$ mathematically correspond to position and momentum operator of mechanic oscillator. We use normalization for which vacuum state $|0\rangle$ will exhibit variance in both quadratures equal to unity $V_x = V_p = 1$. Dimensionless quadrature \hat{x} is proportional to real part of electric intensity and dimensionless quadrature \hat{p} is proportional to the imaginary part of electric intensity. Quadratures satisfy commutation relation

$$[\hat{x}, \hat{p}] = 2i. \tag{6}$$

Fluctuations of electric field can be directly measured by a homodyne detector [35] which will be discussed in detail in Section 2.7.

Single mode of electromagnetic field is described by quantum state with density matrix $\hat{\rho}$. In Fock states representation, quantum state density matrix reads $\hat{\rho} = \sum_{n,m} c_{nm} |n\rangle\langle m|$ where $|n\rangle$ is Fock state and c_{nm} are generally complex coefficients which are real for m=n. Fock states are eigenstates of photon number operator \hat{N} satisfying relation

$$\hat{N}|n\rangle = n|n\rangle \tag{7}$$

and forming the discrete basis. Quadratures mean values of the quantum state are defined as

$$\langle x \rangle = Tr \left[\hat{\rho} \hat{x} \right], \langle p \rangle = Tr \left[\hat{\rho} \hat{p} \right].$$
 (8)

Quadratures second statistical moments are then defined as

$$\langle x^2 \rangle = Tr \left[\hat{\rho} \hat{x}^2 \right], \langle p^2 \rangle = Tr \left[\hat{\rho} \hat{p}^2 \right]$$
 (9)

and variances then reads

$$V_x = \langle x^2 \rangle - \langle x \rangle^2, V_p = \langle p^2 \rangle - \langle p \rangle^2. \tag{10}$$

Heisenberg uncertainty relations for optical quadratures reads

$$V_x V_p \ge 1. \tag{11}$$

Quadratures eigenstates $|x\rangle$ and $|p\rangle$ are infinitely squeezed in position and momentum respectively and they have infinite energy. From this perspective, they are not physical. Both sets of eigenstates form continuous bases $\{|x\rangle\}$ and $\{|p\rangle\}$ respectively. Both bases are orthogonal hence $\langle x'|x\rangle = \delta(x-x')$ and $\langle p'|p\rangle = \delta(p-p')$. Quadrature bases are coupled by Fourier transform

$$|p\rangle = \frac{1}{\sqrt{4\pi}} \int_{-\infty}^{\infty} dx \ e^{ipx/2} |x\rangle$$
 (12)

and overlap of $|x\rangle$ and $|p\rangle$ eigenstates reads

$$\langle x|p\rangle = \frac{1}{\sqrt{4\pi}} e^{ipx/2}.$$
 (13)

In next section, we will discuss Wigner function representation of quantum states.

2.2 Wigner function of quantum states

Wigner function or Wigner quasi-probability distribution [35] is continuous-variable representation of density matrix $\hat{\rho}$. Wigner quasi-probability distribution is defined as

$$W(x,p) = \frac{1}{2\pi} \int_{-\infty}^{\infty} dy \langle x - y | \hat{\rho} | x + y \rangle e^{iyp}$$
 (14)

and it is a real function of expectation values of two complementary variables \hat{x} and \hat{p} . Wigner function is often used because it visualizes behavior in both complementary quadratures at one time. It is called quasi-probability distribution because if Wigner function is positive it can be interpret as probability distribution in phase space. On the other hand, there can be states whose Wigner function attain negative values. Negativity of Wigner function is a witness of high quantum non-classical character. Probability distributions of quadratures can be easily computed from Wigner function by relations

$$P(x) = \int_{-\infty}^{\infty} dp \ W(x, p), \quad P(p) = \int_{-\infty}^{\infty} dx \ W(x, p). \tag{15}$$

Mean values and variances can be computed as well by relations

$$\langle x \rangle = \text{Tr} \left[\hat{\rho} \hat{x} \right] = \int_{-\infty}^{\infty} dp \int_{-\infty}^{\infty} dx \ W(x, p) x,$$

$$V_x = \text{Tr} \left[\hat{\rho} \left(\hat{x} - \langle x \rangle \right)^2 \right] = \int_{-\infty}^{\infty} dp \int_{-\infty}^{\infty} dx \ W(x, p) \left(x - \langle x \rangle \right)^2$$
(16)

and for quadrature \hat{p} similarly. Purity of a state can be computed by formula

$$P = \operatorname{Tr}\left[\hat{\rho}^2\right] = 4\pi \int_{-\infty}^{\infty} dp \int_{-\infty}^{\infty} dx \ W^2(x, p). \tag{17}$$

We will study now special class of quantum states called Gaussian states.

2.3 Gaussian states

Quantum Gaussian states are defined as the states which Wigner function is multidimensional Gaussian function [35]. One mode Gaussian Wigner function reads

$$W(x,p) = \frac{1}{2\pi\sqrt{\text{Det}V}} \exp\left[-\frac{1}{2}(\mathbf{q}\cdot\mathbf{d})^T V^{-1}(\mathbf{q}\cdot\mathbf{d})\right],$$
 (18)

where $\mathbf{q} = (x, p)$ is vector of quadratures and $\mathbf{d} = (\langle x \rangle, \langle p \rangle)$ is vector of mean values and $V_{ij} = \frac{1}{2} \langle q_i q_j + q_j q_i \rangle - \langle q_i \rangle \langle q_j \rangle$ is covariance matrix. If covariance matrix refers to quantum state, its eigenvalues λ_1 and λ_2 have to satisfy relation

$$\lambda_1 \lambda_2 \ge 1. \tag{19}$$

General single-mode Gaussian state can be always adapted by phase to form

$$W(x,p) = \frac{1}{2\pi\sqrt{V_x V_p}} \exp\left[-\frac{(x - \langle x \rangle)^2}{2V_x} - \frac{(p - \langle p \rangle)^2}{2V_p}\right]. \tag{20}$$

Gaussian states purity is then defined as

$$P = V_x V_p. (21)$$

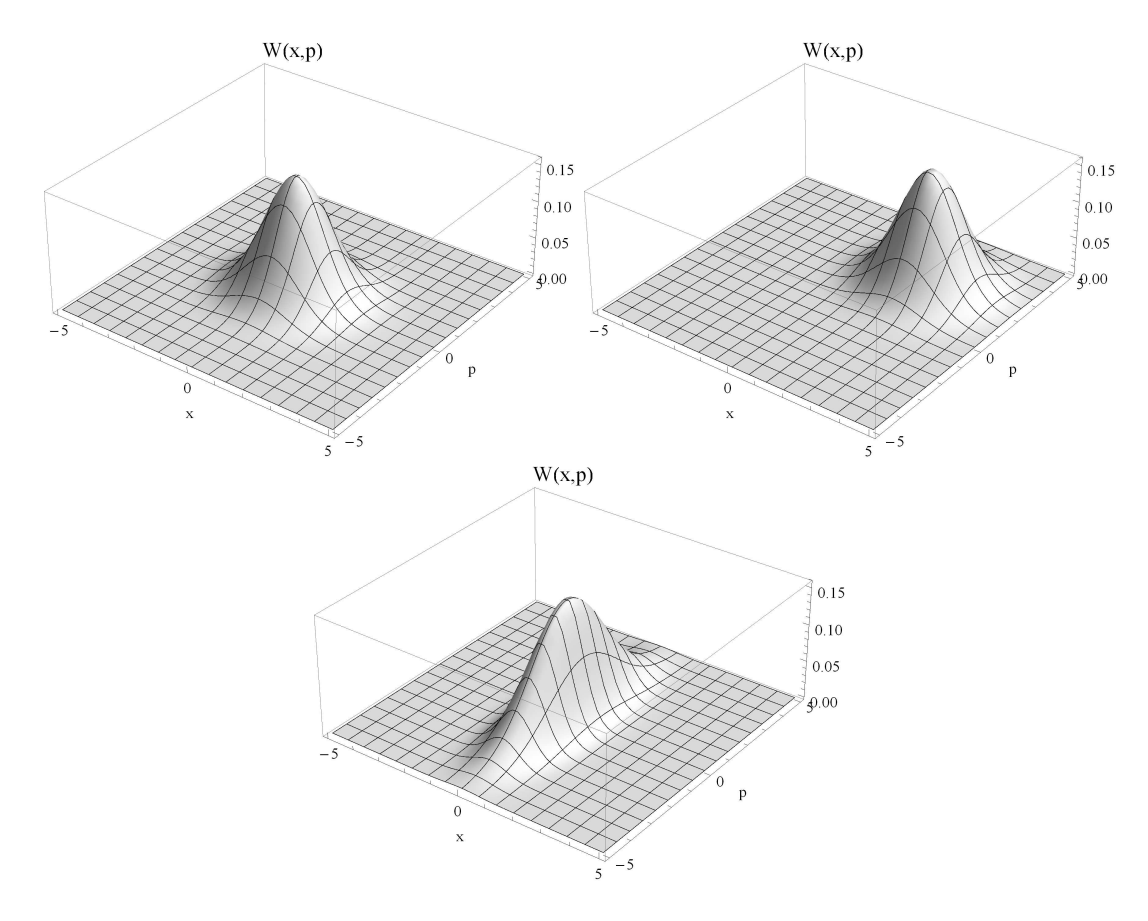


Fig. 1: Wigner quasi-probability distribution of Gaussian states: (top-left) vacuum state, (top-right) coherent state with means values $\langle x \rangle = \langle p \rangle = 2$, (bottom) pure squeezed state with variances $V_x = \frac{1}{3}$ and $V_p = 3$ and with mean values $\langle x \rangle = \langle p \rangle = 0$.

Special cases of Gaussian states are vacuum state, coherent state and squeezed state. Vacuum state is state with minimal energy and minimal uncertainty $V_xV_p=1$. It exhibits zero mean values $\langle x\rangle=\langle p\rangle=0$ in both quadratures and corresponding variances $V_x=V_p=1$ are equal to unity because of normalization. Vacuum state Wigner function depicted in Fig. 1 reads

$$W(x,p) = \frac{1}{2\pi} \exp\left[-\frac{x^2 + p^2}{2}\right].$$
 (22)

Coherent state is eigenstate of annihilation operator. It again exhibits minimal uncertainty and its quadrature variances $V_x = V_p = 1$ are still equal to unity but mean values can be non-zero. Covariance matrix of all coherent states is identity matrix 1. Coherent state Wigner function depicted in Fig. 1 reads

$$W(x,p) = \frac{1}{2\pi} \exp\left[-\frac{(x-\langle x\rangle)^2 + (p-\langle p\rangle)^2}{2}\right]. \tag{23}$$

Squeezed state has one of the quadrature variances smaller than unity. It can exhibit non-zero mean values and higher uncertainty $V_x V_p \ge 1$ than vacuum and coherent state.

Squeezed state with minimal uncertainty depicted in Fig. 1 is called pure squeezed state because its purity reach unity. Vacuum and coherent states are pure as well.

Important difference is between squeezed state and quantum squeezing. Quantum squeezing is a property of every state which has one of the quadrature variances smaller than unity. On the other hand, squeezed states are considered to be Gaussian states. Quantum squeezing is an important resource for many quantum experiments. Squeezed states can be prepared if large number of copies of state with squeezing is available by mixing them on many beam splitters without any detection. Final state will be Gaussified in consequence of quantum central limit theorem [16, 17].

Quantum non-classical states [28] are states which are not a mixture of coherent states in form

$$W(x,p) = \int_{\{\mathbf{d},\mathbb{1}\}} P(\xi)W_{\xi}(x,p)d\xi \tag{24}$$

where integral is over all physical values of parameters $\xi = (\mathbf{d}, \mathbb{1})$. So-called quantum non-Gaussian character [29] means that state is not a mixture of Gaussian states in form

$$W(x,p) = \int_{\{\mathbf{d},V_{ij}\}} P(\xi)W_{\xi}(x,p)d\xi$$
 (25)

where integral is over all physical values of parameters $\xi = (\mathbf{d}, V_{ij})$. Non-Gaussian character is an important witness of quantum non-classical character, weaker than negativity of Wigner function but stronger than non-classicality. Very good examples of quantum non-classical states are Fock states which will be studied now.

2.4 Fock states

The Fock states studied in Ref. [35] are eigenstates of photon number operator \hat{N} and they have no quantum noise in energy. Fock states again form an orthogonal basis $\{|n\rangle\}$ and $\langle m|n\rangle = \delta_{mn}$. Fock-state Wigner function reads

$$W_n(x,p) = \frac{1}{2\pi} (-1)^n L_n(x^2 + p^2) \exp\left[-\frac{x^2 + p^2}{2}\right],$$
 (26)

where $L_n(y)$ is Laguerre polynomial. Single-photon state Wigner function depicted in Fig. 2 is expressed as

$$W_1(x,p) = \frac{1}{2\pi} \exp\left[-\frac{x^2 + p^2}{2}\right] (x^2 + p^2 - 1)$$
 (27)

and two-photon state Wigner function depicted in Fig. 2 is expressed as

$$W_2(x,p) = \frac{1}{2\pi} \exp\left[-\frac{x^2 + p^2}{2}\right] \left(x^4 + p^4 - 4x^2 - 4p^2 + 2p^2x^2 + 2\right). \tag{28}$$

Ideal Fock states are infinitely squeezed in number of photons. It means their energy uncertainty is infinitely squeezed as well. More realistic approximation of real state is attenuated Fock state which can be modeled from pure Fock state by splitting off

some portion of the energy on beam splitter with transmittance η (beam splitter will be discussed in detail later). Density matrix of attenuated single-photon state reads

$$\hat{\rho}_1 = \eta |1\rangle\langle 1| + (1 - \eta)|0\rangle\langle 0| \tag{29}$$

and its Wigner function changes to $W(x,p) = \eta W_1(x,p) + (1-\eta)W_0(x,p)$, where $W_0(x,p)$ is vacuum state Wigner function. Similarly attenuated two-photon state density matrix reads

$$\hat{\rho}_2 = \eta^2 |2\rangle \langle 2| + 2\eta (1 - \eta) |1\rangle \langle 1| + (1 - \eta)^2 |0\rangle \langle 0| \tag{30}$$

and its Wigner function is given as

$$W(x,p) = \eta^2 W_2(x,p) + 2\eta(1-\eta)W_1(x,p) + (1-\eta)^2 W_0(x,p). \tag{31}$$

Measurement of attenuated single-photon state Wigner function was made in Ref. [22]. Fock states have high non-Gaussian character because of their Wigner function attain negative values. Attenuated Fock states negativity vanishes for $\eta < 0.5$ (see Fig. 2) but states still have non-Gaussian character because they cannot be expressed as mixture of Gaussian states [29].

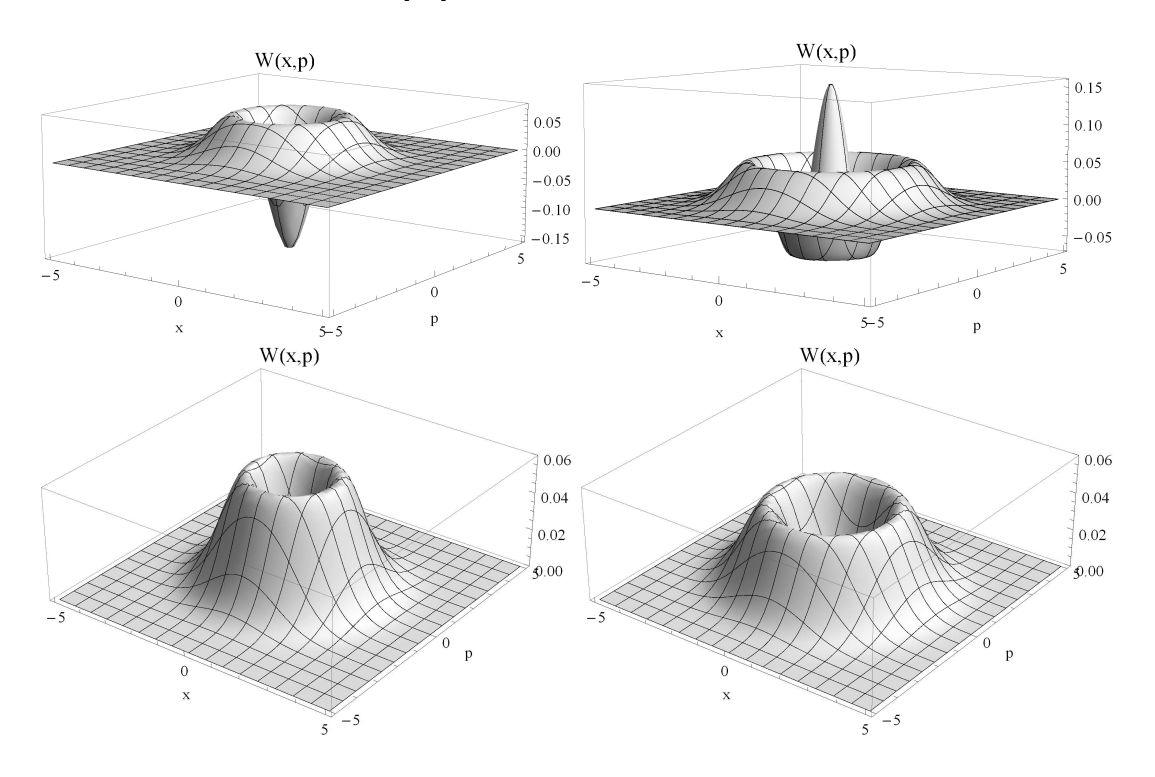


Fig. 2: Wigner quasi-probability distribution of Fock states: (top-left) pure single-photon state, (top-right) pure two-photon state, (bottom-left) attenuated single-photon state with $\eta = 0.5$ and (bottom-right) attenuated two-photon state with $\eta = 0.5$.

In the next section, we will discuss transformations of quantum states.

2.5 Linear Gaussian operations

Transformations mapping Gaussian states to other Gaussian states are called Gaussian operations [35]. Basic unitary Gaussian operations used in this thesis are one-mode coherent displacement and two-mode beam splitter.

Coherent displacement $D(\alpha)$ is unitary operator shifting quantum state in phase space of x and p variables. It can be defined by annihilation and creation operator as

$$\hat{D}(\alpha) = e^{(\alpha \hat{a}^{\dagger} - \alpha^* \hat{a})}.$$
(32)

Displacement transformation of quadratures operators can be written as

$$\hat{x} \to \hat{D}(\alpha)^{\dagger} \hat{x} \hat{D}(\alpha) = \hat{D}(\alpha)^{\dagger} \left(\hat{a}^{\dagger} + \hat{a} \right) \hat{D}(\alpha) = \hat{a}^{\dagger} + \alpha^* + \hat{a} + \alpha = \hat{x} + 2Re(\alpha), \tag{33}$$

$$\hat{p} \to \hat{D}(\alpha)^{\dagger} \hat{p} \hat{D}(\alpha) = \hat{D}(\alpha)^{\dagger} \left(i \hat{a}^{\dagger} - i \hat{a} \right) \hat{D}(\alpha) = i \left(\hat{a}^{\dagger} + \alpha^* - \hat{a} - \alpha \right) = \hat{p} + 2Im(\alpha), \quad (34)$$

and by substitution $\bar{x}=2Re(\alpha)$ and $\bar{p}=2Im(\alpha)$ we can rewrite the transformations to

$$\hat{x} \to \hat{x} + \bar{x}, \quad \hat{p} \to \hat{p} + \bar{p}.$$
 (35)

To perform displacement, quantum filed interaction with "classical" driving field is needed. Driving field α interaction during time $\tau \in (0, t)$ is describe by Hamiltonian

$$H_D^I = i\hbar \left(\delta \alpha \hat{a}^{\dagger} - \delta \alpha^* \hat{a}\right) = \frac{\hbar}{2} \left(\delta x \hat{p} - \delta p \hat{x}\right), \tag{36}$$

where $\delta \alpha = (\delta x + i \delta p)/2$ and displacements then read $\bar{x} = \delta xt$ and $\bar{p} = \delta pt$. In Wigner function representation, displacement is provide by transformation

$$W(x,p) \to W(x' - \bar{x}, p' - \bar{p}). \tag{37}$$

Beam splitter interaction couples two modes together. It uses classical optics beam splitter. In Heisenberg picture interaction is provided by transformation

$$\hat{x}_1' = \sqrt{T}\hat{x}_1 + \sqrt{1 - T}\hat{x}_2, \quad \hat{p}_1' = \sqrt{T}\hat{p}_1 + \sqrt{1 - T}\hat{p}_2,$$

$$\hat{x}_2' = \sqrt{T}\hat{x}_2 - \sqrt{1 - T}\hat{x}_1, \quad \hat{p}_2' = \sqrt{T}\hat{p}_2 - \sqrt{1 - T}\hat{p}_1,$$
(38)

where $T \in (0, 1)$ is beam splitter transmittance and indexes 1 and 2 refer to appropriate modes. Beam splitter interaction can be described by unitary operator [36]

$$\hat{U}_{BS}(T) = T^{\frac{\hat{n}_1}{2}} \exp\left[\sqrt{1 - T}\hat{a}_1^{\dagger}\hat{a}_2\right] \exp\left[-\sqrt{1 - T}\hat{a}_2^{\dagger}\hat{a}_1\right] T^{-\frac{\hat{n}_2}{2}}.$$
 (39)

In Wigner function representation, interaction is described by substitution

$$x_{1} = \sqrt{T}x'_{1} - \sqrt{1 - T}x'_{2}, \quad p_{1} = \sqrt{T}p'_{1} - \sqrt{1 - T}p'_{2},$$

$$x_{2} = \sqrt{T}x'_{2} + \sqrt{1 - T}x'_{1}, \quad p_{2} = \sqrt{T}p'_{2} + \sqrt{1 - T}p'_{1},$$
(40)

and Wigner function is then transformed as

$$W_1(x_1, p_2)W_2(x_2, p_2) \to W_1(\sqrt{T}x_1' - \sqrt{1 - T}x_2', \sqrt{T}p_1' - \sqrt{1 - T}p_2') \times W_2(\sqrt{T}x_2' + \sqrt{1 - T}x_1', \sqrt{T}p_2' + \sqrt{1 - T}p_1'). \tag{41}$$

Now we will discuss measurements of optical mode and operations of quantum states which can be implement by such measurements.

2.6 Threshold detector and photocounters

Threshold detector studied in Ref. [37] is provided by one-mode measurement with two possible results: at least one photon comes to detector or no photons come to detector. To describe threshold detector in operator form, we have to introduce positive operator measure (POVM) formalism which is the most general measurement allowed by Copenhagen interpretation of quantum mechanics [38]. POVM is given by set of positive semidefinite self-adjoin operators which sum to unity. POVM components are not necessarily orthogonal in contrast to projectors. POVM is a direct generalization of projective measurement.

Photon detection in threshold detector is described by POVM component $\Pi = 1 - |0\rangle\langle 0|$. Physically, threshold detector is based on Geiger-like detector where each photon ionizes a single atom in detector chamber and electric pulse is amplified by avalanche process of secondary ionizations to measurable pulse. Avalanche process is the reason why detector cannot distinguish between number of photons incoming to the detector. Threshold detector is sometimes called avalanche photodiode. In Wigner function formalism, POVM component $\Pi = 1 - |0\rangle\langle 0|$ is described by filtration function

$$W_{\Pi}(x,p) = 1 - 4\pi W_0(x,p) \tag{42}$$

where $W_0(x, p)$ is vacuum state Wigner function. Probability of measuring POVM component $\Pi = 1 - |0\rangle\langle 0|$ on state with Wigner function W(x, p) is given as

$$P_{\Pi} = \int_{-\infty}^{\infty} dp \int_{-\infty}^{\infty} dx \ W(x, p) W_{\Pi}(x, p). \tag{43}$$

This measurement returns zero for vacuum state and unity for any other Fock state.

More advanced detectors which can distinguish number of incoming photons are called photon-number resolving detectors. They project to Fock states and the projectors can be written as $\Pi_k = |k\rangle\langle k|$ where k = 1, 2, ... and in Wigner function formalism, measurement is described by filtration function

$$W_{\Pi_k}(x,p) = 4\pi W_k(x,p) \tag{44}$$

where $W_k(x, p)$ is Wigner function of k-photon state. It is challenging to distinguish all Fock states, however, photon number resolving detectors discriminating low Fock states already exist [39].

So far, we assume the ideal cases where every photon incoming to the detector cause measurable pulse but in reality, some photons are reflected from side of the detector and some photons are not detected because after each detection, detector cannot record other photon for certain dead time. It can be described by dimensionless quantum efficiency η representing fraction of all incoming photons which are converted to measurable pulse. Realistic detector can be modeled with ideal detector by splitting the incoming mode on beam splitter with transmittance η . In this thesis, it is dominant imperfection which is considered. We neglect dark counts of photo-counters, since they can be negligibly small for available detectors.

In the next section, we will discuss homodyne and heterodyne detection which are the crucial tools used in this thesis.

2.7 Homodyne and heterodyne detection

Homodyne detection is measurement projected on quadratures eigenstates [35, 37]. Projector of ideal measurement without electronic noise is given as $\Pi_x = |x\rangle\langle x|$ for measuring quadrature \hat{x} and as $\Pi_p = |p\rangle\langle p|$ for measuring quadrature \hat{p} . Homodyne detection is based on beam splitter interaction of signal mode and highly excited classical mode at the same frequency called local oscillator. We use balanced homodyne detection. In balanced homodyne detector, signal mode and local oscillator interfere on symmetric beam splitter and same photodetectors are applied on both output modes to reach statistics of the field quadrature. Measurement of particular quadrature is controlled by phase difference between signal and local oscillator.

In this thesis, balanced homodyne detection and post-selection are used to extract squeezing from single or multiple copies of the general state. Post-selection of quadrature \hat{x}_0 measurement results from narrow interval around \bar{x} is used to prepare final state in an asymptotic regime of low probability of success. In Wigner function formalism, it is provided by transformation

$$W(x_1, p_1, x_0, p_0) \to \frac{1}{N(\bar{x})} \int_{-\infty}^{\infty} dp_0 \ W(x_1, p_1, \bar{x}, p_0) = \tilde{W}(x_1, p_1|\bar{x})$$
 (45)

of two mode Wigner function $W(x_1, p_1, x_0, p_0)$ to conditional Wigner function $\tilde{W}(x_1, p_1|\bar{x})$ where norm of the final Wigner function N reads

$$N(\bar{x}) = \int_{-\infty}^{\infty} dx_1 \int_{-\infty}^{\infty} dp_1 \int_{-\infty}^{\infty} dp_0 \ W(x_1, p_1, \bar{x}, p_0). \tag{46}$$

When selection from narrow interval is used, norm N is infinitely small. Post-selecting from finite interval $[\bar{x}_{min}, \bar{x}_{max}]$ is used to reach state with finite norm of Wigner function. Final Wigner function is then given as

$$\tilde{W}(x_1, p_1 | \bar{x}) = \frac{1}{N(\bar{x})} \int_{\bar{x}_{min}}^{\bar{x}_{max}} d\bar{x} \int_{-\infty}^{\infty} dp_0 \ W(x_1, p_1, \bar{x}, p_0)$$
(47)

and norm is expressed as

$$N(\bar{x}) = \int_{-\infty}^{\infty} dx_1 \int_{-\infty}^{\infty} dp_1 \int_{\bar{x}_{min}}^{\bar{x}_{max}} d\bar{x} \int_{-\infty}^{\infty} dp_0 \ W(x_1, p_1, \bar{x}, p_0). \tag{48}$$

Norm then represents success probability P_S of the measurement. Final state is Gaussian as long as the initial state $W(x_1, p_1, x_0, p_0)$ is Gaussian, however, the transformation of statistical moments of quadratures cannot be generally obtained by any unitary evolution governed by quadratic Hamiltonian [18]. We call this operation Gaussian even if we apply it on non-Gaussian states, since the operation only uses the Gaussian toolbox.

If set-up contains only beam splitters and homodyne detectors measuring just one quadrature and we are interested only in behavior of the same quadrature as was measured, we do not have to work with whole Wigner function because probability distribution of this quadrature carries all desired information. To demonstrate this character,

we consider two states with Wigner functions $W_A(x,p)$ and $W_B(x_0,p_0)$ mixed on beam splitter with transmittance T and selective homodyne measurement of quadrature \hat{x}'_0 applied on one of the output modes. Final state conditional probability distribution of quadrature \hat{x}'_1 reads

$$\tilde{P}(x_1'|\bar{x}) = \int_{-\infty}^{\infty} dp_1' \ \tilde{W}(x_1', p_1'|\bar{x}) = \frac{1}{N(\bar{x})} \int_{-\infty}^{\infty} dp_1' \int_{-\infty}^{\infty} dp_0' \times W_A(\sqrt{T}x_1' - \sqrt{1 - T}\bar{x}, \sqrt{T}p_1' - \sqrt{1 - T}p_0') W_B(\sqrt{T}\bar{x} + \sqrt{1 - T}x_1', \sqrt{T}p_0' + \sqrt{1 - T}p_1'). \tag{49}$$

After backward beam splitter substitution of momentum quadratures

$$p_{1} = \sqrt{T}p'_{1} - \sqrt{1 - T}p'_{0}, \quad p_{0} = \sqrt{T}p'_{0} + \sqrt{1 - T}p'_{1},$$

$$dp_{1}dp_{0} = dp'_{1}dp'_{0}, \tag{50}$$

conditional probability distribution of quadrature \hat{x}'_1 is given as

$$\tilde{P}(x_1'|\bar{x}) = \frac{1}{N} \int_{-\infty}^{\infty} dp_1 \int_{-\infty}^{\infty} dp_0 \ W_A(\sqrt{T}x_1' - \sqrt{1 - T}\bar{x}, p_1) W_B(\sqrt{T}\bar{x} + \sqrt{1 - T}x_1', p_0) = \frac{1}{N(\bar{x})} P_A(\sqrt{T}x_1' - \sqrt{1 - T}\bar{x}) P_B(\sqrt{T}\bar{x} + \sqrt{1 - T}x_1')$$
(51)

where P_A and P_B are coordinate quadrature probability distributions of input states. Similarly, norm is expressed as

$$N(\bar{x}) = \int_{-\infty}^{\infty} dx_1' \int_{-\infty}^{\infty} dp_1' \int_{-\infty}^{\infty} dp_0' \ W_A(\sqrt{T}x_1' - \sqrt{1 - T}\bar{x}, \sqrt{T}p_1' - \sqrt{1 - T}p_0') \times W_B(\sqrt{T}\bar{x} + \sqrt{1 - T}x_1', \sqrt{T}p_0' + \sqrt{1 - T}p_1') = \int_{-\infty}^{\infty} dx_1' \int_{-\infty}^{\infty} dp_1 \int_{-\infty}^{\infty} dp_0 \ W_A(\sqrt{T}x_1' - \sqrt{1 - T}\bar{x}, p_1) W_B(\sqrt{T}\bar{x} + \sqrt{1 - T}x_1', p_0) = \int_{-\infty}^{\infty} dx_1' \ P_A(\sqrt{T}x_1' - \sqrt{1 - T}\bar{x}) P_B(\sqrt{T}\bar{x} + \sqrt{1 - T}x_1').$$
 (52)

This approach can be extended to protocol with selection of measured values from finite interval as well as for more advanced protocols with many beam splitters and homodyne detectors. On the other hand, complementary momentum quadrature is affected by coordinate measurement and we have to compute with whole Wigner function to reach momentum probability distribution.

Heterodyne detection is natural extension of homodyne detection and it is also studied in detail in Ref. [37]. It measures both complementary quadratures at one time. A generalized version of heterodyne detection can be easily implemented by tapping the signal mode on beam splitter with transmittance T and applying homodyne detection measuring coordinate quadrature on transmitted mode and homodyne detection measuring momentum quadrature on reflected mode. Post-selection of quadratures \hat{x} and \hat{p} from narrow interval around \bar{x} and \bar{p} respectively can be used. Note, original version of heterodyne detection is typically for the case T=0.5.

3 Recycling strategies with Gaussian tools

Interconvertibility of quantum resources is important for development of modern quantum physics. Squeezing is an important resource of quantum non-classicallity, being the key element of continuous-variable quantum processing. If the squeezing is not directly observable, there are two fundamentally different types of squeezing extraction: distillation of quantum squeezing and recycling of quantum squeezing. Both methods use general protocol of extraction depicted in Fig. 3. The extraction couples N input states $\hat{\rho}_{in}$ on arbitrary linear optical network consists of beam splitters and mirrors. Trigger then prepares final state $\hat{\rho}_{out}$ by selecting cases when all results \bar{x}_i of M homodyne measurements lay in chosen intervals $\bar{x}_i \in [\bar{x}_{i,min}, \bar{x}_{i,max}]$.

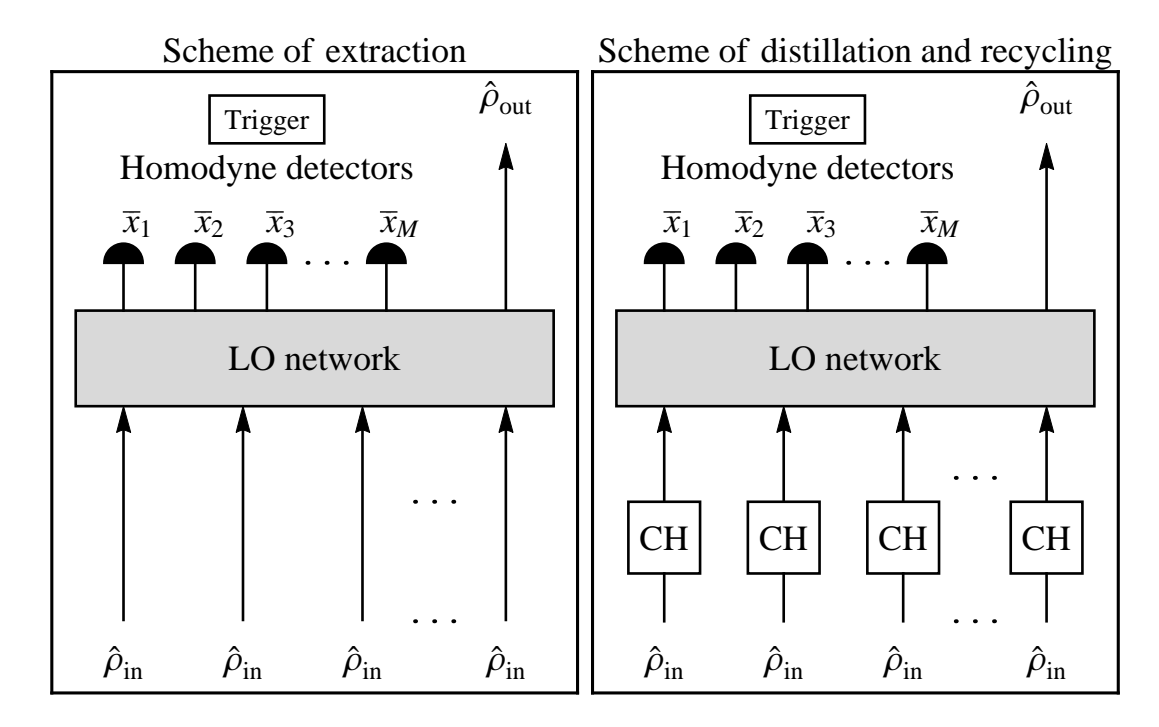


Fig. 3: Schemes of quantum Gaussian extraction, distillation and recycling: (right) quantum Gaussian extraction uses arbitrary linear optical (LO) network and M homodyne detectors to prepare final state $\hat{\rho}_{out}$ from N input state copies $\hat{\rho}_{in}$. Trigger chooses cases only when measurement results \bar{x}_i lay in selected intervals $[\bar{x}_{i,min}, \bar{x}_{i,max}]$ for all i=1,...M. (Left) quantum Gaussian distillation and recycling use extraction protocol to prepare the output state $\hat{\rho}_{out}$ from resource states wasted in a channel CH where the channel represents any disturbing protocol. Difference between quantum Gaussian distillation and recycling is in a type of input state. For distillation, type of the input state is the same as type of the output state $\hat{\rho}_{out}$ in contrast to recycling where the input state could be arbitrary another resource state.

Distillation and recycling apply extraction on resource states wasted in a channel CH to reach useful state again. Squeezing distillation extracts squeezing from state which exhibited squeezing but the squeezing was lost in the channel. For example, the channel could be represented by random coherent displacement. Squeezed state can be distilled

from originally squeezed state disturbed by this channel [10]. For another example, we consider phase averaged squeezed state which no longer exhibits squeezing. Squeezing distillation from that state was described in Ref. [11]. Knowledge of squeezing before the disturbing operation is important for construction of squeezing distillation. It allows to choose the optimal distillation strategy to eliminate the noise in the channel. On the other hand, for general squeezing extraction we do not have to know anything about history of the input state or even the input state do not have to exhibit squeezing at all. Squeezing recycling is another sub task of extraction which transforms useless resource states to useful state of different kind in contrast to squeezing distillation, where crucial property of both resource and final states is quantum squeezing.

The most commonly used resource state for the recycling in this thesis is attenuated single-photon state. Single-photon state with high purity is important resource of quantum optics. It can be used to conditionally prepare any continuous-variable quantum state. On the other hand, wasted single-photon state is highly attenuated with $\eta < 0.5$ exhibiting positive Wigner function and it cannot be used for that purpose. Moreover, distillation of single-photon states towards higher η is impossible with linear optics tools and selective measurement which was proved in Ref. [31]. However we could try to extract squeezing from attenuated single-photon states by recycling. Squeezing is another very important resource of quantum continuous optics in contrast to highly attenuated single-photon state.

To be sure that our procedure do not generate squeezing itself, which will be cheating in our task, we consider squeezing recycling with only Gaussian tools: linear optical components (mirrors and beam splitters) and homodyne or heterodyne detection. Any combination of them cannot generate squeezing from classical states (see Section 2.3). Attenuated single-photon and two-photon states will be considered as input wasted resource states. Commonly generated attenuated single-photon states and homodyne detection in the recycling procedure will be mainly analyzed. Differently to squeezing distillation approach in Ref. [10], we measure the quadrature in which squeezing is generated at the output of the method. Differently to the method in Ref. [11] we will vary post-selection from $\bar{x}=0$ and optimize it for given wasted resource state. Two-photon states and heterodyne detection will be used as extension for fundamental recycling protocols with single-photon states and homodyne detection, to see, whether we can obtain a larger squeezing.

There are several types of schemes we can use for squeezing recycling. We can distinguish universal recycling methods and non-universal methods. The universal squeezing recycling means that the protocol follows an universal receipt which does not depend on specifics of the input state. Explicitly, it considers $\bar{x}_i = 0$ for all indexes i (see Fig. 3). On the other hand, non-universal recycling protocol is optimized for each recycled state. Further, we can sort the methods in respect of number of state copies which are used. Single-copy recycling uses a weak measurement of coordinate of single input state and on the other hand, two-copy recycling uses an interference of two copies of input state in a combination with coordinate measurement. Moreover, we can investigate more complicated multi-copy recycling protocols promising to obtain more squeezing. In this thesis, linear-structure and tree-structure of multi-copy protocols are studied. They will be introduced later in detail.

4 Single-copy Gaussian recycling

The simplest single-copy squeezing recycling depicted in Fig. 4 is based on weak position measurement.

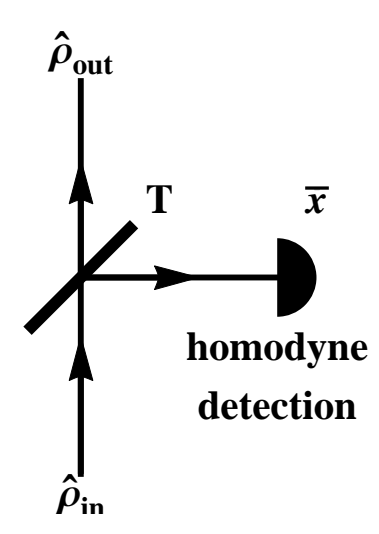


Fig. 4: Scheme of single-copy recycling: input state $\hat{\rho}_{in}$ is tapped on beam splitter with transmittance T and homodyne detection measurement is applied on tapped mode. Post-selecting measured coordinate \bar{x} from $\bar{x} \in [\bar{x}_{min}, \bar{x}_{max}]$ is performed to reach final state $\hat{\rho}_{out}$.

The input state with probability distribution $P_{in}(x)$ of the coordinate is tapped on the beam splitter with the transmittance T. After the coordinate measurement of the tapped mode giving result \bar{x} , the conditional probability density can be expressed as

$$P_{out}(x|\bar{x}) \propto P_{in} \left(\sqrt{T}x - \sqrt{1 - T}\bar{x} \right) \exp \left(-\frac{\left(\sqrt{T}\bar{x} + \sqrt{1 - T}x \right)^2}{2} \right)$$
 (53)

and it can be rearranged by substitution $y = x - \frac{\sqrt{1-T}}{\sqrt{T}}\bar{x}$ to the filtration formula

$$P_{out}(y|\bar{x}) \propto G(y,\bar{x},T) P_{in}\left(\sqrt{T}y\right),$$

$$G(y,\bar{x},T) \propto \exp\left(-\frac{\left(\frac{1}{\sqrt{T(1-T)}}\bar{x}+y\right)^2}{2\frac{1}{1-T}}\right),$$
(54)

where the initial distribution $P_{in}(x)$ is first re-scaled by factor \sqrt{T} and then filtered by the Gaussian filter $G_0(x, \bar{x}, T)$ with the mean value $\frac{1}{\sqrt{T(1-T)}}\bar{x}$ and the variance $\frac{1}{1-T}$. Clearly for weak measurement limit $T\approx 1$ desired to not attenuate the input state, therefore the re-scaling vanishes and the filter $G(x, \bar{x}, T)$ becomes a broader and it can be located at an arbitrary average position controlled by \bar{x} .

When we measure \bar{x} from finite interval $[\bar{x}_{min}, \bar{x}_{max}]$ final probability distribution is given as

$$P_{out}(x) = \frac{1}{N(\bar{x})} \int_{\bar{x}_{min}}^{\bar{x}_{max}} d\bar{x} \ G\left(x - \frac{\sqrt{1-T}}{\sqrt{T}}\bar{x}, \bar{x}, T\right) P_{in}\left(\sqrt{T}x - \sqrt{1-T}\bar{x}\right), (55)$$

which exhibits also the filtration structure in realistic form. Norm N is expressed as

$$N(\bar{x}) = \int_{-\infty}^{\infty} dx \int_{x_{min}}^{x_{max}} d\bar{x} G\left(x - \frac{\sqrt{1-T}}{\sqrt{T}}\bar{x}, \bar{x}, T\right) P_{in}\left(\sqrt{T}x - \sqrt{1-T}\bar{x}\right). (56)$$

These formulas will be used now for specific cases to determine the recycled distributions and the probability of success. Universal recycling will be introduced now.

4.1 Universal single-copy recycling

The universal version of single-copy filtration uses Gaussian filter with $\bar{x}=0$. Universality means that post-selected value \bar{x} does not depend on input state. This filtration method well isolates behavior of P(x) distribution close to origin x=0 and suppresses all peaks of P(x) far from origin. As Variance $\frac{1}{1-T}$ of the filter increases, the filter less attenuates the input state. However, the filtering is less selective, since the filtering function is broader. The transmittance T can therefore be optimized to reach optimal performance. However, the post-selected value $\bar{x}=0$ remains constant, i.e. \bar{x} does not depend on particular P(x).

To understand performance of the filter on general state, it is now described in the operator formalism. The operator can be obtain from a sandwich $\langle x=0|_0\hat{U}_{BS}(T)|0\rangle_0$ of the unitary operator

$$\hat{U}_{BS}(T) = T^{\frac{\hat{n}}{2}} \exp\left(-\sqrt{1 - T}\hat{a}_0^{\dagger}\hat{a}\right) \exp\left(\sqrt{1 - T}\hat{a}^{\dagger}\hat{a}_0\right) T^{-\frac{\hat{n}_0}{2}}$$
(57)

describing the tapping beam splitter by vacuum state $|0\rangle_0$ of the auxiliary mode 0 and position eigen-state $|x=0\rangle_0$ on which we subsequently project the mode 0. Using an asymptotical version $|x=0\rangle$ of physical squeezed state

$$|x=0,s\rangle = (1-s^2)^{\frac{1}{4}} \sum_{n=0}^{\infty} \frac{\sqrt{(2n)!}}{\sqrt{2^n n!}} s^n |2n\rangle$$
 (58)

for $s \to 1$ and Taylor series of $\exp\left(-\sqrt{1-T}a_0^{\dagger}a\right)$, we obtain

$$\langle x = 0 |_0 \hat{U}_{BS}(T) | 0 \rangle_0 \propto T^{\frac{\hat{n}}{2}} \exp\left(-\frac{1-T}{2}\hat{a}^2\right)$$
 (59)

describing the Gaussian filter $\hat{G}(0,T)$ in the operator representation.

The filter is a function of the phase-insensitive operator \hat{a}^2 describing two-photon annihilation, however, it can transform phase insensitive states (symmetrical in phase space) to phase sensitive ones. Clearly, it does not change the single-photon state

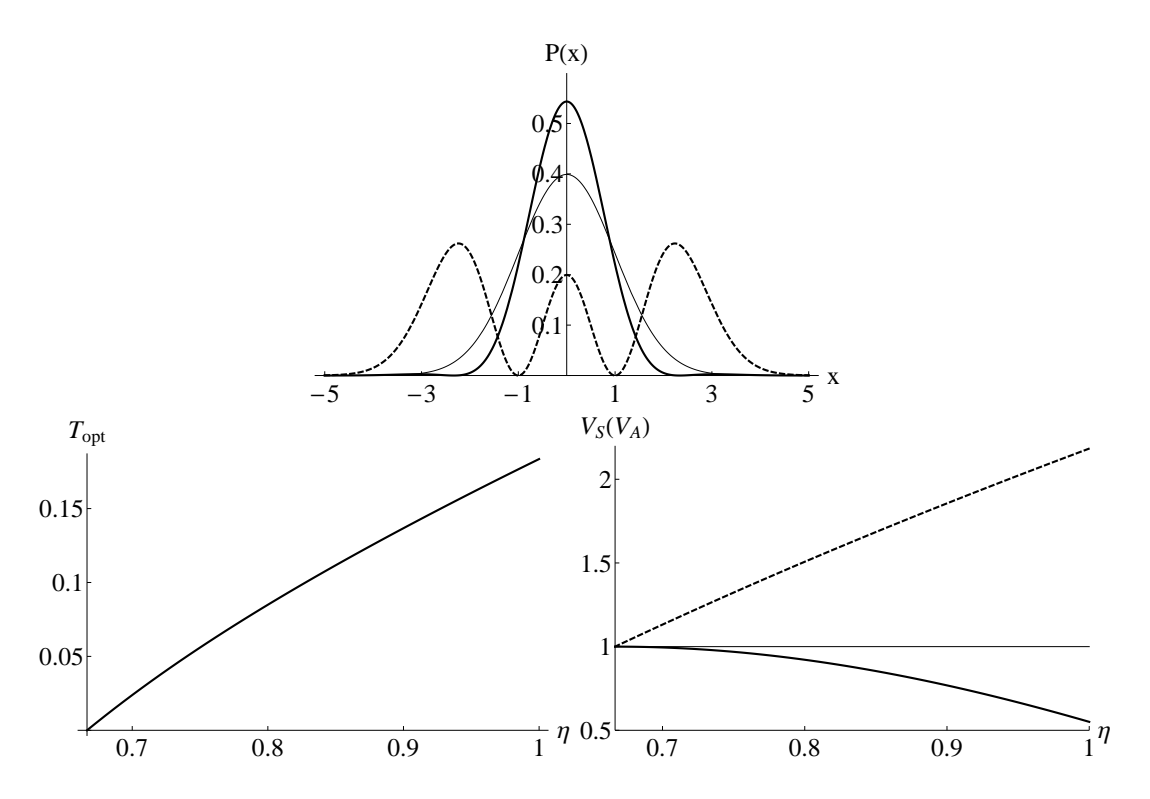


Fig. 5: Single-copy universal recycling: (top) probability distribution of coordinate for state after single-copy recycling from pure two-photon state (full-thick) compared to input state (dashed-thick) and vacuum state (full-thin). (Bottom-left) optimal transmittance to achieve maximal squeezing from two-photon input state. (Bottom-right) minimal variance of the squeezed coordinate extractable from two-photon state (full-thick) and variance of anti-squeezed coordinate (dashed-thick) compared to vacuum noise(full-thin).

|1\rangle. The universal single-copy recycling applied on attenuated single-photon state $\hat{\rho} = \eta |1\rangle\langle 1| + (1-\eta)|0\rangle\langle 0|$ gives the variance

$$V_{out} = 3 - \frac{2(1-\eta)}{1-\eta(1-T)},\tag{60}$$

which does not exhibit any squeezing for any T. In the limit $T \to 1$, the variance V_{out} approaches $V = 1 + 2\eta$ of original attenuated single-photon state. However, implementing the Gaussian filter $\hat{G}(0,T)$ on non-classical Fock state $|2\rangle$, we obtain the superposition

$$\frac{1}{\sqrt{T^2 + \frac{(1-T)^2}{2}}} \left(\frac{1-T}{\sqrt{2}} |0\rangle - T|2\rangle \right) \tag{61}$$

which exhibits squeezing for $T < \frac{1}{3}$ and reach minimal variance $V_S = 3 - \sqrt{6} \approx 0.55$ for $T = 1 - \sqrt{\frac{2}{3}} \approx 0.18$. After single-copy universal recycling, attenuated two-photon

state reach probability distribution of coordinate

$$P_{out}(x) = \frac{e^{-\frac{x^2}{2}} \left(\eta \left(3\eta + \eta T^2 x^4 + 2(2 - 3\eta) T x^2 - 4 \right) + 2 \right)}{\sqrt{2\pi} \left(\eta (T - 1) \left(3\eta (T - 1) + 4 \right) + 2 \right)}$$
(62)

with variance

$$V_S = \frac{\eta(3\eta + 3T(\eta(5T - 6) + 4) - 4) + 2}{\eta(T - 1)(3\eta(T - 1) + 4) + 2}$$
(63)

which exhibits squeezing for $\eta > \frac{2}{3}$. Optimal transmittance is

$$T_{opt} = \frac{3\eta(3\eta - 4) - \sqrt{6}\sqrt{\eta(3\eta - 4) + 2} + 6}{3\eta(3\eta - 2)}$$
(64)

and its dependence on η is depicted in Fig. 5. Transmittance is small in comparison with weak measurement $(T \approx 1)$ which is used for all other cases discussed bellow. Optimal transmittance T_{opt} is increasing function of η and its limit for threshold value $\eta = \frac{2}{3}$ is zero. Minimal variance reaches

$$V_S = 3 - \sqrt{6}\sqrt{\eta(3\eta - 4) + 2} \tag{65}$$

which is depicted in Fig. 5. It is decreasing function of η and $V_S < 1$ appears for any $\eta > \frac{2}{3}$. Evolution of pure two-photon state governed by universal single-copy recycling is depicted in Fig. 5. Input state probability distribution has one central peak and two side peaks. Gaussian filter shifts side peaks a bit further from origin but mainly it suppresses them very much that they are almost negligible. On the other hand, the central peak is raised and it gets narrower than vacuum state distribution.

Squeezing cannot be recycled from single-photon state by universal single-copy protocol but interestingly, it can be recycled from two-photon states for any $\eta > \frac{2}{3}$. It shows that more sophisticated procedures have to be developed to extract squeezing from single-photon states or attenuated two-photon state with positive Wigner function.

4.2 Non-universal single-copy recycling

First, measured position \bar{x} can be optimized to reach maximal squeezing unlike in universal recycling. Gaussian single-copy filter can be set to isolate behavior near any point \bar{x} .

To obtain an operator form of the non-universal single-copy recycling, we now calculate the matrix product

$$\langle x = 0|_0 \hat{D}_0(\bar{x}) \hat{U}_{BS}(T)|0\rangle_0, \tag{66}$$

where $\hat{D}_0(\bar{x}) = \exp(\bar{x}(\hat{a}^{\dagger} - \hat{a}))$ is the displacement operator shifting the measurement of position. Using Baker-Hausdorff theorem

$$e^{A+B} = e^A e^B e^{-[A,B]/2} = e^B e^A e^{[A,B]/2}$$
 (67)

for [A, [A, B]] = [B, [A, B]] = 0, we can decompose the displacement operator

$$\hat{D}_0(\bar{x}) = \exp\left(\frac{\bar{x}^2}{2}\right) \exp\left(-\bar{x}\hat{a}\right) \exp\left(\bar{x}\hat{a}^{\dagger}\right). \tag{68}$$

Using the Baker-Haussdorff theorem once more, we commute

$$\exp\left(-\bar{x}\hat{a}_0\right)\exp\left(-\sqrt{1-T}\hat{a}_0^{\dagger}\hat{a}\right) = \exp\left(-\sqrt{1-T}\hat{a}_0^{\dagger}\hat{a}\right)\exp\left(-\bar{x}\hat{a}_0\right)\exp\left(\bar{x}\sqrt{1-T}\hat{a}\right)$$
(69)

and obtain

$$T^{\hat{n}} \exp\left(\bar{x}\sqrt{1-T}\hat{a}\right) \langle x=0|_0 \exp\left(-\sqrt{1-T}\hat{a}_0^{\dagger}\hat{a}\right) |0\rangle_0, \tag{70}$$

where the last part has been calculated previously. Using it, we derive the operator form of

$$\hat{G}(\bar{x},T) = T^{\hat{n}} \exp\left(\bar{x}\sqrt{1-T}\hat{a} - \frac{1-T}{2}\hat{a}^2\right)$$
(71)

for the single-copy Gaussian filter. If the value of \bar{x} is large and simultaneously $T \to 1$, the filter converges to the asymptotical form $\hat{G}(T) = T^{\hat{n}} \exp\left(\bar{x}\sqrt{1-T}\hat{a}\right)$, being different from the universal symmetrical Gaussian filter described above. For fixed T approaching unity, the attenuated single-photon state cannot be converted to the squeezing since the state almost annihilated by the filter $\hat{G}(T)$.

Considering \bar{x} finite, single-photon state with $\eta = 1$ can be converted by non-universal single-copy filter to a superposition

$$\frac{1}{1+\bar{x}^2(1-T)} \left(\bar{x}\sqrt{1-T}|0\rangle + |1\rangle \right),\tag{72}$$

which after optimization over \bar{x} for given T exhibits minimal variance $V_S = 3/4$. For the single-copy of attenuated single-photon state, the minimum of conditional variance V_S of the output state for a given transmission T of the beam splitter over the post-selection value \bar{x} , it approaches

$$V_S = \frac{4 + \eta(3T - 4)}{4(1 - \eta(1 - T))} \tag{73}$$

for an optimal $\bar{x}_{opt} = \sqrt{3} \sqrt{\frac{1-\eta+\eta T}{\eta(1-T)}}$. Simultaneously, the variance V_A reaches

$$V_A = \frac{2 - \eta(2 - 3T)}{2 - 2\eta(1 - T)}. (74)$$

In a limit $T \to 1$ always exhibits the squeezing

$$V_S = 1 - \frac{\eta}{4} \tag{75}$$

for $\eta > 0$ at a cost of decreasing success rate. For $\eta = 0.5$, the variance approaches $V_S = \frac{7}{8}$. The variance $V_A = 1 + \frac{\eta}{2}$ of complementary variable is always smaller than the variance $V = 1 + 2\eta$ of the original state. This additional purification effect in the complementary momentum variable comes from non-Gaussian structure $W(x, p) \neq 0$

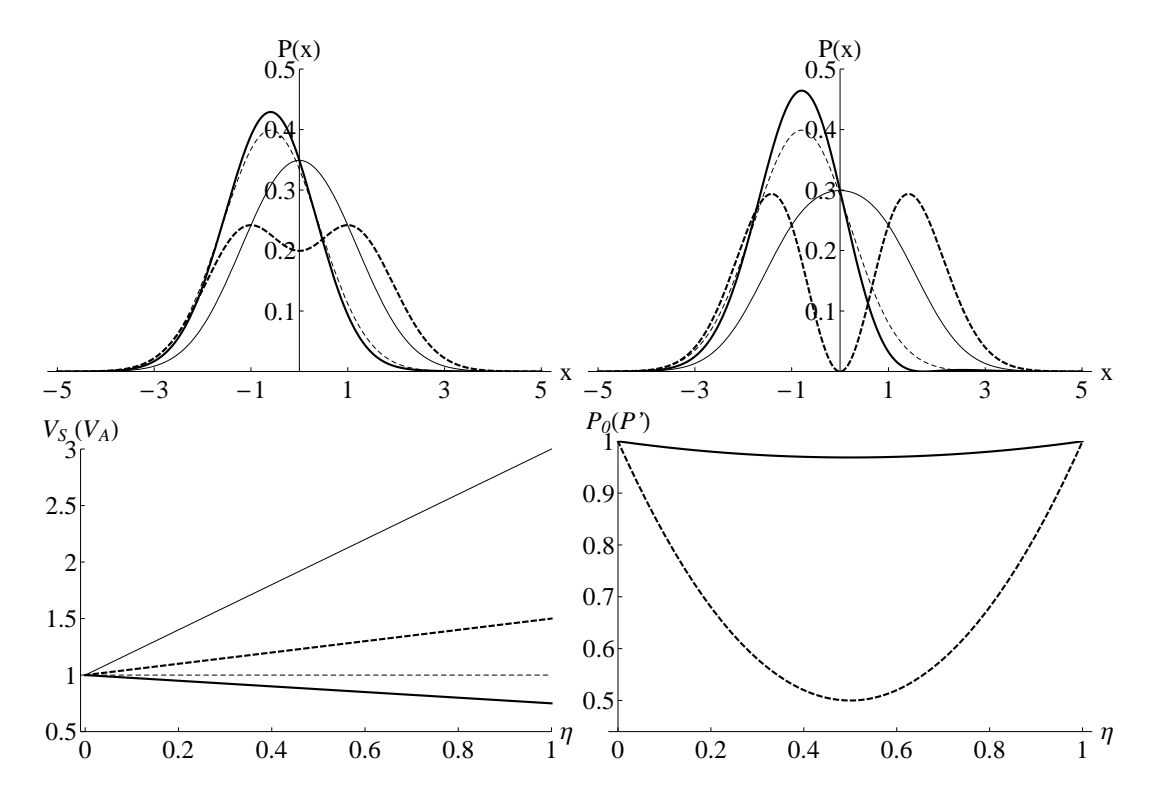


Fig. 6: Optimal single-copy non-universal squeezing recycling from single-photon state: recycled state probability distribution of squeezed quadrature (full-thick) for $\eta=0.5$ (top-left) and $\eta=1$ (top-right) compared to input state probability distribution (dashed-thick), recycled state probability distribution of anti-squeezed quadrature (full-thin) and probability distribution of coherent state (dashed-thin). (Bottom-left) the variance V_S of squeezed quadrature (full-thick), the variance V_A of the complementary quadrature (dashed-thick) compared to vacuum noise (dashed-thin) and variance of attenuated single-photon state (full-thin). (Bottom-Right) purity of the recycled state (full line) compared to purity of input state (dashed line).

W(x)W(p) of the single-photon state. Probability distribution of squeezed quadrature after optimal recycling is depicted in Fig. 6. Evolution of probability distribution is more complicated than in the case of universal single-copy recycling because of the non-universality of the Gaussian filter. Input distribution has two peaks for $\eta > \frac{1}{3}$ but two-peak structure of recycled distribution vanishes for $\eta < 0.84$. For $\eta > 0.84$, only one peak is raised and the other is suppressed and negligible. Raised peak is shifted a bit closer to the origin because the filter cannot completely inhibit the influence of the second peak of input distribution. Recycled distribution is narrower than coherent-state coordinate probability distribution. The dependencies of V_S and V_A for $T \to 1$ are depicted in Fig. 6(bottom-left).

Remarkably, an imperfect single-photon state even with positive Wigner function can be conditionally converted to the directly observable quadrature squeezing by the non-universal recycling for any $\eta > 0$, whereas it is impossible for the universal one. Although the imperfect single photons with the positive Wigner function cannot be

recycled to better single photon with negative Wigner function by a linear optical network and homodyne detectors [31], they can be converted to the squeezing being another important and irreducible resource of quantum technology. It is the simplest example of quantum recycling of resources.

If we use heterodyne detection instead of homodyne detection, the reachable squeezing from single attenuated single-photon state is still the same because minimal achievable variance of squeezed quadrature is still $V_S=1-\frac{\eta}{4}$. Moreover, this is a limit for recycling from attenuated single photon for any projective or selective measurement. This is a limit for photon-counting detectors in combination with displacement as well as for threshold detector. Even ideal projective measurement to superposition $\alpha|0\rangle+\beta|1\rangle$ applied on single-photon state has the same limit of squeezed quadrature variance. Recycling with threshold detector and ideal projective measurement, which are both non-Gaussian detection strategies, will be discussed later in Section 7.2 and Section 7.4, respectively. In summary, homodyne detection reaches maximal squeezing extractable from single-photon state by single-copy recycling.

Now, we will discussed other properties of recycling with homodyne detection. The generated squeezed state is not pure, we can compromise between the achievable squeezing in coordinate and the noise in complementary momentum quadrature. Eliminating \bar{x} and taking a limit $T \to 1$ into account, the optimal trade-off is

$$V_{A,opt} = 1 + \frac{\eta}{2} - \frac{\sqrt{\eta^2 - 4\eta + 4\eta V_S}}{2} \tag{76}$$

with a smaller $V_{A,opt}(V_S)$ comparing to the variance V_A for the maximum of squeezing. Moreover, the state is not exactly Gaussian, therefore purity P of the generated state depicted in Fig. 6 (bottom-right) has to be calculated from the Wigner function, giving

$$P^{(1)} = 1 - \frac{2T\eta(1-\eta)}{(1+\eta(1-T)(\bar{x}^2-1))^2},\tag{77}$$

which is for any η monotonously increasing function of \bar{x} , approaching unity for any T if \bar{x}^2 is high enough. Since $P^{(1)} \geq P_{in}$ where $P_{in} = 1 - 2\eta(1 - \eta)$ is purity of initial single-photon state, the procedure also purifies the state simultaneously with the squeezing extraction. Simultaneously, in a limit of enough large \bar{x} also the purity of Gaussified state $P_G = \frac{1}{4\sqrt{V_X V_P}}$ being $P_G(\eta, T, \bar{x}) \approx 1 - \frac{(1-\eta)T}{8p(1-T)^2\bar{x}^4}$ approaches unity for any η and T < 1, at a cost of the success rate.

Measuring \bar{x} from finite interval is used to count success probability P_S . Measuring $\bar{x} \in [\bar{x}_{min}, +\infty)$ is optimal for single-copy recycling because optimal measured coordinate is for limit $\bar{x} \to \infty$. Transmittancy is given by $T = \frac{\eta \bar{x}_{min}^2 + 3\eta - 3}{\eta(\bar{x}_{min}^2 + 3)}$ which is optimal transmittance for measuring given coordinate \bar{x}_{min} . Trade-off V_S versus P_S is depicted in Fig. 7. For the better squeezing, we unavoidably pay by smaller success probability. For $\eta = 0.3$, squeezing is reached if $P_S < 1.36\%$ which is still very feasible probability of success for many experiments. For $\eta = 0.5$, squeezing is reached if $P_S < 11.87\%$. For $\eta = 0.9$, squeezing is reached if $P_S < 45.73\%$. This implies that squeezing recycling from single-photon states with small η has small success probability but on the other hand squeezing can be recycled from high purity single-photon state with high

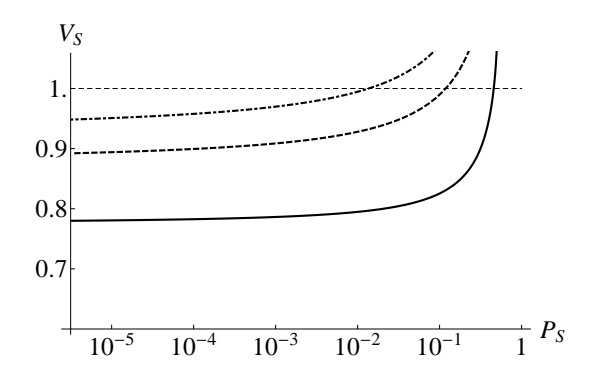


Fig. 7: Single-copy non-universal squeezing recycling from single-photon state success probability versus achieved squeezing: the variance V_S for $\eta = 0.3$ (dot-dashed-thick) and for $\eta = 0.5$ (full-thick) and for $\eta = 0.9$ (dashed-thick) compared to vacuum noise (dashed).

success probability. Since the probability of success can be increased by a rate of single photon production, we consider it as less important and technical parameter. Squeezed quadrature variance goes to limit value $V_S = 1 - \frac{\eta}{4}$ as success probability goes to zero.

Two-photon state is again consider as input state to discussion about single-copy recycling to visualize a tendency for higher Fock states. There are two qualitatively different strategies which recycle squeezing from attenuated two-photon input state. Universal single-copy recycling discussed above and weak measurement recycling like in the case of single-photon state. Both these methods can be compared to reach maximal squeezing. Nearly optimal weak measurement recycling is for measuring \bar{x} from narrow interval around $\bar{x}_{opt} = \frac{\sqrt{3}\sqrt{1-\eta(1-T)}}{\sqrt{\eta(1-T)}}$, which is estimated in analogy with single-photon input state where \bar{x}_{opt} is optimal measured coordinate. In limit $T \to 1$ the variance is given as

$$V_S = 1 - \frac{188\eta}{529},\tag{78}$$

which is numerically verified minimal variance. Estimated nearly optimal measurement reach optimal strategy in limit $T \to 1$. In that limit \bar{x}_{opt} goes to infinity and squeezing is extracted from asymptotic properties of the probability distribution in contrast with universal recycling where squeezing is extracted from behavior of probability distribution near origin. Two-photon input state probability distribution has one central peak and two wing peaks for $\eta=0.9$. One-peak distribution is reached after recycling and distribution has smaller variance than coherent state coordinate probability distribution (see Fig. 8). For $\eta=0.5$, two-peak input state probability distribution is recycled to one-peak distribution which has smaller variance than coherent state probability distribution of coordinate (see Fig. 8). The evolution of the probability distribution is the same as in the case of non-universal single-copy distribution from single-photon state (see Fig. 6). Only more peaks have to be suppressed.

Variances given by formulas Eq. (65) and Eq. (78) are compared to achieve maximal squeezing and result is depicted in Fig. 8. Asymptotic weak measurement is optimal for $\eta < 0.952$, which means that universal single-copy recycling is optimal for two-

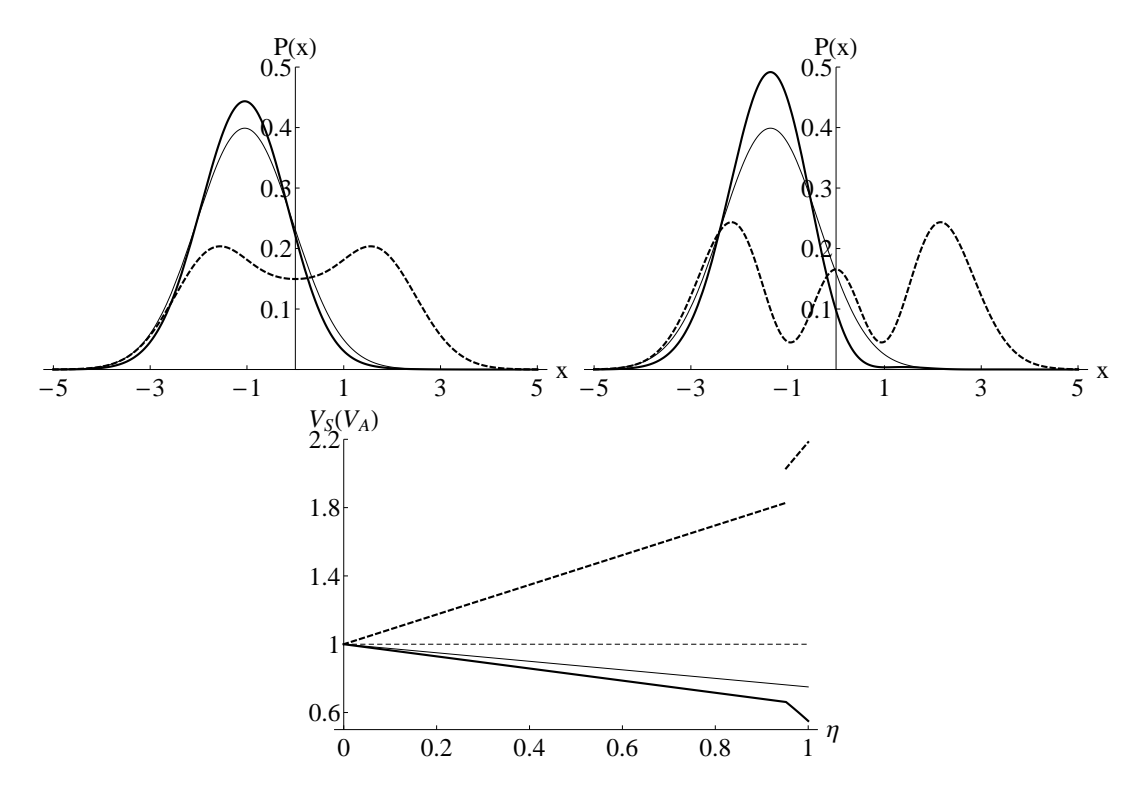


Fig. 8: Single-copy non-universal squeezing recycling from two-photon state: recycled state probability distribution of squeezed quadrature \hat{x} (full-thick) for $\eta = 0.5$ (top-left) and $\eta = 0.9$ (top-right) compared to input state probability distribution (dashed-thick) and coherent state probability distribution (full-thin). (Bottom) the variance V_S of squeezed quadrature (full-thick), the variance V_A of the complementary quadrature (dashed-thick) compared to vacuum noise (dashed-thin) and to extractable variance from single-photon state by non-universal single-copy recycling (full-thin). Variance of quadratures are piecewise functions because for $\eta < 0.952$, asymptotic recycling with $\bar{x} \to \infty$ is optimal and for higher η , universal recycling with $\bar{x} = 0$ is optimal.

photon input state with high purity. From two-photon input state can be extract more squeezing than from single-photon input state for any $\eta > 0$ (see Fig. 8).

Remarkably, squeezing can be recycled from attenuated single-photon state by non-universal single-copy protocol for any $\eta > 0$ even from states with positive Wigner function. It suggests that squeezing is recycled from properties hidden in quantum non-Gaussian character of P(x) distribution. More squeezing can be extracted from two-photon state than from single-photon one for every $\eta > 0$. It shows, that non-Gaussianity of higher Fock states can be used to generate more squeezing.

5 Two-copy Gaussian recycling

Two-copy Gaussian recycling is qualitatively different from single-copy protocol because it uses interference of two copies of input state with distributions $P_{in}(x)$ and then it applies measurement unlike single-copy recycling which uses weak measurement. Two copies of input state interfere on beam splitter with transmittance T and homodyne detection measurement is applied on one of the output modes. Selection of measured coordinate from narrow interval around \bar{x} is applied to achieve final state. Scheme of the recycling is depicted in Fig. 9. The first part of the protocol before optional Gaussian filter uses Hong-Ou-Mandel interference [40], however, homodyne detection is used here instead of the photo-counters.

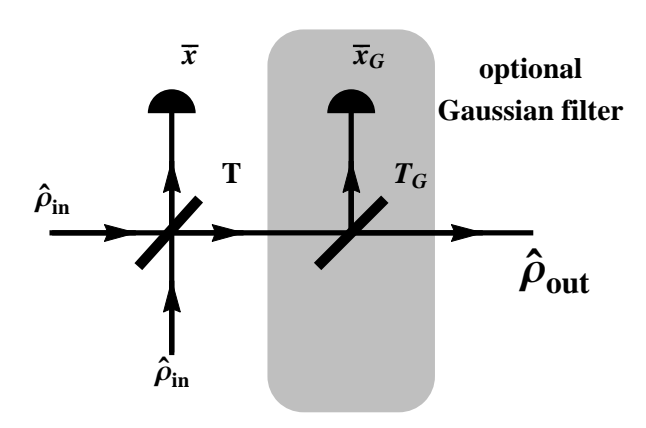


Fig. 9: Scheme of two-copy recycling: two copies of input state $\hat{\rho}_{in}$ are mixed on beam splitter with transmittance T and homodyne detection measurement is applied on one mode. Post-selecting measured coordinate \bar{x} from $\bar{x} \in [\bar{x}_{min}, \bar{x}_{max}]$ is performed. Optional single-copy Gaussian filter composed of beam splitter with transmittance T_G and homodyne detector measuring coordinate from narrow interval around $\bar{x}_G = 0$ can be used to reach final state $\hat{\rho}_{out}$.

Symmetric beam splitter for T=0.5 is optimal for two-copy protocols because of symmetric input states. It can be verified for particular states which we will use as input states. Input modes have marginal probability distribution $P_{in}(x_1)$ and $P_{in}(x_2)$ of generalized coordinates x_1 and x_2 . Coordinates $x_1 = (x'_1 - x'_2)/\sqrt{2}$ and $x_2 = (x'_1 + x'_2)/\sqrt{2}$ are coupled on the beam splitter. Output state has probability distribution in coordinate x'_1 given as

$$P_{out}(x_1'|\bar{x}) = \frac{1}{N(\bar{x})} P_{in} \left(\frac{x_1' - \bar{x}}{\sqrt{2}}\right) P_{in} \left(\frac{x_1' + \bar{x}}{\sqrt{2}}\right)$$

$$(79)$$

after measurement of x_2' in narrow interval around \bar{x} where $N(\bar{x})$ is a norm. Formula can be rearranged by substitution $y = (x_1' - \bar{x})/\sqrt{2}$. Probability distribution is then given as

$$P_{out}(y|\bar{x}) = \frac{1}{N(\bar{x})} P_{in}(y) P_{in}\left(y + \sqrt{2}\bar{x}\right)$$
(80)

and norm is then expressed as

$$N(\bar{x}) = \sqrt{2} \int_{-\infty}^{\infty} dy \ P_{in}(y) P_{in}\left(y + \sqrt{2}\bar{x}\right)$$
(81)

To understand the elementary recycling, output distribution can be redefined to $\tilde{P}_{out}(y|\bar{x})$ expressed as

$$\tilde{P}_{out}(y|\bar{x}) = P_{in}(y) F(y,\bar{x}), \quad F(y,\bar{x}) = \frac{P_{in}(y+\sqrt{2}\bar{x})}{N(\bar{x})}.$$
(82)

Recycling works like filter on probability distribution $P_{in}(y)$ with filtration function $F(y, \bar{x})$. Similar discussion was made in Ref. [19].

If we consider selection of measured coordinate \bar{x} from finite interval $[\bar{x}_{min}, \bar{x}_{max}]$, the output probability distribution is expressed as

$$\tilde{P}_{out}(x|\bar{x}) = \int_{x_{min}}^{x_{max}} d\bar{x} \ P_{in}\left(\frac{x-\bar{x}}{\sqrt{2}}\right) F\left(\frac{x-\bar{x}}{\sqrt{2}}, \bar{x}\right)$$
(83)

and norm changes to

$$N(\bar{x}) = \int_{-\infty}^{\infty} dx \int_{x_{min}}^{x_{max}} d\bar{x} \ P_{in}\left(\frac{x - \bar{x}}{\sqrt{2}}\right) F\left(\frac{x - \bar{x}}{\sqrt{2}}, \bar{x}\right). \tag{84}$$

Norm now represents success probability of this selective measurement.

If output distribution has more than one peak, optional single-copy Gaussian filter can be applied to separate one of the peaks and reach more squeezing. Two-copy recycling can be divided to universal ($\bar{x} = 0$) and non-universal protocol (\bar{x} optimized). These protocols will be studied now in particular.

5.1 Universal two-copy recycling

For universal two-copy recycling is used fixed protocol with $\bar{x} = 0$. The filtration function $F(y, \bar{x} = 0)$ is now just rescaled input state distribution $P_{in}(y)$ by norm $N(\bar{x} = 0)$. Condition for local maxima of probability distribution of output state

$$\frac{d}{dy}\tilde{P}_{out}(y|\bar{x}=0) = \frac{1}{N(\bar{x}=0)}\frac{d}{dy}P_{in}^{2}(y) = \frac{1}{N(\bar{x}=0)}2P_{in}(y)\frac{d}{dy}P_{in}(y)$$
(85)

is equivalent to $\frac{d}{dy}P_{in}(y)=0$ which implies that positions of conditional output distribution $\tilde{P}_{out}(y|\bar{x}=0)$ local maxima x_{out}^{max} are equal to positions of local maxima x_{in}^{max} of input distribution multiplied by $\sqrt{2}$ hence substitution $y=x_1'/\sqrt{2}$. It means that all local maxima are conserved after the transformation and they are just shifted further from origin [19]. Probability distribution less probable values are then suppressed by fitration Eq. (82) and probability distribution $\tilde{P}_{out}(y|\bar{x}=0)$ is peaked up around its global maxima. Due to its process, global maxima get higher and more separate and other local minima are suppressed. If the input state distribution has multiple-global

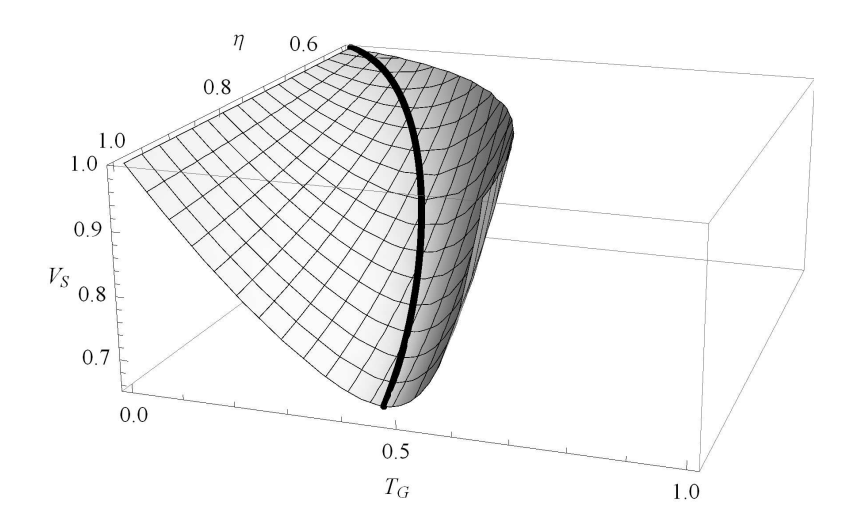


Fig. 10: Two-copy universal recycling from single-photon state after optional Gaussian filter: variance of squeezed quadrature with highlighted optimal squeezing (full-thick line).

maxima, they are conserved by this transformation and single-copy Gaussian filter has to be applied to pick-up one of the peaks. Moreover, relative concavity defined as

$$\frac{\frac{d^2}{dx^2}P(x)}{P(x)}\tag{86}$$

in points of local maxima of the distribution P(x) are conserved in process of two-copy universal recycling [19].

Two-copy universal recycling is a basic element of multi-copy universal recycling which will be discussed later. Therefore, mechanism of two-copy universal recycling is crucial for understanding the multi-copy recycling.

Attenuated single-photon state can be again used as the input resource state. After universal two-copy recycling output state probability distribution

$$P_{out}(x) = \frac{e^{-\frac{x^2}{2}} \left(\eta \left(x^2 - 2\right) + 2\right)^2}{\sqrt{2\pi} (4 - \eta(4 - 3\eta))}$$
(87)

of coordinate x is reached. Variance of quadrature \hat{x} is given as

$$V = \frac{\eta(7\eta + 4) + 4}{4 - \eta(4 - 3\eta)}. (88)$$

This variance is still higher than unity since it can be dominantly influenced by presence of two peaks. Universal single-copy Gaussian filter has to be used to extract squeezing. For $\eta < \frac{1}{3}$, probability distribution $P_{out}(x)$ has single global maximum in the origin and Gaussian filter can be directly applied to reach filtered distribution

$$P_{out,G}(x) = \frac{e^{-\frac{x^2}{2}} \left(\eta \left(T_G x^2 - 2\right) + 2\right)^2}{\sqrt{2\pi} \left(\eta^2 (4 - T_G (4 - 3T_G)) - 4\eta (2 - T_G) + 4\right)}$$
(89)

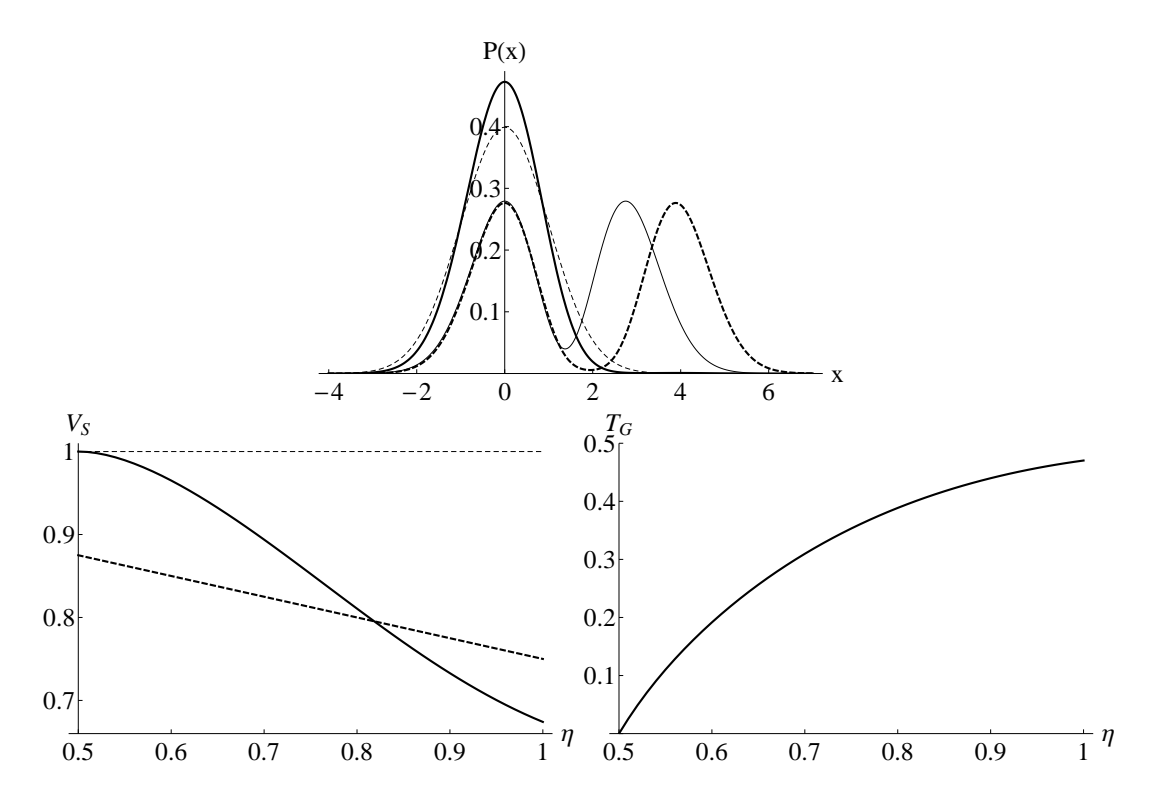


Fig. 11: Two-copy universal recycling from single-photon state after single-copy Gaussian filter: (top) for $\eta = 0.9$, squeezed quadrature probability distributions after filtration (full-thick) and before filtration (dashed-thick) are compared to probability distributions of initial state (full-thin) and vacuum state (dashed-thin). (Bottom-left) minimal variance V_S (full-thick) is compared to vacuum noise (dashed-thin). (Bottom-right) Optimal transmittance of single-copy filter to reach maximal squeezing.

with variance

$$V(x) = \frac{\eta(\eta(3T_G(5T_G - 4) + 4) + 12T_G - 8) + 4}{\eta^2(4 - T_G(4 - 3T_G)) - 4\eta(2 - T_G) + 4}$$
(90)

where T_G is transmittance of beam splitter in Gaussian filter. This filtered state still cannot exhibit any squeezing.

For $\eta > \frac{1}{3}$, the probability distribution $P_{out}(x)$ has two global maxima placed symmetrically around the origin in points $x_{out}^{max} = \pm \sqrt{\frac{6\eta-2}{\eta}}$. State have to be displaced that one of the maxima will be shifted to origin. This can be describe by substitution $x = x' - \sqrt{\frac{6\eta-2}{\eta}}$ and then universal single-copy Gaussian filter can be applied to pick up the peak in the origin and suppress the other one. Alternatively, we can consider displaced input state, which probability distribution in coordinate x has maxima in points $x_{in}^{max} = \pm \sqrt{\frac{3\eta-1}{\eta}}$.

Variance of filtered probability distribution is depicted in Fig. 10. Filtered state exhibits squeezing for $\eta > 0.5$. Numerically optimized variance and optimal transmittance T_G are depicted in Fig. 11. For $\eta > 0.82$, two-copy universal recycling can extract more squeezing from single-photon state than single-copy non-universal recycling (see

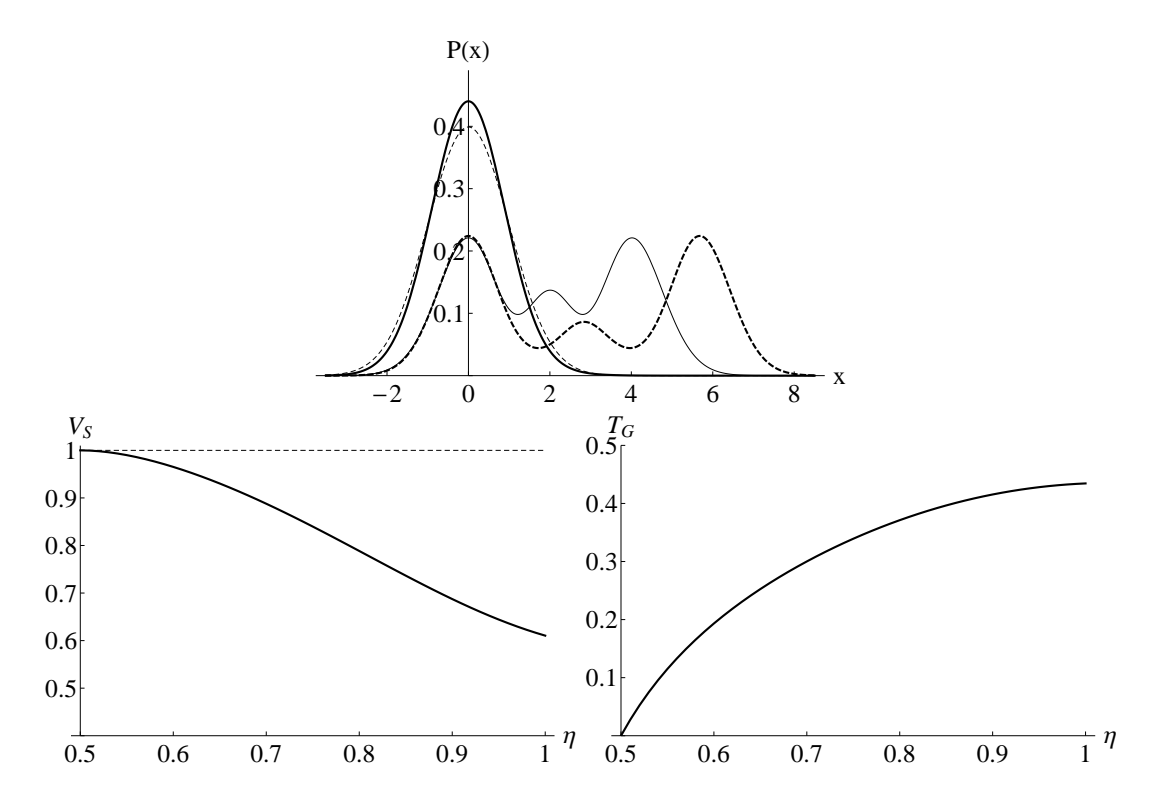


Fig. 12: Two-copy universal recycling from two-photon state after single-copy Gaussian filter extracting squeezing from wing peak: (top) for $\eta = 0.75$, squeezed quadrature probability distributions after filtration (full-thick) and before filtration (dashed-thick) are compared to probability distributions of initial state (full-thin) and vacuum state (dashed-thin). (Bottom-left) minimal variance V_S (full-thick) is compared to vacuum noise (dashed-thin). (Bottom-right) Optimal transmittance of single-copy filter to reach maximal squeezing.

Fig. 11). Displaced input state probability distribution with two peaks is spread by universal two-copy recycling but relative concavity around the global maxima is conserved. Both peaks of the recycled distribution still have the same height. Single-copy filter is used to suppress one of the peaks and raise the other. The recycled distribution then has smaller variance than vacuum state probability distribution of coordinate (see Fig. 11).

To observe behavior for more complex distribution P(x), we consider attenuated two-photon state as the input state again. Probability distribution of coordinate x is given as

$$P_{out}(x) = \frac{e^{-\frac{x^2}{2}} \left(8\eta \left(x^2 - 2\right) + \eta^2 \left(x^4 - 12x^2 + 12\right) + 8\right)^2}{\sqrt{2\pi} \left(\eta \left(15\eta \left(\eta \left(7\eta - 16\right) + 16\right) - 128\right) + 64\right)}$$
(91)

after two-copy recycling. Variance is expressed as

$$V(x) = \frac{\eta(\eta(3\eta(75\eta - 112) + 304) + 128) + 64}{\eta(15\eta(\eta(7\eta - 16) + 16) - 128) + 64}.$$
(92)

This state cannot exhibit squeezing and optional universal single-copy filter has to be

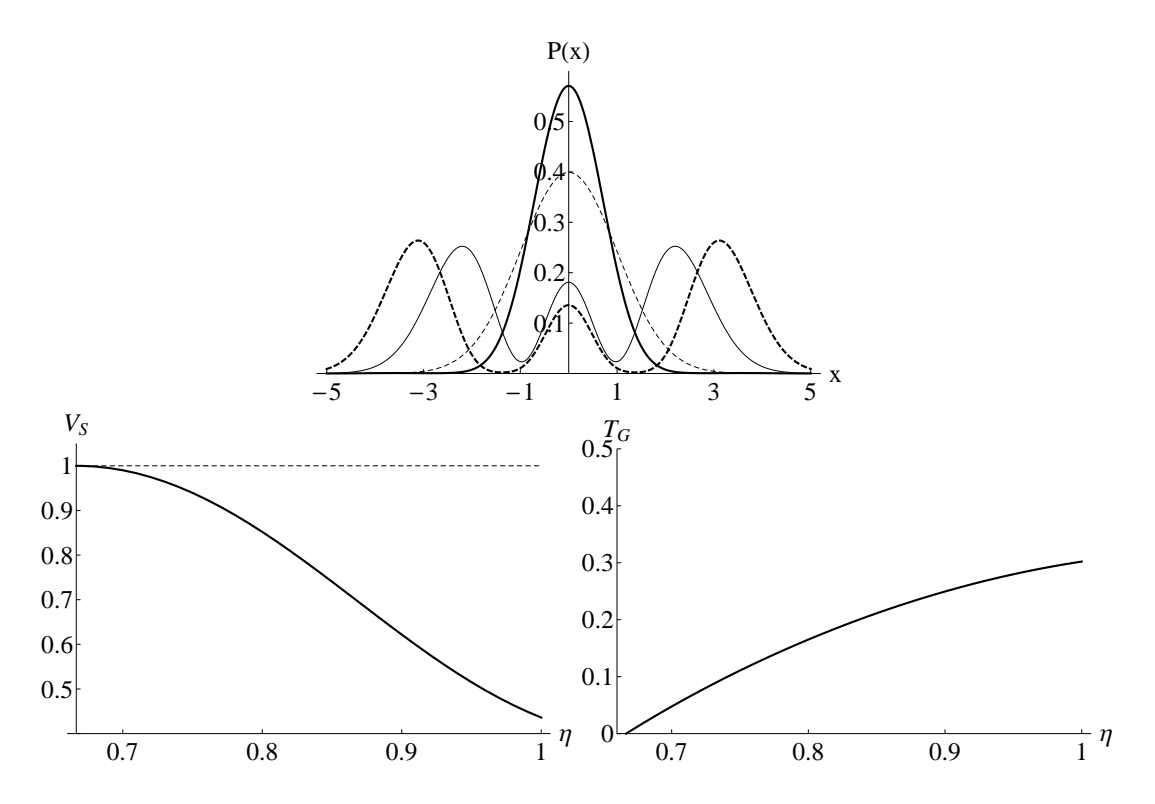


Fig. 13: Two-copy universal recycling from two-photon state after single-copy Gaussian filter extracting squeezing from central peak: (top) for $\eta=0.95$, squeezed quadrature probability distributions after filtration (full-thick) and before filtration (dashed-thick) are compared to probability distributions of initial state (full-thin) and vacuum state (dashed-thin). (Bottom-left) minimal variance V_S (full-thick) is compared to minimal variance extracted by single-copy non-universal recycling from single-photon state (dashed-thick) and to vacuum noise (dashed-thin). (Bottom-right) Optimal transmittance of single-copy filter to reach maximal squeezing.

applied. For $\eta < \frac{1}{15} \left(6 - \sqrt{6} \right) \approx 0.24$, probability distribution of two-photon state has single-global maximum in the origin and state does not have to be displaced before the filtration but in this case squeezing cannot be extracted even after the filtration. For $\eta > 0.24$, probability distribution has two global maxima placed symmetrically around the origin in points

$$x_{in}^{max} = \pm \sqrt{-\frac{-5\eta + \sqrt{2\eta(5\eta - 4) + 2} + 2}{\eta}}$$
 (93)

which are transformed by universal two-copy recycling to global maxima in points $x_{out}^{max} = \pm \sqrt{2} \ x_{in}^{max}$. One of the global maxima is displaced to origin before or after universal two-copy recycling and single-copy filtration is then applied. Filtered state variance of quadrature \hat{x} has to be optimized numerically for parameter T_G . Filtered state exhibits squeezing for $\eta > \frac{1}{2}$ like in the case of universal two-copy recycling from single-photon state. Numerically optimized variance and optimal transmittance T_G are depicted in Fig. 12. Displaced input state probability distribution with three peaks is

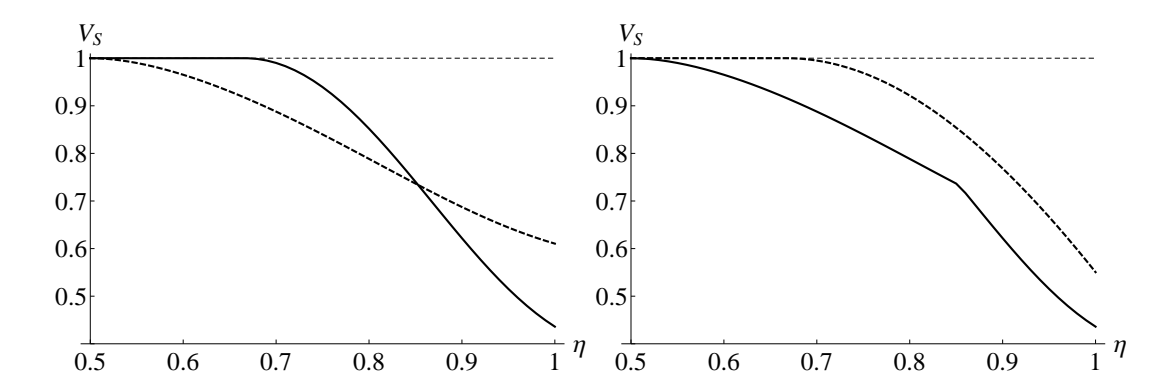


Fig. 14: Two-copy universal recycling from two-photon state after single-copy Gaussian filter: (left) minimal variance in quadrature \hat{x} extractable from central peak (full-thick) and from wing peak (dashed-thick) and vacuum noise (dashed-thin) are compared. (Right) comparison between recyclable variance by two-copy universal recycling (full-thick) and by single-copy universal recycling (dashed-thick) and vacuum noise (dashed-thin) is shown.

spread by universal two-copy recycling and relative concavity around all three maxima is conserved. Central local maximum is slightly suppressed but both side global maxima are insignificantly raised. It is example how the filtration differently affects the local and global maxima. Single-copy filter is used to raised wing peak in the origin and suppress the others. The recycled distribution has smaller variance than vacuum state probability distribution of coordinate (see Fig. 12). Squeezing is now recycled from wing peak of the distribution.

Moreover for $\eta > \frac{1}{15} \left(6 + \sqrt{6} \right) \approx 0.56$, probability distribution of two-photon state has local maximum in the origin. Squeezing can be extracted from it after single-copy filtration. Filtered state variance of quadrature \hat{x} have to be optimized numerically for parameter T_G again. Filtered state exhibits squeezing for $\eta > \frac{2}{3}$ like in the case of universal single-copy recycling from two-photon state. Numerically optimized variance and optimal transmittance T_G are depicted in Fig. 13. Evolution of probability distribution depicted in Fig. 13 is very similar to the former case depicted in Fig. 12. The only difference is that single-copy filter is used to raised central peak and suppress both wing peaks. Squeezing is now recycled from central peak of the distribution.

We have to compare squeezing extracted from central and side maxima to reach maximal squeezing for given η (see Fig. 14). For $\eta > 0.85$, squeezing recycled from center maximum is better than from wing maximum and for $\eta < 0.85$ otherwise. Two-copy universal recycling can extract more squeezing than single-copy one for every $\eta > \frac{1}{2}$ (see Fig. 14).

In this section, properties of universal recycling from two input state copies were demonstrated. Universal two-copy recycling from single-photon state can extract squeezing unlike single-copy one but single-copy Gaussian filter is needed. If we use two-photon state as input state, universal two-copy recycling can extract more squeezing than single-copy one which suggest that extractable squeezing increase with number of input state copies and it is motivation for multi-copy recycling discussed bellow.

5.2 Non-universal two-copy recycling

In the case of two-copy non-universal recycling, filtration function $F(y, \bar{x})$ from Eq. (82) is no longer fixed like in universal recycling and it is optimized over measured coordinate \bar{x} for particular input state. Transformation does not conserve positions of local maxima. Single-copy Gaussian filter is not needed in this case because one peak probability distribution can be extracted by filtration function $F(y,\bar{x})$. The output distribution $\tilde{P}_{out}(y|\bar{x})$ exhibits always global maximum if $|\bar{x}|$ increases, however, the distribution has tendency to converge to vacuum state. We therefore have to optimize the choice of \bar{x} to reach minimal variance.

We again consider single-photon state as the input state. Recycled probability distribution of coordinate x is given as

$$P(x|\bar{x}) = \frac{e^{-\frac{x^2}{2}} \left(-2\eta x^2 \left(\eta \left(\bar{x}^2 + 2\right) - 2\right) + \left(\eta \left(\bar{x}^2 - 2\right) + 2\right)^2 + \eta^2 x^4\right)}{\sqrt{2\pi} \left(\eta^2 \left(\bar{x}^4 - 6\bar{x}^2 + 3\right) + 4\eta \left(\bar{x}^2 - 1\right) + 4\right)}$$
(94)

and variance in x depicted in Fig. 15 is expressed as

$$V_S(\bar{x}) = 1 + \frac{4\eta(2 + \eta - \eta\bar{x}^2)}{4 + \eta(3\eta - 4 + 2(2 - 3\eta)\bar{x}^2 + \eta\bar{x}^4)}.$$
 (95)

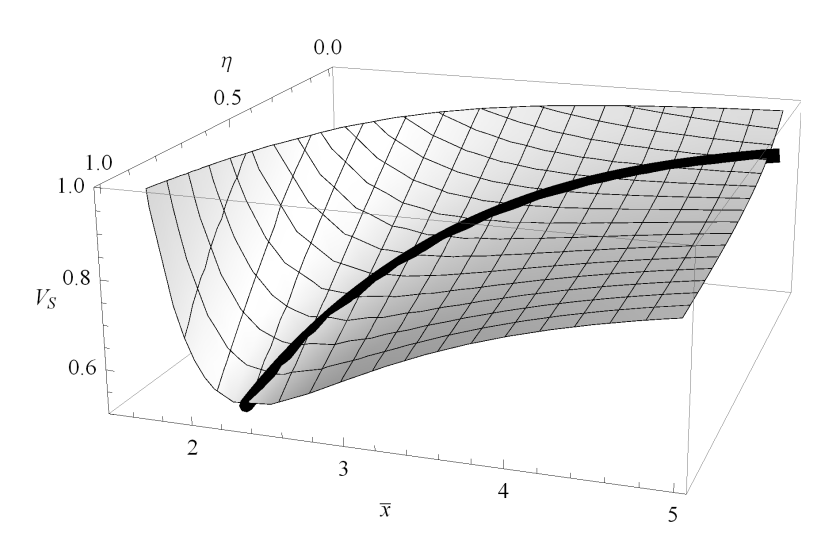


Fig. 15: Two-copy non-universal recycling from single-photon state: variance of squeezed quadrature \hat{x} with highlighted optimal squeezing (full-thick line).

Selecting measured values from narrow interval around $\bar{x}_{opt} = \sqrt{1 + \frac{2+\sqrt{2}\sqrt{8-\eta(4+\eta)}}{\eta}}$ is optimal. For $\eta = 0.5$ and $\eta = 1$, two-peak input state probability distribution is transformed by optimal recycling to one-peak distribution which has smaller variance than vacuum state probability distribution of coordinate (see Fig. 16). Evolution of probability distribution is difficult because of non-universality of Gaussian filter. Recycled distribution always has dominant central peak in the origin because of the symmetric

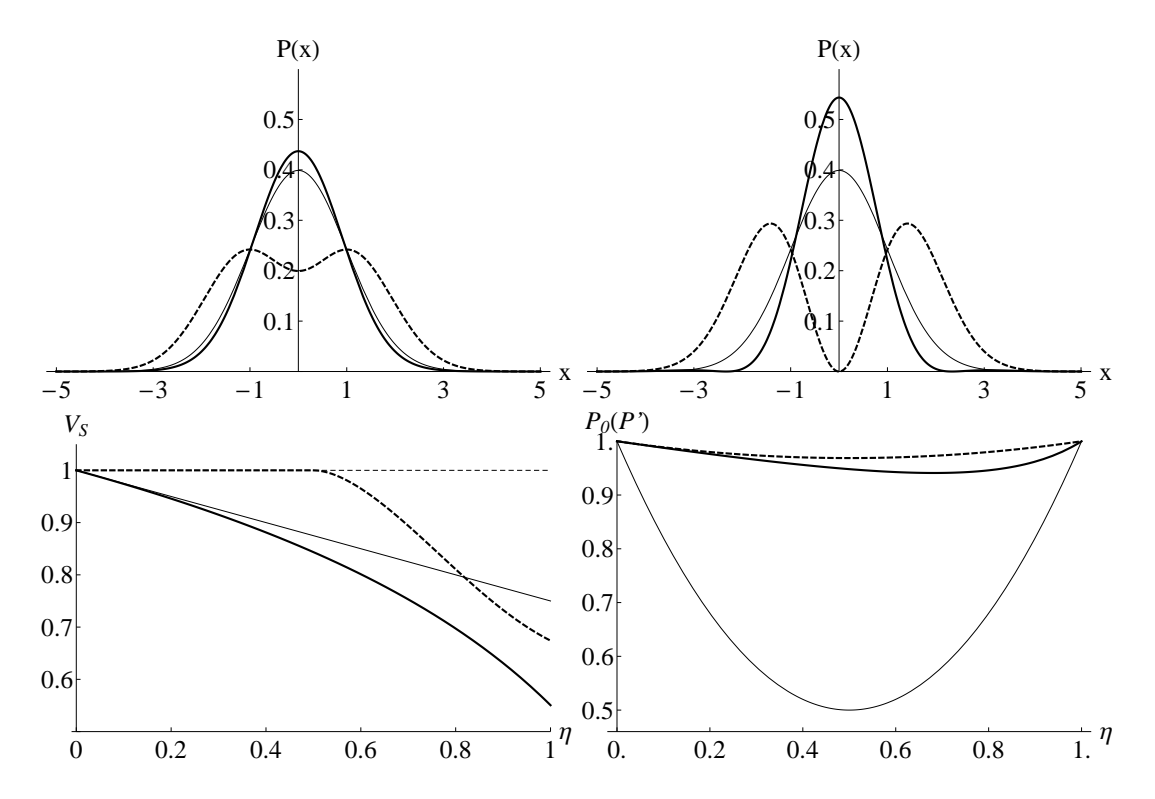


Fig. 16: Two-copy non-universal squeezing recycling from single-photon state: recycled state probability distribution of squeezed quadrature (full-thick) for $\eta=0.5$ (top-left) and $\eta=1$ (top-right) compared to input state probability distribution (dashed-thick) and vacuum state probability distribution (full-thin). (Bottom-left) the variances V_S of squeezed quadrature for non-universal two-copy recycling (full-thick) and for universal two-copy recycling (dashed-thick) and for non-universal single-copy recycling (full-thin) are compared to vacuum noise (dashed-thin). (Bottom-Right) purity of the recycled state (full-thick) compared to purity of input state (full-thin) and to purity of state after single-copy recycling (dashed-thick).

interference of input state copies. For $\eta > 0.92$, the recycled distribution has two negligible side peaks which vanish for smaller η and the recycled distribution then has single peak. Variance in coordinate for optimal measurement reaches

$$V_S = \frac{5\eta - 8 + \sqrt{2}\sqrt{8 - \eta(4 + \eta)}}{(3\eta - 4)}. (96)$$

Probability distribution of squeezed quadrature after optimal recycling is depicted in Fig. 16. Clearly, $V_S < 1$ for any $\eta > 0$. For $\eta = 1$, we reach variance $V_S = 3 - \sqrt{6} \approx 0.55$ like in the case of single-copy recycling from two-photon state. For $\eta = 0.5$, the variance increases to $V_S \approx 0.84$. From the Fig. 16(bottom-right), it is evident that two-copy recycling produces more squeezing than single-copy method dominantly for $\eta > 0.5$, an improvement for $\eta \leq 0.5$ is rather moderate. For every $\eta > 0$, non-universal two-copy recycling extracts more squeezing than universal one (see Fig. 16).

Heterodyne detection can be used instead of homodyne detection again. If we

consider generally unbalanced heterodyne detection with transmittance T and post-selecting measured values from narrow intervals around \bar{x} and \bar{p} . Value $\bar{p} = 0$ is optimal to reach squeezing in quadrature \hat{x} which can be verify numerically. If we measure momentum very close to zero, variance in coordinate is expressed as

$$V_S = \frac{\left(T\left(T\left(\bar{x}^2 - 2\right)^2 - 6\bar{x}^2 + 4\right) - 1\right)\eta^2 + 4\left(T\bar{x}^2 + 1\right)\eta + 4}{\left(T^2\left(\bar{x}^2 - 2\right)^2 - 2T\left(\bar{x}^2 + 2\right) + 3\right)\eta^2 + 4\left(T\bar{x}^2 - 1\right)\eta + 4}$$
(97)

which attain minimum for

$$\bar{x}_{opt} = \sqrt{2 + \frac{2 - \eta + \sqrt{\eta^2 (6 - 8T) + 8\eta (T - 2) + 16}}{\eta T}}.$$
(98)

Global minimum of V_S is in limit $T \to 0$ which means very weak measurement of coordinate. Variance then reads

$$V_S = -\frac{\sqrt{2}\sqrt{3\eta^2 - 8\eta + 8 + \eta - 4}}{\eta}. (99)$$

Squeezing extracted by recycling with heterodyne detection is slightly better than squeezing extracted by recycling with homodyne detection for every $0 < \eta < 1$ (see Fig. 17). This improvement comes from non-factorable form of Wigner function $W(x,p) \neq W(x)W(p)$ of single-photon states. However, ideal projective measurement to superposition $\alpha|0\rangle + \beta|2\rangle$ used for two-copy recycling extracts significantly more squeezing than homodyne or heterodyne detection for every $0 < \eta < 1$. It will be discussed in detail in Section 7.5. Interestingly, extractable squeezing from pure single-photon state is the same for all detectors discussed here and minimal squeezed quadrature variance is still $V_S = 0.55$.

We will discussed now other properties of state extracted by two-copy recycling with homodyne detector. The interference of the single photons does not require phase stability, however, the phase-sensitive homodyne measurement determines the quadrature where the squeezing can be observed. The complementary quadrature exhibits a noise with the variance

$$V_A = \frac{32 + \eta(\eta^2 - 24 - \eta\sqrt{2}\sqrt{8 - \eta(4 + \eta)})}{(4 - 3\eta)(8 - \eta(4 + \eta))}$$
(100)

being below $V_A = 2\eta + 1$ of the initial state. Also here we observe the purification effect, due to non-factorability of position and momentum in the Wigner function of attenuated single-photon state (see Fig. 16).

Similarly as in the case of single-copy recycling measuring \bar{x} from finite interval is used to count success probability P_S which is equal to norm of the output probability distribution $N(\bar{x})$ given by formula Eq. (84). Measuring $\bar{x} \in [\bar{x}_{opt} - \delta, \bar{x}_{opt} + \delta]$ is optimal for two-copy recycling where \bar{x}_{opt} is given as optimal coordinate for measuring values from narrow interval expressed above. Trade-off between V_S versus P_S compared to single-copy recycling is depicted in Fig. 18. For $\eta = 0.3$, squeezing is reached

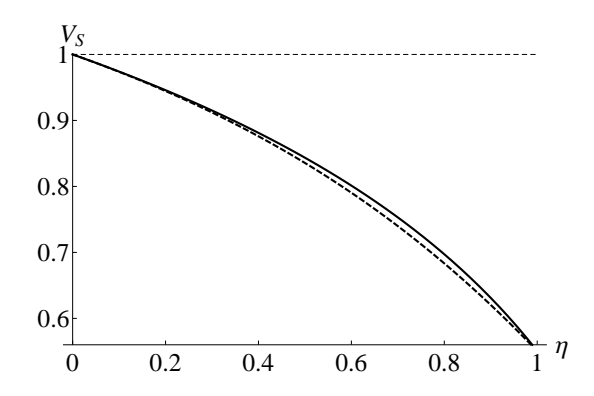


Fig. 17: Two-copy recycling from single-photon state: squeezed quadrature variances of state recycled by protocol with homodyne detector (full-thick) and heterodyne detector (dashed-thick) and vacuum noise (dashed-thin) are compared.

if $P_S < 2.64\%$. For $\eta = 0.5$, squeezing is reached if $P_S < 10.75\%$. For $\eta = 0.9$, squeezing is reached if $P_S < 24.60\%$. For two-copy recycling, squeezed quadrature variance converges faster to limit value with decreasing success probability than for single-copy recycling.

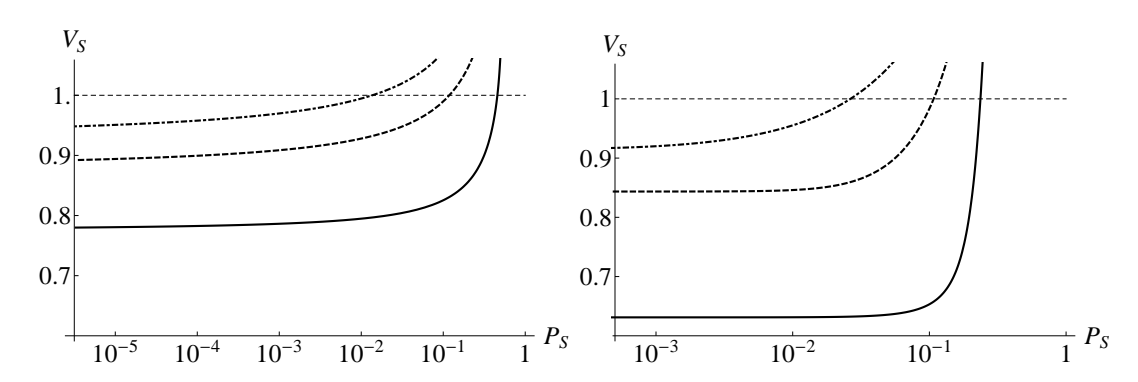


Fig. 18: Single-copy (left) and two-copy (right) non-universal squeezing recycling success probability versus achieved squeezing: the variance V_S for $\eta = 0.3$ (dot-dashed-thick) and for $\eta = 0.5$ (full-thick) and for $\eta = 0.9$ (dashed-thick) compared to vacuum noise (dashed).

Two-photon state will be considered last time as the input state to visualize behavior for higher Fock states. Output state probability distribution of coordinate x can always exhibit one peak character for \bar{x} large enough (see Fig. 19). Variance of squeezed quadrature has to be minimize numerically. Optimal measured coordinate \bar{x}_{opt} is depicted in Fig. 19. Two-peak input state probability distribution for $\eta = 0.5$ and three-peak input state probability distribution for $\eta = 0.9$ are transformed by optimal recycling to recycled distribution with dominant central peak which is narrower than vacuum state probability distribution of coordinate (see Fig. 19). Evolution of probability distribution through recycling is the same as in the case of non-universal two-copy recycling from single-photon state depicted in Fig. 16. Non-universal two-copy recycling can extract more squeezing than single-copy recycling for every $\eta > 0$

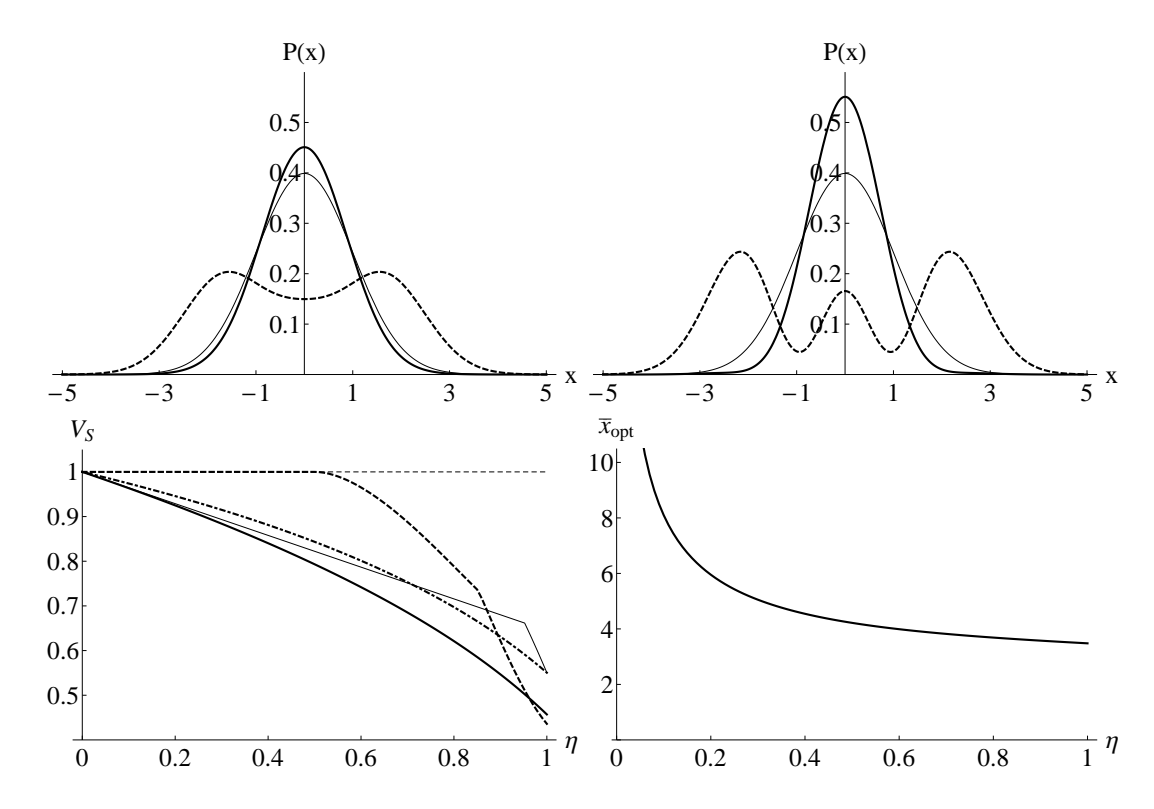


Fig. 19: Two-copy non-universal squeezing recycling from two-photon state: recycled state probability distribution of squeezed quadrature (full-thick) for $\eta=0.5$ (top-left) and $\eta=0.9$ (top-right) compared to input state probability distribution (dashed-thick) and vacuum state probability distribution (full-thin). (Bottom-left) the variances V_S of squeezed quadrature for two-copy non-universal recycling from two-photon state (full-thick) and for two-copy non-universal recycling from single-photon state (dotted-dashed-thick) and for two-copy universal recycling from two-photon state (dashed-thick) and for single-copy non-universal recycling from two-photon state (full-thin) and for vacuum state (dashed-thin) are compared. (Bottom-right) optimal measured coordinate \bar{x}_{opt} for two-copy non-universal recycling from two-photon state.

(see Fig. 19). More squeezing can be extracted from two-photon state than from single-photon state for every $\eta>0$ (see Fig. 19). For $\eta<0.962$, non-universal two-copy recycling can extract more squeezing than universal one and for $\eta>0.962$ otherwise (see Fig. 19) like in the case of single-copy recycling which show that for two-photon state with high purity universal protocols are better than non-universal ones.

Non-universal two-copy recycling can extract more squeezing than single-copy recycling for every $\eta > 0$ and for both single-photon and two-photon states as the input states. Moreover, non-universal two-copy recycling can extract more squeezing from single-photon than universal one. In the case of two-photon state, situation is more difficult and universal squeezing is better for states with high purity.

6 Multi-copy Gaussian recycling

6.1 Tree-structure multi-copy Gaussian recycling

We have $N = 2^k$, where $k \in \mathbb{N}$, copies of input quantum state $\hat{\rho}_{in}$ with the probability distributions $P(x_i)$ of a generalized positions x_i , where i = 1, ..., N. Particularly, attenuated single-photon states are taken as $\hat{\rho}_{in}$ but the setup is general and it does not matter on particular $\hat{\rho}_{in}$. Linear-optical implementation of general Gaussian recycling protocol for quantum states of light is schematically depicted in Fig. 20.

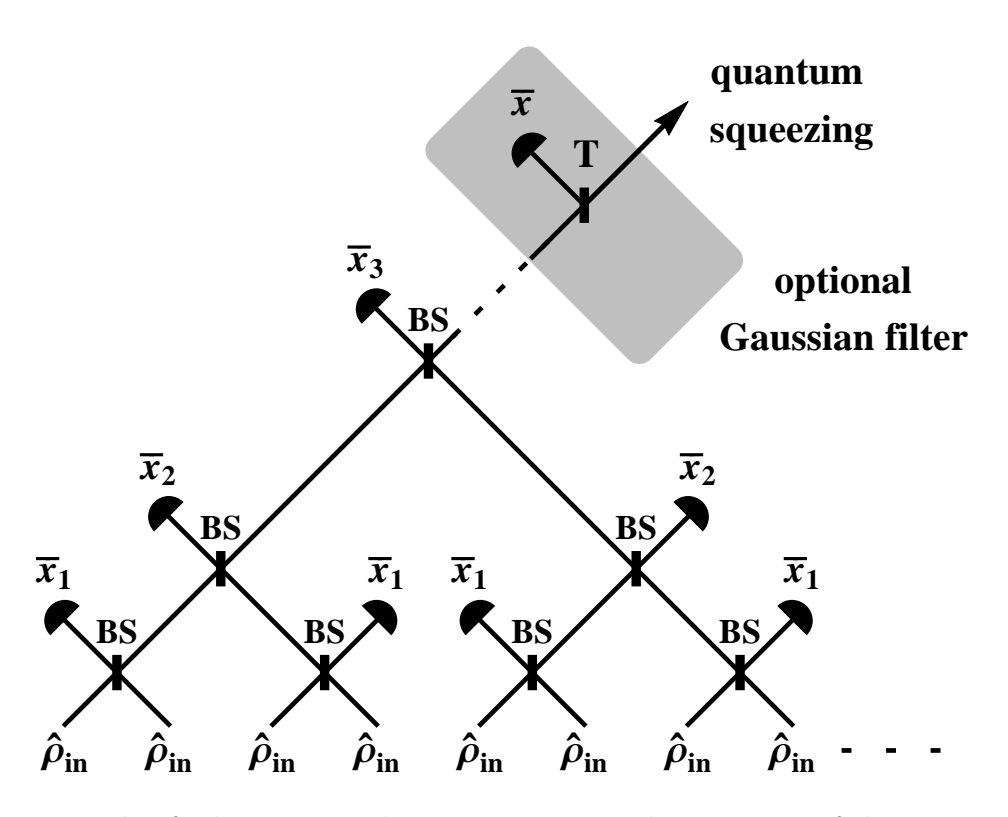


Fig. 20: Example of a linear optical tree-structure implementation of the non-universal recycling of $N=2^n$ wasted states with the probability distribution $P_{in}(x)$ of the generalized position: symmetric beam splitters with transmittance $T_{BS}=0.5$ and homodyne detectors measuring coordinates \bar{x}_i , $i=1,\ldots,n$ are used. Optional single-copy Gaussian filter is composed of beam splitter with transmittance T and homodyne detector measuring coordinate from narrow interval around $\bar{x}=0$.

It is based on a network consisting from the symmetrical beam splitters (BS) and projective measurement of the generalized coordinate \bar{x}_j , $j=1,\ldots,k$, which can be represented by homodyne detectors for linear-optic implementation. On the symmetric beam splitter two coordinates x_1 and x_2 are combined to produce coupled output coordinates $x'_1 = (x_1 + x_2)/\sqrt{2}$ and $x'_2 = (x_2 - x_1)/\sqrt{2}$. Choice of measured coordinates can be made to reach squeezing. Optimally, we can use single-copy quantum Gaussian filters at the end of the protocol. This set up can be easily transformed to another experimental platform. We proved that heterodyne detection is producing slightly more

squeezing than homodyne measurement. However, in the following calculations we use only homodyne detection since it gives simpler analysis and generates almost optimal amount of squeezing.

6.2 Linear-structure multi-copy Gaussian recycling

To reduce complexity of multi-mode interference effects exhibiting in the tree-structure multi-copy recycling, we consider linear-structure multi-copy recycling which uses $N \in$ N copies of input quantum state $\hat{\rho}_{in}$. Structure of this protocol is depicted in Fig 21. Single-copy Gaussian filter is applied if state coordinate probability distribution has multiple global maxima.

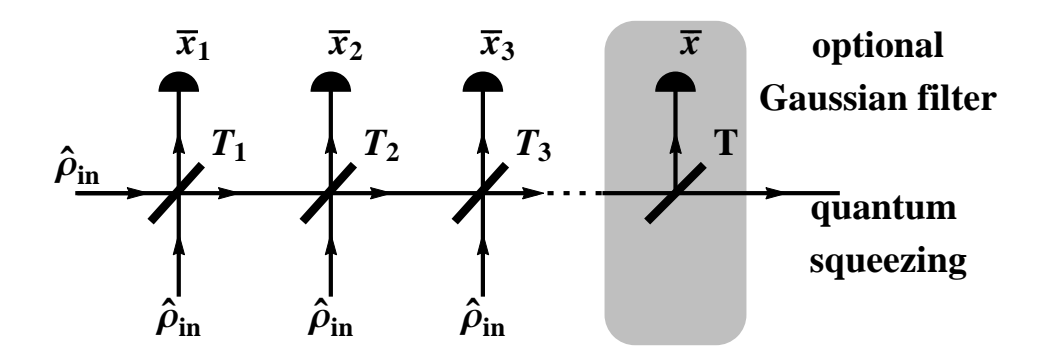


Fig. 21: Example of a linear optical linear-structure implementation of the non-universal recycling of N=2 states with the probability distribution $P_{in}(x)$ of the generalized position: beam splitters with transmittances $T_i = \frac{i}{i+1}$ and homodyne detectors measuring coordinates \bar{x}_i , $i=1,\ldots,N-1$ are used. Optional single-copy Gaussian filter is composed of beam splitter with transmittance T and homodyne detector measuring coordinate from narrow interval around $\bar{x}=0$.

6.3 Universal multi-copy recycling

Universal recycling follows same recipe for every input state. It is therefore the method to universally extracts squeezing from any state. Choice of measured values \bar{x}_j does not depend on particular input probability distribution. For both multi-copy structures we can implement universal recycling by considering $\bar{x}_j = 0$ [19]. Protocols combine N copies into the output distribution $P_{out}(x) \propto \left[P_{in}\left(\frac{x}{\sqrt{N}}\right)\right]^N$, which can be filtered by single-copy filter to a distribution with the variance

$$V_S = \frac{P_{in}(x_{max})}{|P''_{in}(x_{max})|},\tag{101}$$

where x_{max} is a position of a global maximum of $P_{in}(x)$. The initial displacement of all the states is irrelevant for the variance Eq. (101), the output distribution will be only shifted. If $P_{in}(x)$ has single global maximum, then asymptotical variance directly

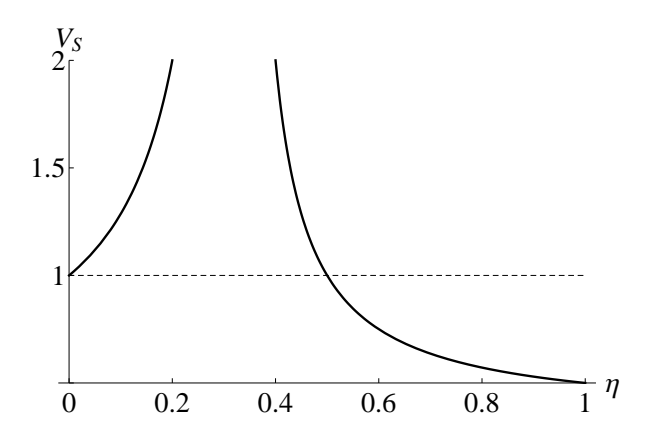


Fig. 22: Variance V_S produced by universal recycling as a function of η (full line) compared to vacuum noise (dashed line).

approaches V_S . If the distribution $P_{in}(x)$ has optionally more than single global maximum, the variance of $P_{out}(x)$ can be still very large. The variance V_S can be approached if the single-copy filtration depicted in the Fig. 21 is applied to isolate a single global maximum. Moreover, the relative concavity defined as

$$\frac{P''(x)}{P(x)} \tag{102}$$

in the point of global maximum of probability distribution is invariant of universal recycling [19]. It means than relative concavity in the point of global maximum of probability distribution is the same after each universal step in multi-copy recycling. From Ref. [19], for attenuated single-photon state with $\eta < \frac{1}{3}$ the universal recycling produce state with variance

$$V_S = \frac{1 - \eta}{|3\eta - 1|} \ge 1. \tag{103}$$

For $\eta > \frac{1}{3}$, single-photon state has two global maxima. If one of the global maxima is shifted to origin and universal single-copy recycling is applied after universal recycling, minimal variance reads

$$V_S = \frac{\eta}{|3\eta - 1|}. (104)$$

Formulas Eq. (103) and Eq. (104) can be derived from (101) and they are numerically verified for large N. Squeezing is reached only for $\eta > \frac{1}{2}$. The squeezing is limited and for the non-classical states with positive Wigner function is not achievable. The variance V_S from Eq. (103) and Eq. (104) is depicted in Fig. 22. To demonstrate properties of this method marginal probability density P(x) before and after single-copy filtration is depicted in Fig. 23 (top). At first, two-peak input state probability distribution is spread by universal recycling but relative concavity near both global maxima is conserved. Both global maxima still have the same height. Single-copy filter is then used to suppress the peak far from the origin and raised the one in the origin. Recycled probability distribution is narrower than vacuum state probability

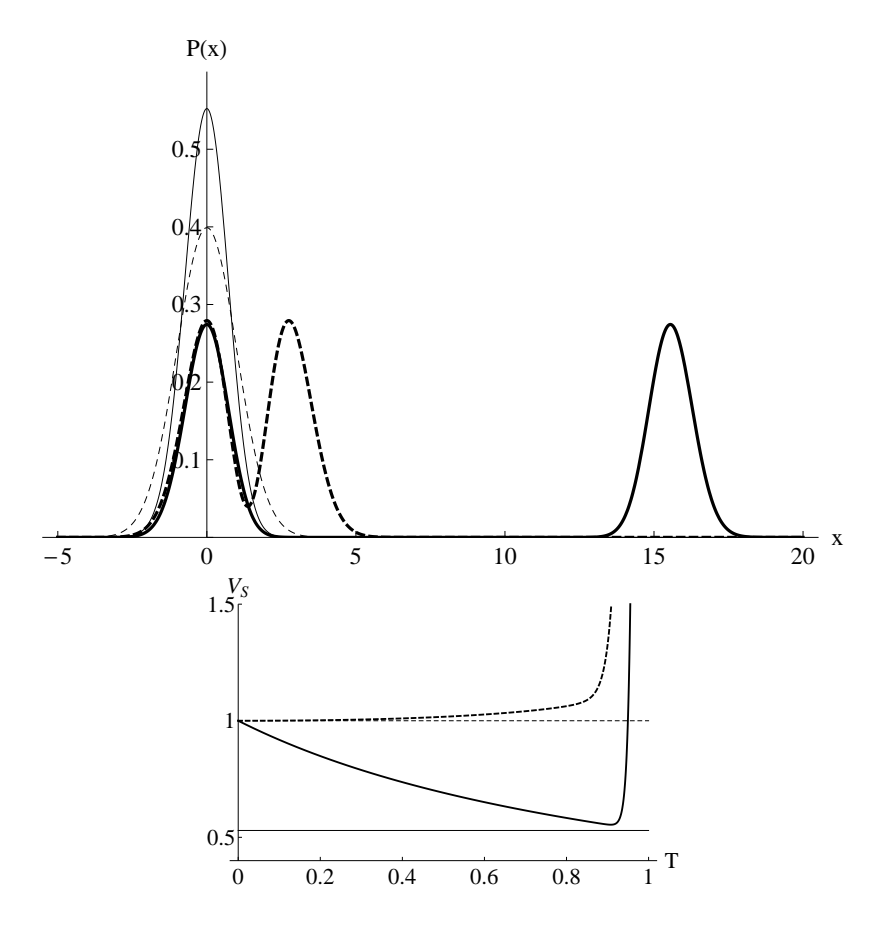


Fig. 23: Universal multi-copy squeezing recycling from displaced single-photon state with optional universal single-copy filter with transmittance T. (Top) for $\eta=0.9$: initial displaced state (dashed-thick), recycled state for N=32 before single-copy filtration (full-thick) and after single-copy filtration for T=0.912 (full-thin) compared to vacuum state (dashed-thin). (Bottom) variance V_S of squeezing as the function of transmittance of beam splitter and number of copies N=32: after recycling $\eta=0.9$ (full-thick), prediction of formula Eq. (104) (full-thin), after recycling $\eta=0.5$ (dashed-thick), variance of vacuum noise (dashed-thin).

distribution of coordinate. Variance after universal recycling and universal single-copy filtration is compared to Eq. (104) in Fig. 23 (bottom).

Similarly as for recycling from two copies squeezing can be extracted for universal multi-copy recycling but only in combination with single-copy Gaussian filter where transmittance T have to be optimized. Moreover, squeezing is reachable just for $\eta > 0.5$ in contrast to any non-universal method discussed above which can extract squeezing for every $\eta > 0$. Minimal variance extractable from pure single-photon state is just $V_S = 0.5$. There is still need for seeking better recycling strategies.

6.4 Single-layer partially-universal multi-copy recycling

Before fully non-universal recycling partially-universal Gaussian recycling is analyzed. Our main motivation is to realize from how can non-universal method extract squeezing differently to universal one. Partially-universal method use tree-structure protocol (see Fig. 20) with optimized non-zero measured position \bar{x}_1 in first layer followed by the universal part with all others values $\bar{x}_2, \ldots, \bar{x}_n = 0$. For the output distribution

$$P_{out}(x|\bar{x}) \propto \left[P_{in} \left(\frac{x/\sqrt{M} - \bar{x}_1}{\sqrt{2}} \right) P_{in} \left(\frac{x/\sqrt{M} + \bar{x}_1}{\sqrt{2}} \right) \right]^M,$$
 (105)

where M=N/2 is number of copies entering the universal part of the recycling. The achievable variance for limit of large number of input state copies can be derived from Eq. (105) and expressed as

$$\frac{1}{V_S(\bar{x}_1)} = \frac{\frac{d^2}{dx^2} \left[P_{in} \left(\frac{x - \bar{x}_1}{\sqrt{2}} \right) P_{in} \left(\frac{x + \bar{x}_1}{\sqrt{2}} \right) \right]_{x = x'_{max}}}{P_{in} \left(\frac{x - \bar{x}_1}{\sqrt{2}} \right)_{x = x_{max}} P_{in} \left(\frac{x + \bar{x}_1}{\sqrt{2}} \right)_{x = x_{max}}}, \tag{106}$$

where x_{max} is position of global maximum of the distribution

$$P_1(x|\bar{x}_1) \propto P_{in} \left(\frac{x - \bar{x}_1}{\sqrt{2}}\right) P_{in} \left(\frac{x + \bar{x}_1}{\sqrt{2}}\right)$$
 (107)

after first non-universal layer of the recycling and \bar{x}_1 is optimized. The recycled variance $V_S(\bar{x}_1)$ can be further given as

$$\frac{1}{V_{S}(\bar{x}_{1})} = \frac{1}{2} \left| \frac{P_{in}''(y)}{P_{in}(y)} \right|_{y = \frac{x_{max} + \bar{x}_{1}}{\sqrt{2}}} + \frac{P_{in}''(y)}{P_{in}(y)} \Big|_{y = \frac{x_{max} - \bar{x}_{1}}{\sqrt{2}}} + \frac{2P_{in}'(y)}{P_{in}(y)} \Big|_{y = \frac{x_{max} + \bar{x}_{1}}{\sqrt{2}}} \frac{P_{in}'(y)}{P_{in}(y)} \Big|_{y = \frac{x_{max} - \bar{x}_{1}}{\sqrt{2}}} \right|.$$
(108)

The reachable variance after the universal part recycling does not depend on the displacement of distribution $P_{in}(x)$ for the limit of large number of copies.

We can consider that global maximum of the distributions $P_1(x|\bar{x}_1)$ before the universal recycling is shifted to the origin and then we simply get $x_{max} = 0$. The formula Eq. (108) is then simplified. Global maximum of the distribution remains in origin after universal procedure and in the case of multiple global maxima the universal single-copy filtration can be used to extract the single peak and reach the minimal variance expressed as

$$\frac{1}{V_S(\bar{x}_1)} = \frac{1}{2} \left| \frac{P_{in}''(y)}{P_{in}(y)} \right|_{y = \frac{\bar{x}_1}{\sqrt{2}}} + \frac{P_{in}''(y)}{P_{in}(y)} \bigg|_{y = -\frac{\bar{x}_1}{\sqrt{2}}} + 2 \left(\frac{P_{in}'(y)}{P_{in}(y)} \bigg|_{y = \frac{\bar{x}_1}{\sqrt{2}}} \right) \left(\frac{P_{in}'(y)}{P_{in}(y)} \bigg|_{y = -\frac{\bar{x}_1}{\sqrt{2}}} \right) \right|.$$
(109)

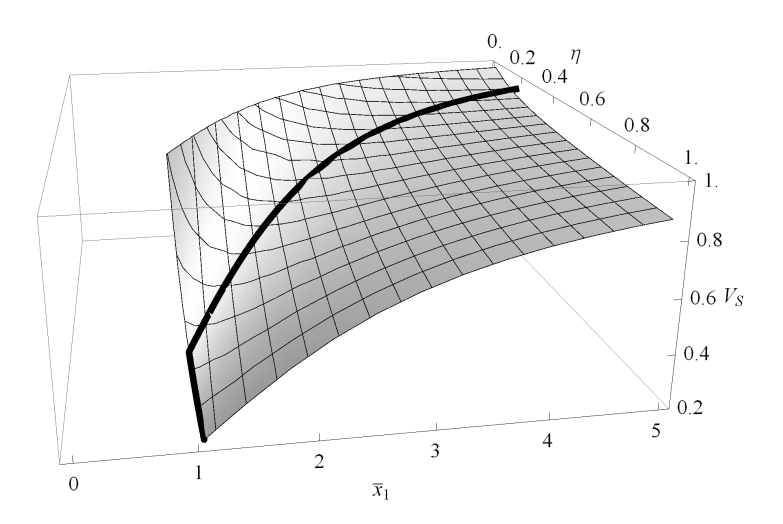


Fig. 24: Variance of squeezed coordinate after single-layer partially-universal multi-copy recycling from single-photon state for global maximum in origin after first non-universal layer given by Eq. (113). Full thick line shows optimal measurement.

The variance $V_S(\bar{x}_1)$ is achieved from an average of the relative concavity $\frac{P''_{in}(y)}{P_{in}(y)}$ in points $\pm \frac{\bar{x}_1}{\sqrt{2}}$ and the product of the relative steepness $\frac{P'_{in}(y)}{P_{in}(y)}$ taken in that points $\pm \frac{\bar{x}_1}{\sqrt{2}}$. For the universal Gaussian recycling, the relative concavity has been only the resource of squeezing. The signs of relative concavity and relative steepness strongly depend on the choice of \bar{x} . Note, relative concavity and relative steepness are features of input state distribution on the other hand global maximum position x_{max} is feature of distribution of the state after first non-universal layer. We newly extract the non-classicality hidden in a relatively steepness of $P_{in}(x)$ distribution, by using the partially-universal approach.

If attenuated single-photon state is used as $\hat{\rho}_{in}$, state with density probability distribution in coordinate x

$$P_1(x|\bar{x}_1) = \frac{e^{-\frac{x^2}{2}} \left(\eta^2 x^4 + (4\eta - 4\eta^2 - 2\eta^2 \bar{x}_1^2) x^2 + (2 - 2\eta + \eta \bar{x}_1^2)^2 \right)}{\sqrt{2\pi} \left(\eta^2 \bar{x}_1^4 + (-6\eta^2 + 4\eta) \bar{x}_1^2 + 3\eta^2 - 4\eta + 4 \right)}$$

is reached after first non-universal layer. Distribution multi-peak structure appearing for $\eta > \frac{1}{3}$ is vanishing by increasing \bar{x}_1 . For $\bar{x}_1 \to \infty$, the distribution converges to the vacuum state. To apply Eq. (109), the parameter \bar{x}_1 has to be therefore chosen that the global maximum will appear in the origin, not in the wings of the distribution. Higher squeezing can be recycled from maximum in the origin than from side maxima even if side maximum is shifted to origin and universal single-copy filter is applied. Local maximum

$$P_1(0) = \frac{1}{4} \exp\left(-\frac{\bar{x}_1^2}{2}\right) \left(2 + \eta(\bar{x}_1^2 - 2)\right)^2 \tag{110}$$

in the origin x = 0 has to be higher than maxima

$$P_{1}(x'_{max}) = 2 \exp\left(\frac{1}{\eta} - \bar{x}_{1}^{2} - 2 - \sqrt{1 - \frac{2(1-\eta)\bar{x}_{1}^{2}}{\eta}}\right) \times \eta^{2} \left(1 + \sqrt{1 - \frac{2(1-\eta)\bar{x}_{1}^{2}}{\eta}}\right)$$
(111)

in the points $\pm x'_{max}$ satisfying

$$x_{max}^{'2} = 4 - \frac{2}{\eta} + \bar{x}_1^2 + 2\sqrt{1 - \frac{2(1-\eta)\bar{x}_1^2}{\eta}}.$$
 (112)

For $\frac{1}{3} \leq \eta \leq \frac{2}{7}(3-\sqrt{2}) \approx 0.45$, \bar{x}_1 is lower bounded by $\bar{x}_{min}^2 = 2\sqrt{\frac{4-3\eta}{\eta}} - \frac{2}{\eta}$. For $\eta > \frac{2}{7}(3-\sqrt{2})$, lower bound \bar{x}_{min} is given by cross-section of the formulas Eq. (110) and Eq. (111) and numerical solution is depicted in Fig. 28 (top-right). Within that interval, \bar{x}_1 is optimized to reach minimal $V_S(\bar{x}_1)$. For $\eta = 0.9$, we need $\bar{x}_1 > 1.01$, for $\eta = 0.5$, we require $\bar{x}_1 > 0.7$ to have single global maximum (in the origin) and use Eq. (109). For $\bar{x}_1 > \bar{x}_{min}$, the variance (see Fig. 24) approaches

$$V_S(\bar{x}_1) = \frac{(2 + \eta(\bar{x}_1^2 - 2))^2}{4 + 4\eta(\bar{x}_1^2 - 4) + \eta^2(\bar{x}_1^4 + 12)}.$$
 (113)

If the value, of $\bar{x}_1 = \sqrt{\frac{6(1-\eta)}{\eta}}$ for which the minimum of Eq. (113) is achieved, lies in $\langle \bar{x}_{min}, \infty \rangle$ (see Fig. 28), the variance V_S can reach

$$V_S = \frac{4 - 4\eta}{4 - 3\eta}.\tag{114}$$

For $\eta=0.3$, depicted in Fig. 25, the lowest variance $V_S(\bar{x}_1)=0.903$ is approached for $\bar{x}_1=\sqrt{14}\approx 3.742$. For $\eta=0.5$, the lowest variance $V_S(\bar{x}_1)=\frac{4}{5}$ is approached for $\bar{x}_1=\sqrt{6}\approx 2.45$. For $\eta=0.9$, corresponding to the Fig. 26, we could reach $V_S(\bar{x}_{opt})=0.308$ from Eq. (113) but only for $\bar{x}_1=0.816$ which is, however, below $\bar{x}_{min}=1.01$. For the threshold value $\bar{x}_1=1.01$, we can reach $V_S=0.326$, which is fully corresponding to numerical results. For $\eta=1$, we could reach variance $V_S(\bar{x}_1)$ arbitrary small as \bar{x}_1 decreases, but we are limited by $\bar{x}_{min}=1.055$, which corresponds to $V_S=0.218$. When optimal measured position $\bar{x}_1=\sqrt{\frac{6(1-\eta)}{\eta}}$ lies in area where P_1 has central global maxima the squeezing recycled by nearly optimal method is the same as squeezing obtained from global optimization over all measured positions which will be analyzed later. Maximal value of η when it is satisfied can be reach as cross-section of optimal position $\bar{x}_1=\sqrt{\frac{6(1-\eta)}{\eta}}$ and boundary values which are depicted in Fig. 28. The maximal value is $\eta=0.86$.

Development of probability distribution is depicted in Fig. 25 and Fig. 26. For $\eta=0.3$, probability distributions after first layer for $\bar{x}_1=0$ and for optimal $\bar{x}_1=2.55$

are compared to vacuum noise probability distribution in Fig. 25 (top-left). Distributions after four other universal layers are compared again to vacuum noise probability distribution in Fig. 25 (top-right). For $\bar{x}_1=0$, all layers are universal and single-peak distribution is just spread and single peak is suppressed. However, for $\bar{x}_1=2.55$, distribution is raised and narrower than vacuum-state distribution even after first layer and the distribution is moderately raised by other universal layers. Similarly for $\eta=0.9$, probability distributions after first layer for $\bar{x}_1=0$ and for optimal $\bar{x}_1=2.55$ are compared to vacuum noise probability distribution in Fig. 26 (top-left). Distributions after four other universal layers are compared again to vacuum noise probability distribution in Fig. 26 (top-right). For $\bar{x}_1=0$, all layers are universal. The distribution still has two-peaks of the same height and the same relative concavity and the distribution is just spread. For $\bar{x}_1=1.2$, distribution after first layer has one central peak and two smaller wing peaks. Subsequent universal layers suppresses the wing peaks and raises the central peak. Final distribution is narrower than vacuum-state probability distribution.

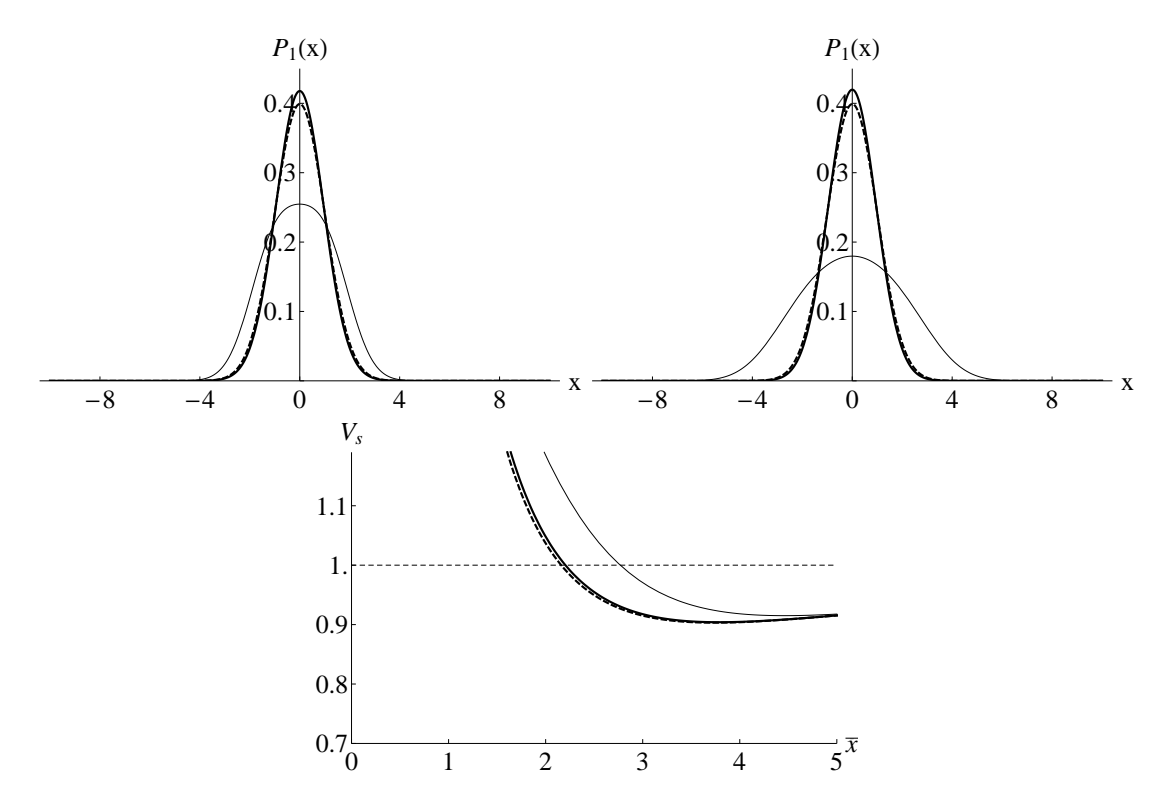


Fig. 25: Nearly optimal non-universal multi-copy squeezing recycling from single-photon state for $\eta=0.3$. (Top-Left) after first non-universal two-copy recycling and before universal multi-copy recycling M=1: $\bar{x}_1=0$ (full-thin), optimal $\bar{x}_1=3.742$ (full-thick), vacuum state (dashed-thick). (Top-Right) after nearly optimal recycling M=16: $\bar{x}_1=0$ (full-thin), optimal $\bar{x}_1=2.45$ (full-thick), vacuum (dashed-thick). (Bottom) recycled variance V_S : optimal two-copy (M=1) non-universal recycling (full-thin), nearly optimal multi-copy recycling for M=16 (full-thick), asymptotical nearly optimal multi-copy recycling for $M\to\infty$ (dashed-thick).

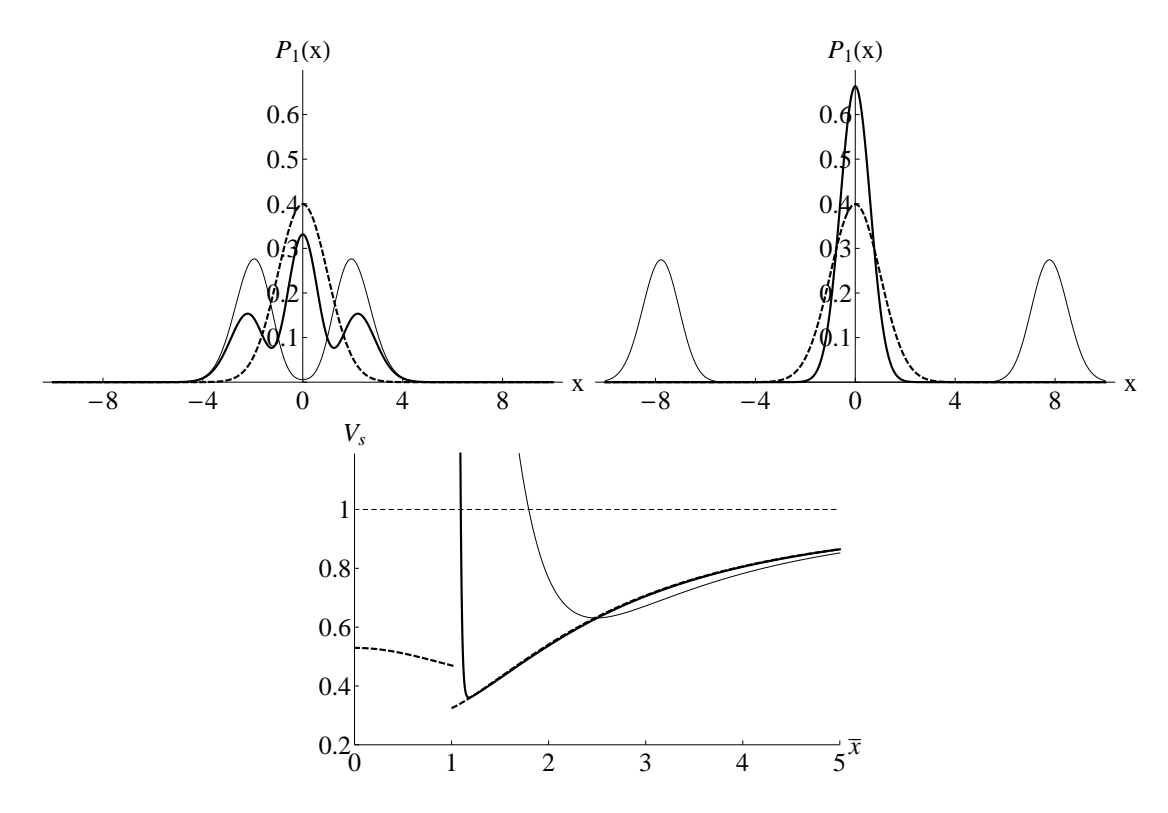


Fig. 26: Nearly optimal non-universal multi-copy squeezing recycling from single-photon state for $\eta=0.9$. (Top-Left) after first non-universal two-copy recycling and before universal multi-copy recycling M=1: $\bar{x}_1=0$ (full-thin), $\bar{x}_1=1.2$ (full-thick), vacuum state (dashed-thick). (Top-Right) after nearly optimal recycling M=16: $\bar{x}_1=0$ (full-thin), $\bar{x}_1=1.2$ (full-thick), vacuum (dashed-thick). (Bottom) recycled variance V_S : optimal two-copy (M=1) non-universal recycling (full-thin), nearly optimal multi-copy recycling for M=16 (full-thick), asymptotical nearly optimal multi-copy recycling for $M\to\infty$ (dashed-thick).

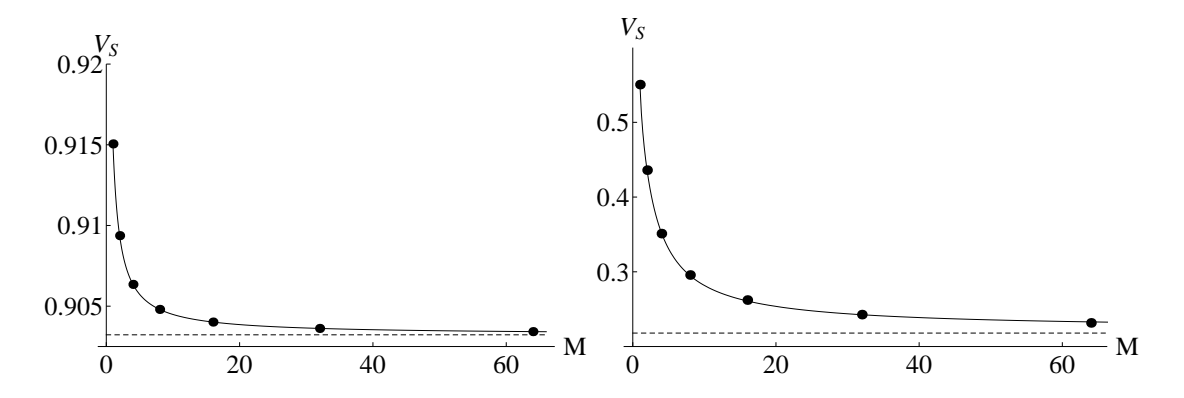


Fig. 27: Nearly optimal non-universal multi-copy squeezing recycling from single-photon state: Numerical values of minimal variance V_S for $\eta = 0.3$ (left) and $\eta = 1$ (right) fitted by rational function and compared to theoretical limits (dashed-thin).

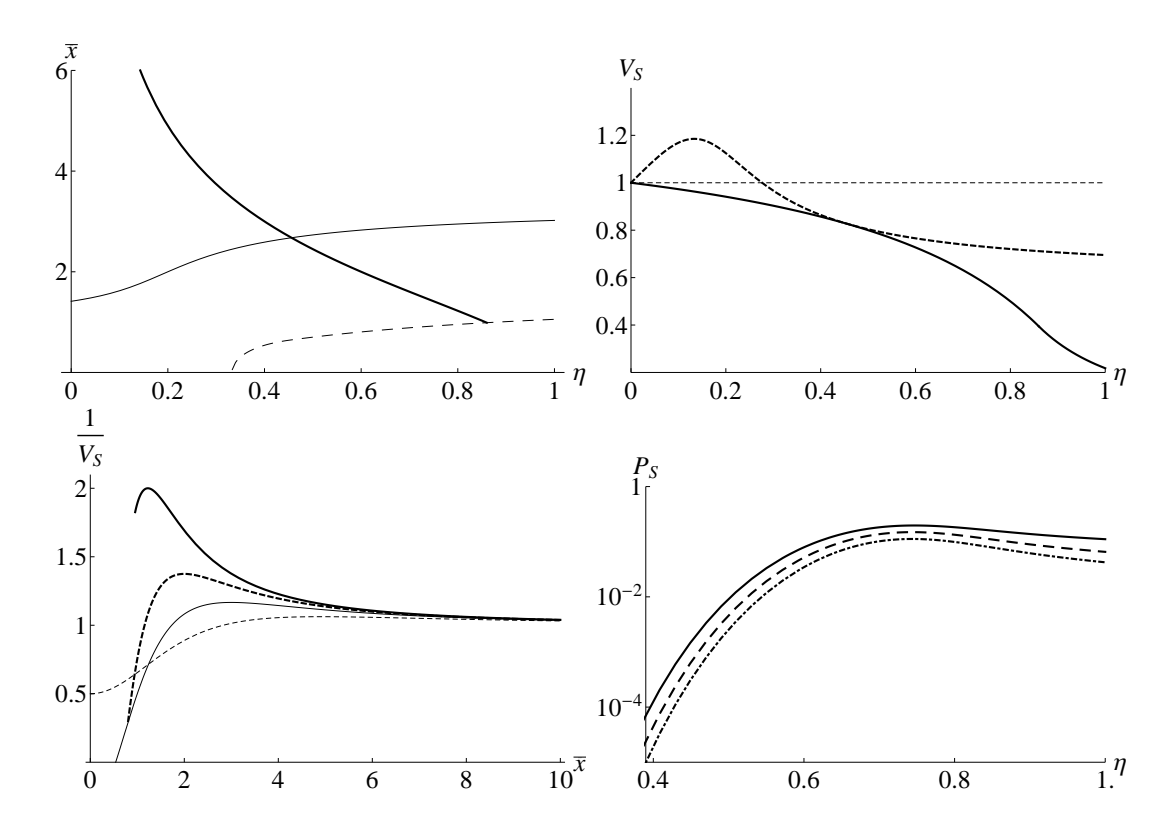


Fig. 28: (Top-left) formula Eq. (109) is valid in area above the dashed-thin line. Optimal position in dependence of η (full-thick). Relative concavity is equal to zero for \bar{x}_1 lying on full-thin line. (Top-right) variance reached just from relative steepness (dashed-thick) compared to minimal reachable variance (full-thick) and to vacuum noise variance (dashed-thin). (Bottom-left) sum of relative concavity and relative non-stationarity for $\eta = 0.2$ (dashed-thin) and for $\eta = 0.4$ (full-thin) and for $\eta = 0.6$ (dashed-thick) and for $\eta = 0.8$ (full-thick). (Bottom-right) dependence of success probability P_S of optimal measurement on η for N = 8 and for m = 1 (full line) and for m = 2 (dashed line) and for m = 3 (dot-dashed line).

If $\bar{x}_1 \leq \bar{x}_{min}$ then the equal symmetrical maxima on the sides are global maxima and the universal recycling separates them and concentrates the distribution around them. We need to shift one of the maxima to origin and apply the universal single-copy filtration after the nearly optimal recycling to filter-out only single peak. We can use formula Eq. (108) with x'_{max} given by Eq. (112) to calculate the minimal variance

$$V_S(\bar{x}_1) = \frac{\eta \left(1 + \sqrt{1 - \frac{2(1-\eta)\bar{x}_1^2}{\eta}}\right)}{\left|4\bar{x}_1^2(1-\eta) - 2\eta + (2-4\eta - \eta\bar{x}_1^2)\sqrt{1 - \frac{2(1-\eta)\bar{x}_1^2}{\eta}}\right|}$$
(115)

achievable after the optimized single-copy filtration. However, we can numerically verify that V_S from Eq. (115) with $\bar{x}_1 \in \langle 0, \bar{x}_{min} \rangle$ is always larger than V_S from Eq. (113) with $\bar{x}_1 \in \langle \bar{x}_{min}, \infty \rangle$, as is visible from Fig. 26 (for $\eta = 0.9$).

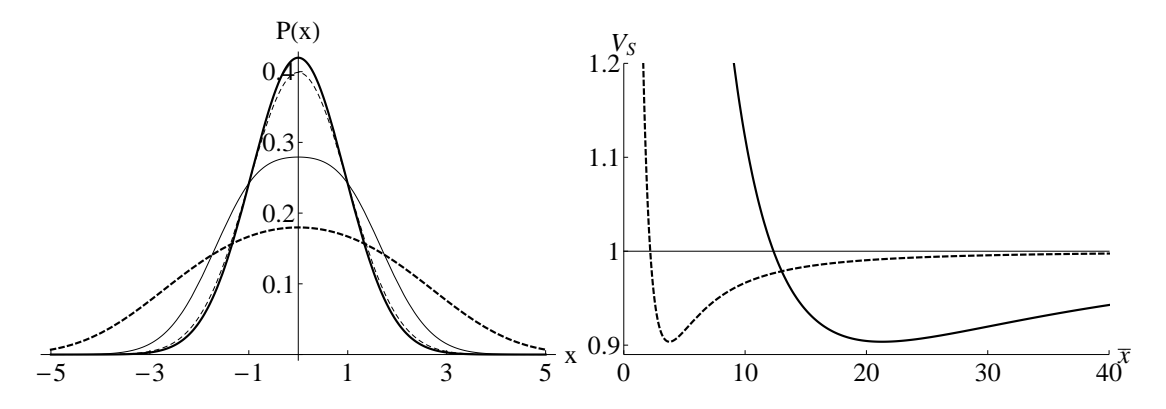


Fig. 29: Partially-universal multi-copy squeezing recycling from single-photon state for $\eta=0.3$ with non-universal last layer. (Left) probability distribution of coordinate: after 5 universal layers and before last non-universal layer (dashed-thick), after 6th non-universal layer for optimal measured coordinate (full-thick), input state (full-thin) and vacuum (dashed-thin). (Right) variance of the squeezed coordinate for N=32 in dependence of measured position for measuring in the last layer (full-thick) and for measuring in the first layer (dashed-thick) compared to vacuum noise (full-thin).

The relative concavity can vanish for some points $\pm \frac{\bar{x}_1}{\sqrt{2}}$, then the squeezing is achieved just from the relative steepness and the partially-universal recycling goes completely beyond the universal one. More often, combination of relative concavity and relative steepness is used to reach maximal squeezing. Relative concavity is equal to zero for

$$\bar{x}_1 = \frac{\sqrt{\sqrt{24\eta^2 - 8\eta + 1} + 6\eta - 1}}{\eta}$$

and squeezing is generated just from relative steepness. Variance achievable just from steepness is compared to minimal reachable variance for partially-universal multi-copy recycling in Fig. 28 (top-right). For $\eta = \frac{1}{15}(10-\sqrt{10}) \approx 0.45$, overall minimal variance is achieved just from the steepness.

In summary, the nearly optimal recycling uses $\bar{x}_1 \in \langle \bar{x}_{min}, \infty \rangle$ and minimal extractable variance is determined by the formula Eq. (113). For $\eta < 0.86$, minimal variance reachable for $\bar{x}_1 = \sqrt{\frac{6(1-\eta)}{\eta}}$ coincides with fully non-universal recycling. For $\eta > 0.86$, maximum squeezing is achieved for $\bar{x}_1 = x_{min}$ and the protocol reaches just nearly optimal result because fully non-universal recycling extract higher squeezing.

Other remarkable fact is that it does not matter which measured position is non-zero. Minimal variance is still the same. Final state recycled from N copies with non-zero measured position in mth layer has probability density function

$$P_m(x|\bar{x}_m) \propto \left[P_{in} \left(\frac{\bar{x}_m}{\sqrt{2^m}} + \frac{x}{\sqrt{N}} \right) P_{in} \left(\frac{\bar{x}_m}{\sqrt{2^m}} - \frac{x}{\sqrt{N}} \right) \right]^{N/2}. \tag{116}$$

Final states are almost the same. Only difference is in scaling of \bar{x} which causes just decreasing of success probability of optimal measurement with increasing m. In Fig.

28(bottom-right) is depicted dependence of success probability on m. For $\eta=0.3$, proses is shown in Fig. 29 where each universal layer spreads the single-peak input distribution and as it is wider it is closer to Gaussian distribution. Despite to process of Gaussification, we can still extract squeezing after finite number of universal layers by applying non-universal layer which raises the global maximum in the origin and makes the distribution narrower than vacuum-state probability distribution of coordinate. For N=64, optimal measured position for m=1 is $\bar{x}_{1,opt}=3.764$ and for m=6 is $\bar{x}_{6,opt}=21.294$. In both cases same variance $V_S=0.904$ is reached and optimal measured coordinates satisfy formula $\bar{x}_{m,opt}/\bar{x}_{n,opt}=\sqrt{2^{m-n}}$. Particularly, $\bar{x}_{6,opt}/\bar{x}_{1,opt}=\sqrt{2^5}$.

Single-layer partially-universal multi-copy recycling extracts better squeezing than single-copy and two-copy recycling and than universal multi-copy recycling. For $\eta < 0.86$, this method is optimal for all measured coordinate optimization. For input states with higher purity, single-layer multi-copy recycling reaches just nearly optimal squeezing.

6.5 Multi-layer partially-universal multi-copy recycling

The partially-universal protocol can be further extend to more non-universal layers in the tree-structure scheme. Non-universal part is again followed by multi-copy universal recycling.

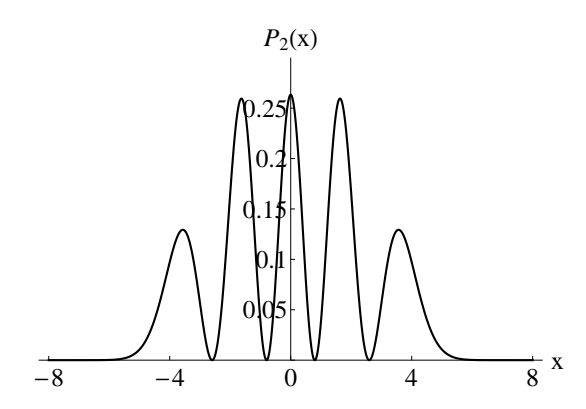


Fig. 30: Probability distribution of coordinate of state after two non-universal layers for $\bar{x}_1 = 1.2$ and $\bar{x}_2 = 0.9$ and $\eta = 1$.

For the distribution with global maximum shifted to the origin after k non-universal layers, the universal recycling finally achieves the squeezed variance given by

$$\frac{1}{V_S} = \frac{1}{2^k} \left| \sum_{i=1}^k \frac{P_{in}''(y_i)}{P(y_i)} + \frac{P_{in}'(y_i)}{P(y_i)} \frac{P_{in}'(-y_i)}{P(-y_i)} \right|$$
(117)

where y_i represents all different combinations $\sum_{j=1}^k \pm \frac{\bar{x}_j}{2^{\frac{j}{2}}}$ over all possible signs \pm . The formula Eq. (117) is valid for any distribution, because the global maximum can be always displaced to the origin. If it is done before the universal recycling, it does not change the asymptotically reachable squeezing. Because global maxima change with

 \bar{x}_j , it produce multiple minima of the variance, which all have to be compared. In formula Eq. (117) can be seen, that for multi-layer partial non-universal recycling, the squeezing is still extracted from the relative concavity and the relative steepness.

For two non-universal layers, achievable variance from pure state according to formula Eq. (117) is $V_S = 0.127$ for measured coordinates $\bar{x}_1 = 1.2$ and $\bar{x}_2 = 0.9$, which is higher squeezing than for single-layer partially-universal method with extractable variance $V_S = 0.218$ from pure single-photon state. Corresponding probability distribution of coordinate of state after optimal two non-universal layers and before next universal part of recycling is depicted in Fig. 30.

Multi-layer partially-universal multi-copy recycling can extract more squeezing than single-layer method attenuated single-photon state with $\eta > 0.86$. On the other hand, the multi-copy method is more difficult to optimization and cannot reach better squeezing for $\eta < 0.86$.

6.6 Non-universal multi-copy recycling

Fully non-universal multi-copy recycling can be numerically analyzed for small number of input copies N, but for large N the situation is too complex and many parameters have to be optimized. It is impossible to analytically predict achievable variance for large N and uncover all generic features which determines extractable squeezing.

Two structures are studied for resource of N single-photon states. For tree structure, measured coordinates are the same in the same level of tree-structure scheme so $n = \log_2 N$ measured coordinates have to be optimized. It means that number of parameters increases logarithmically which is the advantage of this structure. Variance of the the final state has to be numerically minimized. Minimal variance V_S as the function of η is depicted in Fig. 31. Tree-structure recycling can reach better squeezing than single-copy and two-copy recycling. Simple non-universal single-copy Gaussian recycling is still very efficient for the states with $\eta \leq 0.5$, for states with positive Wigner function. For $\eta > 0.86$, limit value for infinite number of copies remains unanswered. For N = 16, we can reach variance $V_S = 0.136$ for pure single-photon state. Optimal recycling again extracts squeezed one-peak probability distribution from two-peak input probability distribution (see Fig. 31 top-left). Recycled distribution is symmetrically placed around origin because of symmetric interference on every beam splitter. Development of distribution through recycling is nontrivial because complicated non-universal protocol of recycling is followed.

Minimal reachable variance dependence on number of copies depicted in Fig. 31 (bottom-left) suggests that arbitrary high squeezing can be achieved for infinite number of copies but we cannot compute optimal variance for more copies. Numerical results are fitted by linear rational function with limit $V_S = 0.00546$ for $N \to \infty$. Numerical comparison between single-layer partially-universal and fully non-universal protocols are depicted in Fig. 31 (bottom-right). The improvement is evident for $\eta = 1$, however, for $\eta \leq 0.9$ the improvement is temperate. From comparison can be seen a nearly optimal character of the single-layer partially-universal method, which well responds to fully non-universal method for $\eta < 0.9$.

For the linear-structure optimal scheme is when transmittance in successive step is

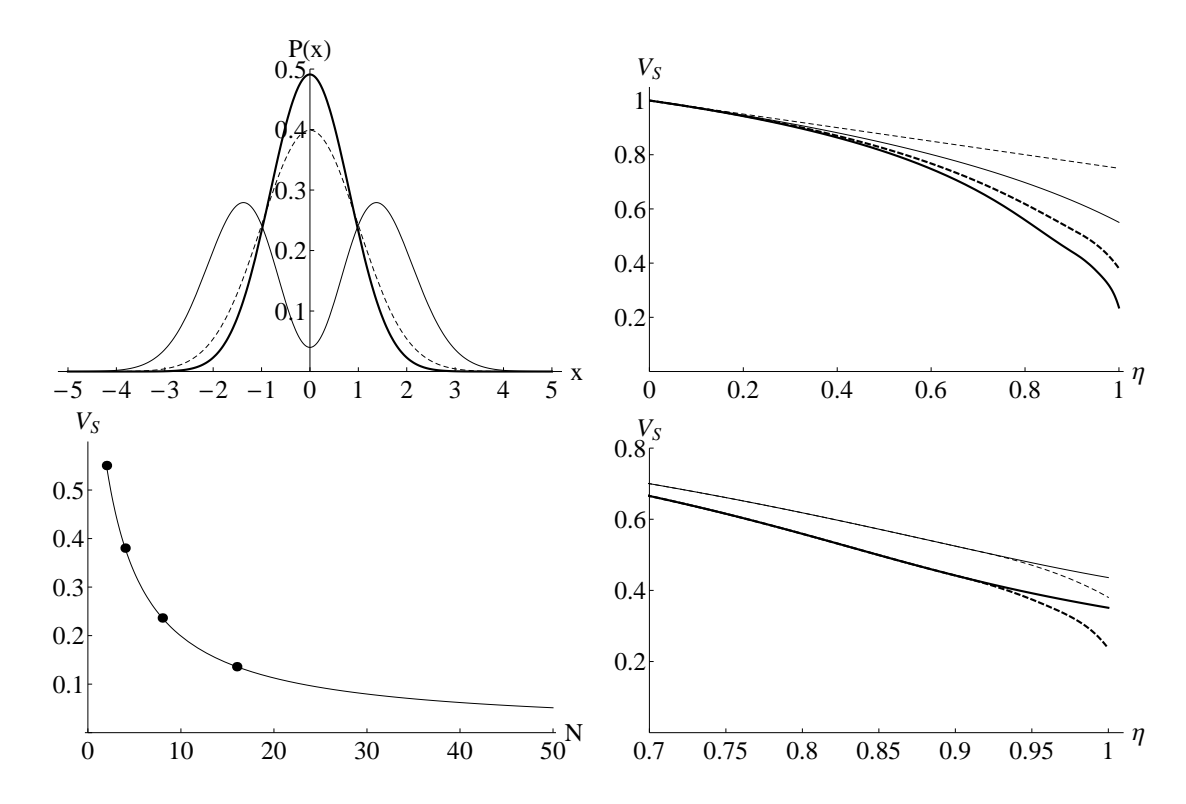


Fig. 31: Non-Universal multi-copy tree-structure squeezing recycling from single-photon state. (Top-left) final state (full-thick) recycled state from 8 input states for $\eta=0.9$ (full-thin) compared to vacuum state (dashed-thin). (Top-right) variance of final state for 4 (dashed-thick) and 8 (full-thick) input states compared to single-copy (dashed-thin) and two-copy (full-thin) recycling. (Bottom-left) minimal reachable variance in dependence on number of input state copies fitted by linear rational function. (Bottom-right) comparison between partially-universal and full non-universal multi-copy method: variance of squeezed quadrature for N=4 partially-universal (full-thin) and full non-universal (dashed-thin) and for N=8 partially-universal (full-thick) and full non-universal (dashed-thick).

given by $T_i = \frac{i}{i+1}$. Number of detectors increases linearly with increasing number of input states. Number of measured coordinates, which we have to optimize, increases linearly, too. This is disadvantage of linear structure. Variance of the the final state have to be minimized numerically. Minimal variance V_S as the function of η is depicted in Fig. 32. Linear-structure recycling can reach better squeezing than two-copy recycling. Both structures give the same squeezing for N=4 for every η which suggests that both structures reach same squeezing for given number of copies of input state. For linear structure, number of parameters increases very fast so we cannot analyze more than five input state copies.

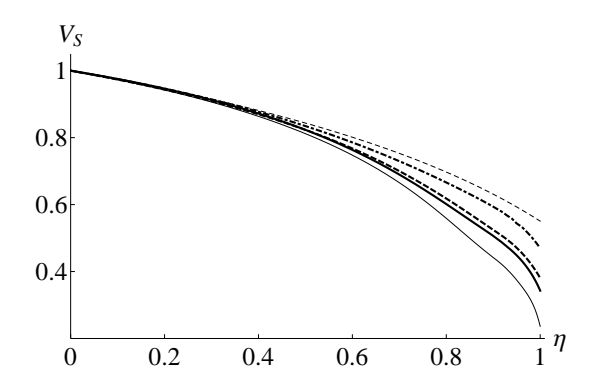


Fig. 32: Non-universal multi-copy linear-structure squeezing recycling from single-photon state. Variance of final state for 3 (dot-dashed-thick) and 4 (dashed-thick) and 5 (full-thick) initial states compared to two-copy recycling (dashed-thin) and tree-structure recycling with 4 (dashed-thick) and 8 (full-thin) initial states.

In conclusion, tree structure is better than linear structure because of less parameters which have to be optimized for given number of input states. Moreover, partially-universal protocol was involved and for tree-structure protocol and it allowed us to analyze very good estimation of fully non-universal multi-copy recycling which is very complex problem. We can determine limit of infinite number of input state copies for single-layer partially-universal multi-copy recycling in contrast to fully non-universal one where we can analyze output state only for small number of input state copies. Minimal squeezed state variance recycled from large number of pure single-photon state copies was not determined because it is problem of minimization of high degree polynomial of many variables. It suggests that very high squeezing might be reached but there is not enough data for good estimation.

7 Non-Gaussian detectors

It is interesting to know if quantum recycling can be achieved without homodyne detector, using only coherently displaced avalanche photodiode working as a threshold detector. It is actually non-Gaussian detector. Now we will consider threshold detector as an extension for two basic recycling protocols which are single-copy and two-copy recycling. Moreover we will consider ideal non-Gaussian projective measurement to determine maximal squeezing extractable by these two protocols based on linear optics with arbitrary detector.

7.1 Threshold detectors

Alternatively to homodyne detection, if it is not available, we can use another detector in combination with coherent displacement. Threshold detector described by the POVM component $1-|0\rangle\langle 0|$ can be used. Measurement with that detector is no longer Gaussian operation. Protocols for one and two input state copies are depicted in Fig. 33. This detector is many cases more feasible than homodyne detection. However, inefficiency of this detector is serious problem, therefore it has to be analyzed.

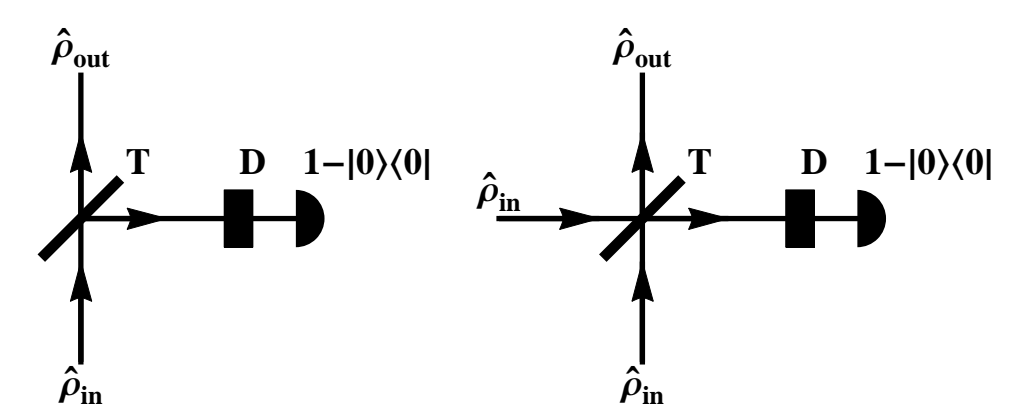


Fig. 33: Schemes for single-copy (left) and two-copy (right) recycling with non-Gaussian measurement $1-|0\rangle\langle 0|$ and coherent displacement D. Beam splitter with transmittance T is used for interference of the input states.

Both single-photon state and vacuum state are phase insensitive as well as beam splitter and threshold detector so the displacement can be applied just in quadrature \hat{x} . To describe these measurement we need whole input state Wigner function $W_{in}(x,p)$ in contrast to homodyne detection where coordinate probability density is enough. Input state is at first tapped on beam splitter which is described by substitution

$$x = \sqrt{T}x' - \sqrt{1 - T}x'_0, \quad p = \sqrt{T}p' - \sqrt{1 - T}p'_0,$$

$$x_0 = \sqrt{T}x'_0 + \sqrt{1 - T}x', \quad p_0 = \sqrt{T}p'_0 + \sqrt{1 - T}p',$$
(118)

then displacement is applied on tapped mode which can be expressed by substitution

 $x'_0 = x''_0 - D$ and $p'_0 = p''_0$. Joint distribution is given as

$$W_D(x', p', x_0'', p_0'') \propto W_{in}(\sqrt{T}x' - \sqrt{1 - T}x_0' + \sqrt{1 - T}D, \sqrt{T}p' - \sqrt{1 - T}p_0') \times W_A(\sqrt{T}x_0' + \sqrt{1 - T}x' - \sqrt{T}D, \sqrt{T}p_0' + \sqrt{T}p_0')$$
(119)

where W_A is either Wigner function W_0 of vacuum state for single-copy scheme or input state Wigner function for two-copy scheme. We consider imperfect detectors with detection inefficiencies. It can be described as additional beam splitter with transmittance η_L placed before the detector. It is again describe by transformation

$$x_0'' = \sqrt{\eta_L} \tilde{x}_0 - \sqrt{1 - \eta_L} x_L', \quad p_0'' = \sqrt{\eta_L} \tilde{p}_0 - \sqrt{1 - \eta_L} p_L',$$

$$x_L = \sqrt{\eta_L} x_L' + \sqrt{1 - \eta_L} \tilde{x}_0, \quad p_L = \sqrt{\eta_L} p_L' + \sqrt{1 - \eta_L} \tilde{p}_0. \tag{120}$$

Wigner function is then expressed as

$$W_{L}(x', p', \tilde{x}_{0}, \tilde{p}_{0}) \propto \int_{-\infty}^{\infty} dx'_{L} \int_{-\infty}^{\infty} dp'_{L} W_{D}(x', p', \sqrt{\eta_{L}}\tilde{x}_{0} - \sqrt{1 - \eta_{L}}x'_{L}, \sqrt{\eta_{L}}\tilde{p}_{0} - \sqrt{1 - \eta_{L}}p'_{L}) \times W_{0}(\sqrt{\eta_{L}}x'_{L} + \sqrt{1 - \eta_{L}}\tilde{x}_{0}, \sqrt{\eta_{L}}p'_{L} + \sqrt{1 - \eta_{L}}\tilde{p}_{0}).$$
(121)

Finally, threshold detector is applied on tapped mode to reach output Wigner function

$$W_{out} \propto \int_{-\infty}^{\infty} d\tilde{x}_0 \int_{-\infty}^{\infty} d\tilde{p}_0 \ W_L(x', p', \tilde{x}_0, \tilde{p}_0) \left(1 - W_0(\tilde{x}_0, \tilde{p}_0)\right).$$
 (122)

Derived formulas will be discussed now for particular cases.

7.2 Single-copy non-Gaussian recycling with threshold detector

Wigner function W_A is now represented by vacuum state Wigner function W_0 and attenuated single-photon state is used as input state. Final Wigner function, probability distribution of quadratures and their variances can still be computed analytically but results are too complicated to show them here. Optimization of parameters to reach maximal squeezing have to be performed numerically.

Squeezing is observed in quadrature \hat{x} which was displaced. In limit $T \to 1$ and $D \to 0$, we can reach the same minimal variance $V_S = 1 - \frac{\eta}{4}$ for the threshold detector as for the homodyne detection. Moreover, the reachable variance does not depend on detector losses, because in that limit influence of detector losses vanishes. For $\eta = 0.5$ and $\eta = 0.9$, probability distributions of squeezed and anti-squeezed quadrature after optimal displacement are depicted in Fig. 36. Single-peak distribution narrower than coherent state coordinate distribution can be recycled again. Although the evolution of probability distributions is carried by evolution of whole Wigner function, recycled distributions is very similar to the case of single-copy non-universal recycling with homodyne detection. But the mechanism of extraction is nontrivial because whole Wigner

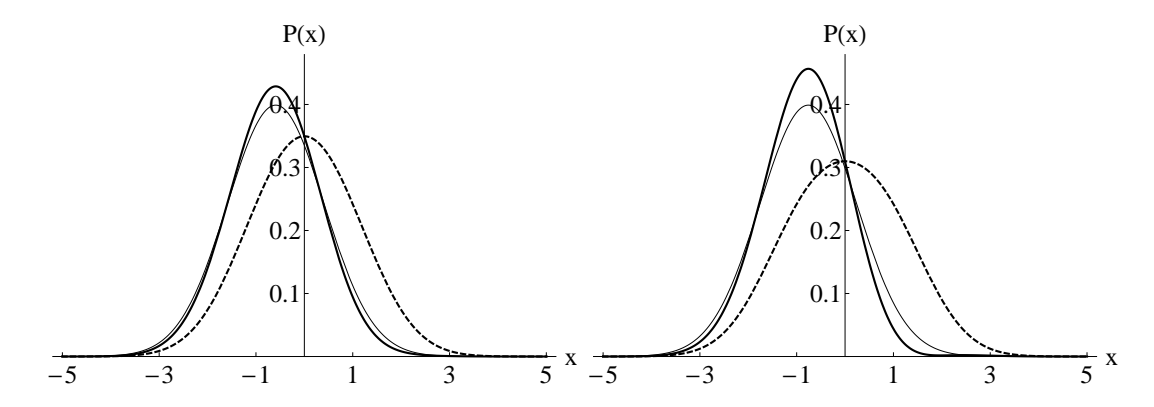


Fig. 34: Single-copy non-Gaussian recycling for T=0.99 and $\eta_L=0.5$ and optimal displacement: recycled state probability distribution of squeezed quadrature (full-thick) and anti-squeezed quadrature (dashed-thick) for $\eta=0.5$ (left) and $\eta=0.9$ (right) are compared to coherent state probability distribution (full-thin).

function have to be carried in contrast to single-copy recycling with homodyne detection. For $\eta=0.5$ and T=0.99, optimal displacement is d=0.082 and corresponding variance is $V_S=0.876$ which is close to limit variance $V_S=0.875$. The influence of losses η_L is very moderate. In whole range $\eta_L \in (0,1)$ variance V_S differs just on fourth fractional digit. For $\eta=0.9$ and T=0.99, optimal displacement is d=0.11 and corresponding variance is $V_S=0.777$ which is again close to limit variance $V_S=0.775$. Dependence of variance V_S on η_L is very similar to the case for $\eta=0.5$.

For single-copy non-Gaussian recycling, the same squeezing can be extracted as for Gaussian one. Actually, it is a maximum of squeezing extractable from the attenuated single-photon state by linear optical tap and arbitrary measurement, as will be proved in Section 7.4. Threshold detector is a good substitution for homodyne detector in that protocol. We do not require photon-number resolving detector to reach optimal performance. Moreover, influence of detector losses on extractable variance is very moderate for optimal measurement.

7.3 Two-copy non-Gaussian recycling with threshold detector

For two-copy protocol, Wigner function W_A is represented by input state Wigner function W_{in} and input state is single-photon state again. For this protocol, squeezing cannot be extracted. We have to consider more difficult scheme with two threshold detectors depicted in Fig. 35 and non-symmetrical interference of input state copies in contrast to other two-copy recycling protocols where symmetrical interference is optimal.

We have to split ancillary mode of state described by Wigner function $W_L(x', p', \tilde{x}_0, \tilde{p}_0)$

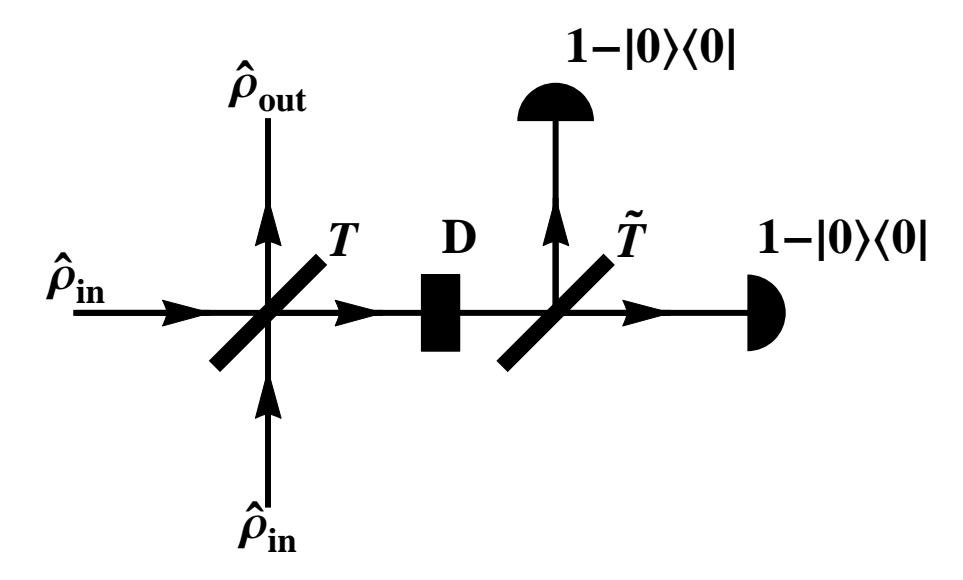


Fig. 35: Schemes of two-copy recycling with two threshold detectors $1 - |0\rangle\langle 0|$ and coherent displacement D. Beam splitter with transmittance T is used for interference of the input states. And symmetric beam splitter with transmittance $\tilde{T} = 0.5$ are applied on measured mode and two threshold detectors is then applied.

on symmetrical beam splitter. It can be described by substitution

$$\tilde{x}_0 = \frac{\tilde{x}_1 - \tilde{x}_2}{\sqrt{2}}, \quad \tilde{p}_0 = \frac{\tilde{p}_1 - \tilde{p}_2}{\sqrt{2}},$$

$$\tilde{x} = \frac{\tilde{x}_2 + \tilde{x}_1}{\sqrt{2}}, \quad \tilde{p} = \frac{\tilde{p}_2 + \tilde{p}_1}{\sqrt{2}}.$$
(123)

Wigner function then reads

$$W_B(x', p', \tilde{x}_1, \tilde{p}_1, \tilde{x}_2, \tilde{x}_2) \propto W_L(x', p', \frac{\tilde{x}_1 - \tilde{x}_2}{\sqrt{2}}, \frac{\tilde{p}_1 - \tilde{p}_2}{\sqrt{2}}) W_0(\frac{\tilde{x}_2 + \tilde{x}_1}{\sqrt{2}}, \frac{\tilde{p}_2 + \tilde{p}_1}{\sqrt{2}}),$$
 (124)

where W_0 is vacuum state Wigner function. Than we apply threshold detector on both ancillary modes. Output state Wigner function is expressed as

$$W_{out} \propto \int_{-\infty}^{\infty} d\tilde{x}_1 \int_{-\infty}^{\infty} d\tilde{p}_1 \int_{-\infty}^{\infty} d\tilde{x}_2 \int_{-\infty}^{\infty} d\tilde{p}_2 \ W_B(x', p', \tilde{x}_1, \tilde{p}_1, \tilde{x}_2, \tilde{x}_2) \times$$

$$(1 - W_0(\tilde{x}_1, \tilde{x}_1)) (1 - W_0(\tilde{x}_2, \tilde{x}_2)) .$$
(125)

We use single-photon state again as input state. Formulas for output state Wigner function and variances in quadratures are to complicated to show them here. State exhibits squeezing in quadrature \hat{x} which was displaced. Minimization of its variance has to be performed numerically. The optimal measurement is in limit $T \to 1$ and $D \to 0$. Limit $T \to 0$ is optimal as well because of the symmetry of input states. Minimal squeezed quadrature variance reads $V_S = 1 - \frac{\eta}{4}$ which is the same result as for single-copy recycling but it is worse than reachable squeezed quadrature variance by

two-copy recycling with homodyne detector. For optimal limit measurement, reachable variance does not depend on detectors losses because influence of losses vanished in that limit. Difference between output states after single-copy recycling with threshold detector and two-copy recycling with two threshold detectors is very slight and the difference vanishes in limit $T \to 1$ and $D \to 0$. For $\eta = 0.5$ and $\eta = 0.9$, probability distributions of squeezed and anti-squeezed quadrature after optimal displacement are depicted in Fig.36. One-peak distribution narrower than coherent state coordinate distribution can be recycled again. Although the evolution of probability distributions is carried by evolution of whole Wigner function, recycled distributions are very similar as in the case of single-copy non-universal recycling with homodyne detection.

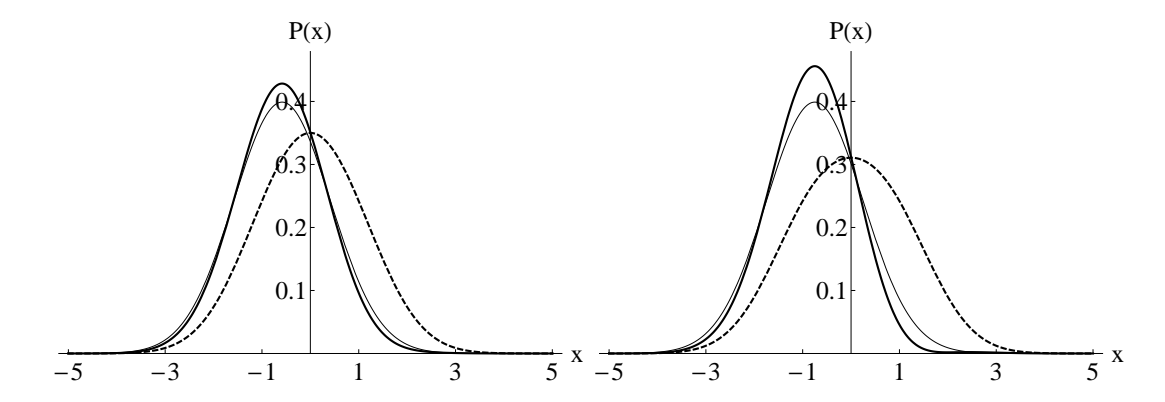


Fig. 36: Two-copy non-Gaussian recycling for T=0.99 and $\eta_L=0.5$ and optimal displacement: recycled state probability distribution of squeezed quadrature (full-thick) and anti-squeezed quadrature (dashed-thick) for $\eta=0.5$ (left) and $\eta=0.9$ (right) are compared to coherent state probability distribution (full-thin).

For $\eta=0.5$ and T=0.99, optimal displacement is d=0.082 and corresponding variance is $V_S=0.877$ which is close to limit variance $V_S=0.875$. The influence of losses η_L is very moderate. In whole range $\eta_L \in (0,1)$ variance V_S differs just on fourth fractional digit. For $\eta=0.9$ and T=0.99, optimal displacement is d=0.11 and corresponding variance is $V_S=0.78$ which is again close to limit variance $V_S=0.775$. Dependence of variance V_S on η_L is very similar to the case for $\eta=0.5$ and in whole range $\eta_L \in (0,1)$. Variance V_S differs just on third fractional digit.

For two-copy recycling, threshold detector is not effective. It extracts less squeezing than recycling with homodyne detection and the extracted squeezing is same as squeezing extracted by single-copy recycling for every η . This imply that two threshold detectors in combination with displacement do not work like projection to superposition $\alpha|0\rangle + \beta|2\rangle$ because these projective measurement extract significantly more squeezing. Optimal projective measurement is required to extract more squeezing as it will be shown in next two sections.

7.4 Optimal single-copy recycling with projective measurement

Now we will consider optimal projective measurement of attenuated single-photon state. Single-photon state is tapped on beam splitter and projective measurement on superposition $\alpha|0\rangle + \beta|1\rangle$, where $|\alpha|^2 + |\beta|^2 = 1$, is applied on tapped mode. Two-mode input state density matrix reads

$$\hat{\rho}_{in} = \eta |10\rangle_{AB}\langle 10| + (1-\eta)|00\rangle_{AB}\langle 00|. \tag{126}$$

After coupling on beam splitter with transmittance T, density matrix is transformed to

$$\hat{\rho}_{BS} = \eta T |10\rangle_{AB} \langle 10| + \eta (1-T)|01\rangle_{AB} \langle 01| + \eta \sqrt{T(1-T)}|10\rangle_{AB} \langle 01| + \eta \sqrt{T(1-T)}|01\rangle_{AB} \langle 10| + (1-\eta)|00\rangle_{AB} \langle 00|.$$
(127)

Projective measurement on state $|\psi\rangle_B = \alpha |0\rangle_B + \beta |1\rangle_B$ is used on tapped mode B. Density matrix is proportional then to

$$\hat{\rho}_{\psi} \propto Tr_{B} \left[\hat{\rho}_{BS} |\psi\rangle_{B} \langle \psi| \right] = \langle \psi|_{B} \hat{\rho}_{BS} |\psi\rangle_{B} =$$

$$\eta \left(|\alpha|^{2} T |1\rangle_{A} \langle 1| + \alpha^{*} \beta \sqrt{T(1-T)} |1\rangle_{A} \langle 0| + \alpha \beta^{*} \sqrt{T(1-T)} |0\rangle_{A} \langle 1| \right) +$$

$$\left(\eta |\beta|^{2} (1-T) + (1-\eta) |\alpha|^{2} \right) |0\rangle_{A} \langle 0|.$$
(128)

Norm of the density matrix $\hat{\rho}_{\psi}$ is given as

$$N = |\alpha|^2 (\eta T + 1 - \eta) + |\beta|^2 \eta (1 - T). \tag{129}$$

Mean value of quadrature \hat{x} reads

$$\langle x \rangle = Tr_A \left[\hat{\rho}_{\psi}(a_A + a_A^{\dagger}) \right] = 2\eta Re(\alpha^* \beta) \sqrt{T(1-T)}/N.$$
 (130)

Second moment of quadrature \hat{x} is given as

$$\langle x^2 \rangle = Tr_A \left[\hat{\rho}_{\psi} (a_A + a_A^{\dagger})^2 \right] = 1 + \frac{2\eta T |\alpha|^2}{N}. \tag{131}$$

Quadrature \hat{x} variance reads

$$V_x = 1 + \frac{2\eta T|\alpha|^2}{N} - \frac{4\eta^2 \left(Re(\alpha^*\beta)\right)^2 T(1-T)}{N^2}.$$
 (132)

Variance is decreasing with increasing term $(Re(\alpha^*\beta))^2$. It implies that real α and β are optimal. If normalization of $|\psi\rangle_B$ expressed as $|\alpha|^2 + |\beta|^2 = 1$ is used, it can be shown that optimal coefficient α reads

$$\alpha_{opt} = \frac{\sqrt{\eta(T-1)}}{\sqrt{(1-T)(2\eta(T-1)+3)}}$$
 (133)

and variance for $\alpha = \alpha_{opt}$ is expressed as

$$V_x = \frac{4 - \eta(4 - 3T)}{4 + 4\eta(T - 1)}. (134)$$

Variance reads $V_x = 1 - \frac{\eta}{4}$ in limit of weak measurement $T \to 1$.

This is a prove that minimal variance of squeezed quadrature reachable by weak measurement is $V_S = 1 - \frac{\eta}{4}$. Remarkably, this threshold can be achieved by single-copy recycling with homodyne detector as well as with threshold detector. $V_S = 1 - \frac{\eta}{4}$ is maximal squeezing extractable from one attenuated single-photon state using linear optics with any detection technique.

7.5 Optimal two-copy recycling with projective measurement

Now we will consider projective measurement on ancillary mode after interference of two single-photon state copies on symmetric beam splitter. Ancillary mode will be projected to superposition $\alpha|0\rangle + \beta|1\rangle + \gamma|2\rangle$, where $|\alpha|^2 + |\beta|^2 + |\gamma|^2 = 1$.

Input state density matrix reads

$$\hat{\rho}_{in} = \eta^2 |11\rangle_{AB} \langle 11| + \eta(1-\eta)|10\rangle_{AB} \langle 10| + \eta(1-\eta)|01\rangle_{AB} \langle 01| + (1-\eta)^2 |00\rangle_{AB} \langle 00|.$$
(135)

Interference on symmetric beam splitter transforms density matrix to

$$\hat{\rho}_{BS} = \frac{\eta^2}{2} \left(|20\rangle_{AB} \langle 20| + |02\rangle_{AB} \langle 02| - |20\rangle_{AB} \langle 02| - |02\rangle_{AB} \langle 20| \right) + \eta(1 - \eta) \left(|10\rangle_{AB} \langle 10| + |01\rangle_{AB} \langle 01| \right) + (1 - \eta)^2 |00\rangle_{AB} \langle 00|.$$
(136)

Projective measurement on state $|\psi\rangle_B = \alpha |0\rangle_B + \beta |1\rangle_B + \gamma |2\rangle_B$ with normalization condition $|\alpha|^2 + |\beta|^2 + |\gamma|^2 = 1$ is used on tapped mode B. Density matrix is then expressed as

$$\hat{\rho}_{\psi} \propto Tr_{B} \left[\hat{\rho}_{BS} | \psi \rangle_{B} \langle \psi | \right] = \langle \psi |_{B} \hat{\rho}_{BS} | \psi \rangle_{B} =$$

$$\frac{\eta^{2}}{2} \left(|\alpha|^{2} |2\rangle_{A} \langle 2| - \alpha \gamma^{*} |0\rangle_{A} \langle 2| - \alpha^{*} \gamma |2\rangle_{A} \langle 0| \right) + |\alpha|^{2} \eta (1 - \eta) |1\rangle_{A} \langle 1| +$$

$$\left(|\alpha|^{2} (1 - \eta)^{2} + |\beta|^{2} \eta (1 - \eta) + |\gamma|^{2} \frac{\eta^{2}}{2} \right) |0\rangle_{A} \langle 0|.$$
(137)

Norm of the density matrix $\hat{\rho}_{\psi}$ is given as

$$N = \left(\frac{\eta^2}{2} - \eta + 1\right) |\alpha|^2 + \eta(1 - \eta)|\beta|^2 + \frac{\eta^2}{2}|\gamma|^2.$$
 (138)

Mean value of quadrature \hat{x} is equal to zero and variance is given then as

$$V_x = \langle x^2 \rangle = Tr_A \left[\hat{\rho}_{\psi} (a_A + a_A^{\dagger})^2 \right] = 1 + \frac{2|\alpha|^2 - \sqrt{2}\eta^2 Re(\alpha \gamma^*)}{N}.$$
 (139)

Variance is decreasing with increasing term $(Re(\alpha^*\gamma))^2$. It implies that real α and γ are optimal. It can be shown that optimal value of coefficient β is equal to zero. Normalization of $|\psi\rangle_B$ is then expressed as $|\alpha|^2 + |\gamma|^2 = 1$. If we use normalization condition to exclude γ , variance reads

$$V_x = \frac{2\alpha^2(\eta + 1) + \eta^2 - 2\sqrt{2 - 2\alpha^2}\alpha\eta^2}{2\alpha^2(1 - \eta) + \eta^2}.$$
 (140)

Optimal coefficient α is given as

$$\alpha_{opt} = \frac{\eta}{\sqrt{2}\sqrt{(\eta - 1)\eta + \sqrt{2}\sqrt{(\eta - 2)\eta + 4} + 3}}$$
(141)

and minimal variance is expressed as

$$V_x = \frac{\eta^2 - \sqrt{2}\sqrt{(\eta - 2)\eta + 2\sqrt{2}\sqrt{(\eta - 2)\eta + 4} + 6\eta} + \sqrt{2}\sqrt{(\eta - 2)\eta + 4} + 4}{(\eta - 2)\eta + \sqrt{2}\sqrt{(\eta - 2)\eta + 4} + 4}.$$
 (142)

For $\eta=1$, there is freedom in choice of optimal parameters. Minimal variance $V_x=0.55$ is reached for arbitrary $\alpha<0.303$ if $\beta=0$ if $\gamma=\left(\sqrt{2}+\sqrt{3}\right)\alpha$. Homodyne and heterodyne detections are then sufficient to reach maximal squeezing. However, for $0<\eta<1$, the freedom in choice of parameter α vanishes and optimal parameter α_{opt} is given by Eq. (141). Homodyne and heterodyne detections then cannot reach maximal squeezing given by formula Eq. (140) (see Fig. 37). Optimal coefficients are depicted in Fig. 37 where can be seen that optimal values of coefficient γ are very close to unity.

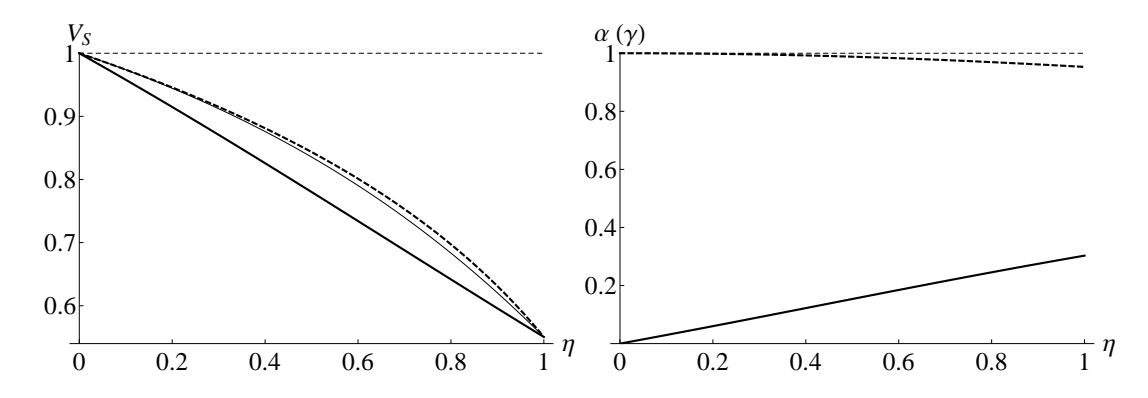


Fig. 37: Two-copy recycling with projective measurement on superposition $\alpha|0\rangle + \gamma|2\rangle$: (left) minimal variance of squeezed quadrature (full-thick) is compared to minimal squeezed quadrature variance extracted by two-copy recycling with homodyne (dashed-thick) and heterodyne (full-thin) detectors and to vacuum noise (dashed-thin). (Right) optimal values of coefficients α (full-thick) and γ (dashed-thick) are compared to unity (dashed-thin).

In this section was shown that two-copy recycling with homodyne detector even with heterodyne detector cannot extract maximal squeezing extractable from two single-photon state copies for every $0 < \eta < 1$. Heterodyne detection projects to superposition

 $\alpha|0\rangle + \beta|1\rangle + \gamma|2\rangle$ but it cannot do projection with all required coefficients. For $\eta=1$, homodyne and heterodyne detectors are enough to extract maximal squeezing thanks to the freedom of choice of optimal parameters of projective measurement.

8 Conclusion

Remarkably, we demonstrated that squeezing can be recycled from arbitrary attenuated single-photon state with linear optics components and Gaussian homodyne or heterodyne detection only. Moreover, the squeezing recycling has purification effect on quantum states as well. We pay by success probability for higher squeezing but success probability is just less important technical parameter since it can be increased by rate of single photon production. Recycled squeezing can be increased with more single-photon state copies on input. The improvement is considerable for single-photon state with high purity but also for single-photon state with positive Wigner function, the progress is observable. Multi-copy recycling protocol is more complex, more difficult to analyze and very difficult for experimental realization without integrated optical technology but still interesting enough to study. We studied the tree-structure and the linear-structure multi-copy recycling protocols. Extractable squeezing from both of them is the same for given number of input state copies. However, the tree-structure protocol uses less homodyne detectors thus there are less parameters to optimize. The tree-structure protocol is then easier to analyze than the linear-structure protocol. On the other hand it requires more complicated interference of input state copies.

Moreover, we developed partially-universal method for tree-structure multi-copy recycling. Partially-universal strategy uses single non-universal layer in tree-structure protocol and all other layers are universal. The partially-universal method extracts the same squeezing as fully non-universal method for almost every attenuated single-photon states. Only for single-photon states with high purity, partially-universal method is worse than fully non-universal method. To improve the partially-universal method, we can consider more than one non-universal layers in tree-structure protocol. If we consider partially-universal method with finite number of non-universal layers ordered before all other universal layers, the limit squeezing for infinite number of input state copies is determined by relative concavity and relative steepness of input state probability distribution in points controlled by measured values in non-universal layers. It extends the universal approach where extractable squeezing is determined just by relative concavity of distribution of input resource state [19]. Moreover, ordering of universal and non-universal layers are irrelevant because the extractable squeezing is still the same. It means that limit determined for specific ordering is valid for any other ordering, since infinite number of universal layers still follow after last non-universal layer.

Exchangeability of universal and non-universal layers has interesting consequence. If we consider input state with single-peak probability distributions of quadratures and we apply finite number of universal layers, the state will by closer to Gaussian state with every other applied universal layer. However, if we add last non-universal layer, squeezing still can be extracted despite squeezing cannot be recycled from Gaussian state at all. Extractable squeezing is the same as if we firstly apply the non-universal layer and then we add all universal layers. Remarkably, essential ingredient for squeezing hidden in the input state survives despite the Gaussification of the state caused by universal recycling. Only thing, which we pay for ordering the non-universal layers on the end of the recycling, is less probability of success.

We showed that optimal projective measurement for single-copy recycling from attenuated single-photon state can be reached by homodyne detector, heterodyne detector and threshold detector as well. However, for two-copy recycling, optimal projective measurement cannot be reached with neither of them. Two-copy recycling from attenuated single-copy state with heterodyne detection can extract more squeezing than the same protocols with the other two detectors and on the other, hand threshold detector is worse than the rest.

Our main target is to produce quantum squeezing in the cases when the standard sources of squeezing are not available but still we can produce many interfering single photons. It seams to be relevant for ultraviolet region of electromagnetic spectrum where parametric nonlinear processes in optical crystals are challenging but still single photon sources are existing [32, 33]. Our analysis is a first step to produce continuous-variable quantum states in this ultraviolet region.

9 Outlook

Natural extension of studied resources will be higher Fock states than two-photon state. They exhibit nontrivial multi-peak probability distributions of quadratures with high curvature. Two-photon state was proven to be better resource than single-photon one. It suggests that higher squeezing could be extracted from multi-photon states. On the other hand, multi-photon states are very complex and difficult to generate.

Other interesting issue is whether a better resource is large number of single-photon state copies or smaller number of multi-photon state copies or even only one multi-photon state with high energy. In other words, if better strategy is to fuse single-photon states to multi-photon state before the recycling or to use them directly for recycling. For two copies of pure single-photon state, both strategies are equal but for attenuated single-photon state, they differ and optimal strategy depends on attenuation factor η . Situation is more complicated for higher number of input states.

Everything about single-photon state resource is not still answered. Optimal projective measurement for single-copy recycling from attenuated single-photon state can be reached by homodyne or heterodyne detection but for two-copy recycling, optimal projective measurement cannot be reached with neither of them. Therefore, there is a need for better detector. Optimal projective measurement should be studied for multicopy recycling but it is very complex problem because Hilbert space expands with increasing number of input states. For pure single-photon state, homodyne detection is sufficient to reach optimal extractable squeezing by two-copy recycling but on the other hand, question of limit squeezing for large number of pure single-photon state copies is not answered. Non-universal multi-copy recycling and multi-layer partially-universal recycling suggest that arbitrarily high squeezing could be achieved for large number of input state copies but we cannot compute enough data to make a good estimation of the limit. To solve this problem, Fock state representation could be better than Wigner function formalism, because only pure single-photon states are considered.

All tools developed for quantum optics could be transformed to different platforms like solid-state physics or atomic systems. Moreover, all squeezing recycling strategies could be transformed to extract different quantum processing resource. For example, slightly squeezed states with high purity are another important resource for quantum information processing. Studied squeezing recycling tools have purification effect as well. It means that recycling protocols could be optimized to produce states with high purity in condition that recycled state exhibits at least slight squeezing.

Finally, we plan to investigate novel class of recycling strategies based on active coherent manipulation of sources generating single-photon states. We believe it can be a resource to produce more squeezing and break limitations given by Gaussian methods.

References

- [1] D. F. Walls, Squeezed states of light, Nature **306**, 141 (1983).
- [2] R. E. Slusher, L. W. Hollberg, B. Yurke, J. C. Mertz and J. F. Valley, Observation of Squeezed States Generated by Four-Wave Mixing in an Optical Cavity, Phys. Rev. Lett. 55, 2409 (1985).
- [3] L.-A. Wu, M. Xiao and H. J. Kimble, Squeezed states of light from an optical parametric oscillator, J. Opt. Soc. Am. B 4, No. 10 (1987).
- [4] T. Eberle, S. Steinlechner, J. Bauchrowitz, V. Händchen, H. Vahlbruch, M. Mehmet, H. Müller-Ebhardt and R. Schnabel, *Quantum Enhancement of the Zero-Area Sagnac Interferometer Topology for Gravitational Wave Detection*, Phys. Rev. Lett. 104, 251102 (2010).
- [5] S. Takeda, T. Mizuta, M. Fuwa, P. van Loock and A. Furusawa, *Deterministic* quantum teleportation of photonic quantum bits by a hybrid technique, Nature **500**, 315 (2013).
- [6] S. Yokoyama, R. Ukai, S. C. Armstrong, C. Sornphiphatphong, T. Kaji, S. Suzuki, J. Yoshikawa, H. Yonezawa, N. C. Menicucci and A. Furusawa, *Ultra-large-scale* continuous-variable cluster states multiplexed in the time domain, Nat. Phot. 7, 982 (2013).
- [7] L. S. Madsen, V. C. Usenko, M. Lassen, R. Filip and U. L. Andersen, *Continuous variable quantum key distribution with modulated entangled states*, Nat. Commun. **3**, 1083 (2012).
- [8] A. Furusawa, P. van Loock, Quantum Teleportation and Entanglement, (WILEY-VCH, Weinheim, Germany, 2011).ISBN: 978-3527409303
- [9] B. Kraus, K. Hammerer, G. Giedke and J. I. Cirac, Entanglement generation and Hamiltonian simulation in continuous-variable systems, Phys. Rev. A 67, 042314 (2003).
- [10] J. Heersink, Ch. Marquardt, R. Dong, R. Filip, S. Lorenz, G. Leuchs and U. L. Andersen, *Distillation of Squeezing from Non-Gaussian Quantum States*, Phys.

- Rev. Lett. **96**, 253601 (2006).
- [11] J. Fiurášek, P. Marek, R. Filip and Roman Schnabel, Experimentally feasible purification of continuous-variable entanglement, Phys. Rev. A. **75**, 050302 (2007).
- [12] B. Hage, A. Franzen, J. DiGuglielmo, P. Marek, J. Fiurášek and R. Schnabel, On the distillation and purification of phase-diffused squeezed states, New J. Phys. 9, 227 (2007).
- [13] O. Glöckl, U. L. Andersen, R. Filip, W. P. Bowen and G. Leuchs, *Squeezed-State Purification with Linear Optics and Feedforward*, Phys. Rev. Lett. **97**, 053601 (2006).
- [14] A. Franzen, B. Hage, J. DiGuglielmo, J. Fiurášek and R. Schnabel, Experimental Demonstration of Continuous Variable Purification of Squeezed States, Phys. Rev. Lett. 97, 150505 (2006).
- [15] P. Marek, J. Fiurášek, B. Hage, A. Franzen, J. DiGugliemo and R. Schnabel, Multiple-copy distillation and purification of phase-diffused squeezed states, Phys. Rev. A 76, 053820 (2007).
- [16] E. T. Campbell and J. Eisert, Gaussification and Entanglement Distillation of Continuous-Variable Systems: A Unifying Picture, Phys. Rev. Lett. 108, 020501 (2012).
- [17] E. T. Campbell, M. G. Genoni and J.Eisert, Continuous-variable entanglement distillation and noncommutative central limit theorems, Phys. Rev. A 87, 042330 (2013).
- [18] M. Lassen, L. S. Madsen, M. Sabuncu, R. Filip and U. L. Andersen, Experimental demonstration of squeezed-state quantum averaging, Phys. Rev. A 82, 021801 (2010).
- [19] R. Filip, Distillation of quantum squeezing, Phys. Rev. A 88, 063837 (2013).
- [20] H. J. Kimble, M. Dagenais and L. Mandel, *Photon Antibunching in Resonance Fluorescence*, Phys. Rev. Lett. **39**, 691 (1977).

- [21] P. Grangier, G. Roger and A. Aspect, Experimental Evidence for a Photon Anticorrelation Effect on a Beam Splitter: A New Light on Single-Photon Interferences, Europhys. Lett. 1, 173 (1986).
- [22] A. I. Lvovsky, H. Hansen, T. Aichele, O. Benson, J. Mlynek and S. Schiller, Quantum State Reconstruction of the Single-Photon Fock State, Phys. Rev. Lett. 87, 050402 (2001).
- [23] S. A. Babichev, J. Appel and A. I. Lvovsky, Homodyne Tomography Characterization and Nonlocality of a Dual-Mode Optical Qubit, Phys. Rev. Lett. 92, 193601 (2004).
- [24] Q. Wang, W. Chen, G. Xavier, M. Swillo, T. Zhang, S. Sauge, M. Tengner, Z.-F. Han, G.-C. Guo and A. Karlsson, Experimental Decoy-State Quantum Key Distribution with a Sub-Poissionian Heralded Single-Photon Source, Phys. Rev. Lett. 100, 090501 (2008).
- [25] R. Alléaume, F. Treussart, G. Messin, Y. Dumeige, J.-F. Roch, A. Beveratos, R. Brouri-Tualle, J.-P. Poizat and P. Grangier, *Experimental open-air quantum key distribution with a single-photon source*, New J. Phys. **6**, 92 (2004).
- [26] E. Knill, R. Laflamme and G. J. Milburn, A scheme for efficient quantum computation with linear optics, Nature 409, 46 (2001).
- [27] M. Dakna, J. Clausen, L. Knöll and D.-G. Welsch, Generation of arbitrary quantum states of traveling fields, Phys. Rev. A 59, 1658 (1999).
- [28] R. J. Glauber, Coherent and Incoherent States of the Radiation Field, Phys. Rev. 131, 2766 (1963).
- [29] R. Filip and L. Mišta, Jr., Detecting Quantum States with a Positive Wigner Function beyond Mixtures of Gaussian States, Phys. Rev. Lett. 106, 200401 (2011).
- [30] M. Ježek, I. Straka, M. Mičuda, M. Dušek, J. Fiurášek and R. Filip, Experimental Test of the Quantum Non-Gaussian Character of a Heralded Single-Photon State, Phys. Rev. Lett. 107, 213602 (2011).

- [31] D. W. Berry and A. I. Lvovsky, *Preservation of loss in linear-optical processing*, Phys. Rev. Lett. **105**, 203601 (2010).
- [32] K. Edamatsu, G. Oohata, R. Shimizu and T. Itoh, Generation of ultraviolet entangled photons in a semiconductor, Nature 431, 167 (2004).
- [33] S. Buckley, K. Rivoire, J. Vuckovic, Engineered Quantum Dot Single Photon Sources, Rep. Prog. Phys. **75**, 126503 (2012).
- [34] R. J. Glauber, Quantum Theory of Optical Coherence: Selected Papers and Lectures, (WILEY-VCH, Weinheim, Germany, 2007).
 ISBN: 978-3527406876
- [35] E. Wolf, *Progress in Optics, Volume 53*, (Elsevier B.V., 2009) Chapter 6: Quantum Feed-Forward Control of Light ISBN: 978-0444533609
- [36] R. A. Campos, B. E. A. Saleh, and M. C. Teich, Quantum-mechanical lossless beam splitter: SU(2) symmetry and photon statistics, Phys. Rev. A 40, 1371 (1989).
- [37] H. A. Bachor, T. C. Ralph, A Guide to Experiments in Quantum Optics, (WILEY-VCH, Weinheim, Germany, 2004). ISBN: 978-3527403936
- [38] A. Peres, Quantum Theory: Concepts and Methods, (Springer, New York City, New York 1993).
 ISBN: 978-0792336327
- [39] R. H. Hadfield, Quantum Theory of Optical Coherence: Selected Papers and Lectures, Nat. Phot. 3, 696 (2009). ISBN: 978-3527406876
- [40] C. K. Hong, Z. Y. Ou and L. Mandel, Measurement of subpicosecond time intervals between two photons by interference, Phys. Rev. Lett. **59**, 2044 (1987).